MICROFLUIDIC STUDIES OF PULSATILE CXCL12 STIMULATION ON PROSTATE CANCER CELLS

by

Yao-Kuang Chung

A dissertation submitted in partial fulfillment
of the requirements for the degree of
Doctor of Philosophy
(Biomedical Engineering)
in The University of Michigan
2009

Doctoral Committee:

Associate Professor Shuichi Takayama Chair
Professor Kenneth J Pienta
Associate Professor Alan J Hunt
Assistant Professor Xiaoxia Lin

Dedication

This dissertation is dedicated to my lovely family and friends, especially my grandmother, who passed away peacefully at Mar, 7th, 2009.

Acknowledgements

I would like to thank Professor Pienta and his lab for the help of this prostate cancer research. Also thank Dr. Nobuhiro Kato, Dr. Yi-chung Tung, and Dr. Yunseok Heo for assisting of device fabrication. Moreover, thank Dr. Nobuyuki Futai and Dr. Jonathan Song for assisting of culture media modification. Especially thank my advisor, Professor Takayama, for all the teaching and help during these five years. This research is based upon work supported in part by NIH and the Wilson foundation.

TABLE OF CONTENTS

List of Figures

Chapter II

Chapter III

Chapter IV

List of Tables

List of Appendices

List of Abbreviations

PDMS: poly(dimethysiloxane)

SDF-1: stromal cell-derived factor 1

Chapter I

Introduction And Research Overview

Introduction

This thesis investigates how different fluid flow patterns and temporal CXCL12 stimulation patterns affect prostate cancer PC3 cell adhesion and migration. Prostate carcinoma (PCa) is the most frequently diagnosed cancer in men and the second leading cause of cancer death in American males. Clinical results show that prostate cancer expresses great variability in its ability to metastasize to bone, which not only results in significant complications such as bone pain, impaired mobility, and pathological fracture that severely diminish the quality of life in suffered patients but also is the main reason for the high mortality rate. Bone metastasis is known to be exacerbated by the CXC chemokine receptor 4 (CXCR4) signaling pathway.

Physiology significance of prostate cancer metastasis, PC3 cells, and CXCL12

Prostate cancer happens when cells of the prostate mutate and start to proliferate or differentiate out of control. Prostate cancer cells prefer spreading (metastasizing) from the prostate especially to the bones and lymph nodes and metastasis is responsible for ~90% of cancer death. According to the American Cancer Society, about 30000 men died from prostate cancer in 2008, which is about 10% of total cancer death in men.

One man out of six will be diagnosed with prostate cancer in his life time. In this research, PC3 cell lines, originally derived from advanced bone metastasized prostate cancer are used.

CXC chemokine ligand-12 (CXCL12) or stromal cell-derived factor 1 (SDF-1) is a chemokine highly correlated with cancer metastasis. CXCL12 through its receptor CXCR4 emerge as a crucial regulator of trafficking of various types of cancer cells [15-21]. Also, positive correlations were established between SDF-1 levels and tumor metastasis. Moreover, neutralization of CXCR4 has been shown to limit the number and growth of metastasis in vivo [21, 22]. Finally, PC3 cells are known to migrate across bone marrow endothelial cell monolayer in response to CXCL12 [23].

Need for a new microfluidic cell migration system

Although inhibition of CXCR4 is known to modulate cancer metastasis *in vivo*, the detailed mechanisms are still ambiguous. In vitro studies are useful but lack many physiological features and may not reveal the full range of cancer cell behaviors. For example, the temporal patterns of CXCR4 stimulation by CXCL12 in vivo may be pulsatile rather than continuous. The pulsatile exposure to CXCL12 is expected due to pulsatile release, active degradation by proteases, scavenging by CXCR7 expressing cells, binding to extracellular matrix, and by presence of interstitial flows. Active scavenging by CXCR7 has been shown to be critical for cell directed sensing and polarizing toward CXCL12 stimuli in vivo [24] further reinforcing the potentially important role of temporal patterns of stimulation. Pulsatile stimulation makes mechanistic sense also since CXCR4 is a G-protein coupled receptor (GPCR) and continuous stimulation would

simply lead to receptor desensitization [25]. Because conventional in vitro cell culture systems are static and bioactive chemicals simply added as a bolus, this type of physiological pulsatile exposure of cells to CXCL12 is difficult or not possible to control. There are also other drawbacks of conventional cell migration assay systems. For example, transwell assays (Boyden chambers) [26], which are easy to use and can be high throughput, provide only endpoint results and are not able to visualize and analyze cell migration. Microfluidic devices such as T-channels [27]and premixer gradient generators [28] enable visualization cell adhesion and migration but require tedious seeding procedures to properly position cells inside microhannels as well as tubing to external actuation mechanisms for active flow control. In this research, I not only develop a microfluidic cell migration assay chamber that enables exposure of cells to pulsatile flow and CXCL12 stimulation, the devices are easy to setup, straightforward to position cells, self-contained, and enable real-time visualization of cell movements.

Research Overview

This research focuses on flow and CXCL12 effects on PC3 adhesion and migration by using microfluidic devices. Specific goals and detail motives are as follows.

Despite the critical importance of cell adhesion and migration in cancer, there are surprisingly few studies on the effect of flow on cancer cell responses. This research applied a microfluidic system that is able to generate both pulsatile and steady flow patterns. Effects of not only flow rate but also flow patterns on adhesion and migration of metastatic prostate cancer cell line (PC3 cells) were investigated and analyzed in this

research. From experiment results, it is interesting that PC3 cells showed significantly better adhesion and migration behavior under pulsatile flow than under steady flow.

Biologically, there are several lines of evidence to suggest that, physiologically, the CXCL12 stimuli are temporally patterned as described above. Interestingly, no study has yet studied the effect of different temporal patterns on the directed migration of cancer cells, perhaps in part due to the lack of convenient tools to perform the studies. Therefore, in this research, a new microfluidic device has been designed and pulsatile patterns of CXCL12 stimuli applied to explore PC3 cell migration response such as directionality and speed. Experiment results showed that short exposure time of CXCL12 (2 min exposure of CXCL12 stimuli for every 10 min interval) was able to induce PC3 cell migration with significantly higher directionality than PC3 cells with continuous exposure or longer duration pulses of CXCL12 stimulation. Pulsatile stimuli therefore are important for cell sensing and reacting with extracellular chemical cues in vitro and may better mimic in vivo situations.

Chapter II

Microfluidic pulse and gradient generation system (MPGS) for chemotaxis experiments

Introduction

Chemotaxis plays a crucial role in numerous physiological and pathological processes. The term "Chemotaxis" was first coined by W. Pfeffer in 1884 to describe the attraction of fern sperm to the ova, but since then the phenomenon has been described in bacteria and many eukaryotic cells in many different situations. The most common method for study of chemotaxis is the use of Boyden chambers where chemotaxis is measured by the number of cells migrating from one compartment to another compartment that is a chemoattractant source via a porous filter [26, 29]. The Boyden chamber has the advantage of being easy to set up, straightforward to seed and position cells, and being self-contained, requiring no external tubings or controls for creation of a gradient. Despite their convenience and popularity, Boyden chambers typically provide only endpoint results and thus little information about complex cellular movement during the chemotaxis process [30-32]. Alternative visual assays such as the Zigmond chamber [33-35], Dunn chamber [35], and pipette tip methods to locally dispense chemoattractants

[36-41] have been developed but are time-consuming to setup, challenging to perform, and does not always provide precise microscale control over the spatio-temporal evolution of the gradient. Recently, a number of microfluidic chemotaxis devices have been developed [28, 42-44] to overcome the limitations of conventional chemotaxis systems and enable generation of gradients with higher stability and control. While these systems are useful and cleverly take advantage of microfluidic phenomena, they also have accompanying drawbacks typical of microfluidic systems such as requiring tedious seeding procedures to properly position cells inside microhannels and needing tubing to external actuation mechanisms for active flow control. In this research, we develop a programmable microfluidic chemotaxis system that has the user-friendly features of Boyden chambers of being easy to setup, straightforward to position cells, and self-contained, but also realizes the strengths of microfluidic assays such as real-time visualization of cell movements, precise microscale control of gradients, and active programmable controls (Fig.1). The system, which we call microfluidic pulse and gradient generation system (MPGS), is composed of a PDMS microfluidic chip, Braille display-based microfluidic pumping system [45, 46], and a transparent indium tin oxide on-chip heating system [47, 48]. Fig.2 shows the structure of MPGS: (1) four 2 * 4-pin Braille display modules, (2) a machined aluminum monolithic fingerplate with two hold-down clamps, (3) PDMS microfluidic chip, (4) a transparent heater unit. Pulsatile flow can be easily generated and controlled in a microchannel using Braille system and pumping frequency can be controlled precisely by computer program as fast as 10 Hz. The bulk volume flow rate can be controlled to as low as 0.05nL/sec. Therefore, desired gradient can be generated and maintained precisely in MPGS by changing pumping

frequency, pumping time, and pumping period. The precision of the pumping and relatively slow speed of diffusion enables the gradient generated to be maintained steady and constant even though the pumping is pulsatile in nature. Also, with modified culture media, transparent heater and temperature control system, we are able to conduct chemotaxis experiments outside the incubator and to get real time images for quantitative studies.

Before the cell migration experiments, PDMS microfluidic chip was plasma oxidized for hydrophilicity and sterilized by ultraviolet light. Then microfluidic channel and cell inlet reservoir were coated with 100 ng/ml collagen type I, the major component of the bone matrix, inside the incubator for at least an hour. Finally, the microfluidic chip was washed twice by Dulbecco's Phosphate-Buffered Saline (DPBS) and then a culture media modified to allow carbon dioxide independent media on chip outside of an incubator (for brevity, I will refer to this media as the "modified media" hereafter).

For the cell migration assay, cells were first starved for 18 hours in the incubator with serum free media (RPMI 1640 + antibiotic/antimicotic + 0.1% BSA) and then rinsed with a few mL of sterile DPBS. Next, cells were removed from the culture flask using cell dissociation buffer, centrifuged down, resuspended in modified media, and counted by a hemocytometer. Finally, cells were loaded and seeded in MPGS for six hours before pumping chemoattractant. Table A describes the pumping pin actuation frequency, pumping duration, and stimulation interval for each condition. Fig. 3 shows simulation results of the concentration gradient along the symmetry line of migration semicircle after 12 hours under the diffusivity 4.3×10^{-11} m^2/s. Though there are numerous pumping conditions to try, we first selected several conditions for comparison. Pumping condition

1 and 2 have the same pulses per hour (120 pulses/hour) but delivered in different patterns to produce different gradients. Therefore, cells will be exposed to the same amount of chemoattractant but under different gradients. Pumping condition 3 has higher and sharper gradients than 1 and 2 due to having more pulse inputs per hour. Pumping condition 4 is the opposite condition with fewer inputs and gentler gradients. Using the MPGS, we are able to generate chemical gradients conveniently to investigate cell reactions under different conditions.

Primary results

From Fig. 4, we can see that PC3 cells migrate into the semicircle area under a CXCL12 gradient. These proof-of-principle results show basic function of MPGS for chemotaxis experiments with real time imaging.

Discussions

From simulation results, by changing pumping pin actuation frequencies, pumping duration, and stimulation intervals, MPGS was able to generate various gradient shapes to investigate cell chemotaxis behavior. PC3 cells did migrate into the channel under the effect of SDF-1 in MPGS. However, from simulation, slopes of the gradients decrease as cells migrate toward the source of chemicals and gradients are not stable due to pulsatile nature of Braille pumping. While many microfluidic gradient generators cite the stability of gradients as a strength, the results led me to ask the question of whether stable gradients are physiological or necessary for cell to react. Actually, pulsatile exposure of cancer cells to the chemokine CXCL12 may be more physiologically relevant. It is

known that CXCL12 release in vivo is pulsatile [49] and that there is active scavenging [24] and degradation of CXCL12 [50] as well to make in vivo levels fluctuate rapidly. When active scavenging is inhibited, cells do not migrate well in vivo. Therefore, instead of focusing on generating steady gradient, I decided to study the effect of pulsatile simulation and temporally patterned chemical gradients as described in subsequent chapters.

Conclusion

MPGS was useful to generate various gradients to investigate cell chemotaxis behavior under substantially steady chemical gradients. However, pulsatile stimulation and temporal gradient may be more efficient for cell to react and has more physiological relevance. Therefore, instead of forming steady gradients, I changed the design to apply pulsatile stimulation and temporal gradients (see chapter IV).

Table 1 Experimental conditions.
Pumping pin actuation frequency, pumping duration, and stimulation intervals for pumping conditions 1 to 4

Conditions	Actuation Frequency	Pumping Duration	Stimulations Intervals
Condition 1	10 Hz	16 sec	20 minutes
Condition 2	5Hz	16sec	10minutes
Condition 3	10Hz	12sec	10minutes
Condition 4	10Hz	12sec	20minutes

Figure 1 Schematic design of the top view of a PDMS microfluidic chip.
It includes a cell seeding and culture area (big semi-circle on left); cell migration area (small semicircle in the center of left side); microfluidic channel (thin line in middle); and chemoattractant reservoir (square reservoir on right). Cells can be simply loaded by pipette tips and seeded in cell inlet. Dissolved chemoattractants can be loaded in the media inlet and pumped through pumping channel by Braille pins. Chemoattractant pulse generates desired concentration gradient inside the small semicircle for cell to migration in. Cell migration inside the semicircle area can be seen under microscope.

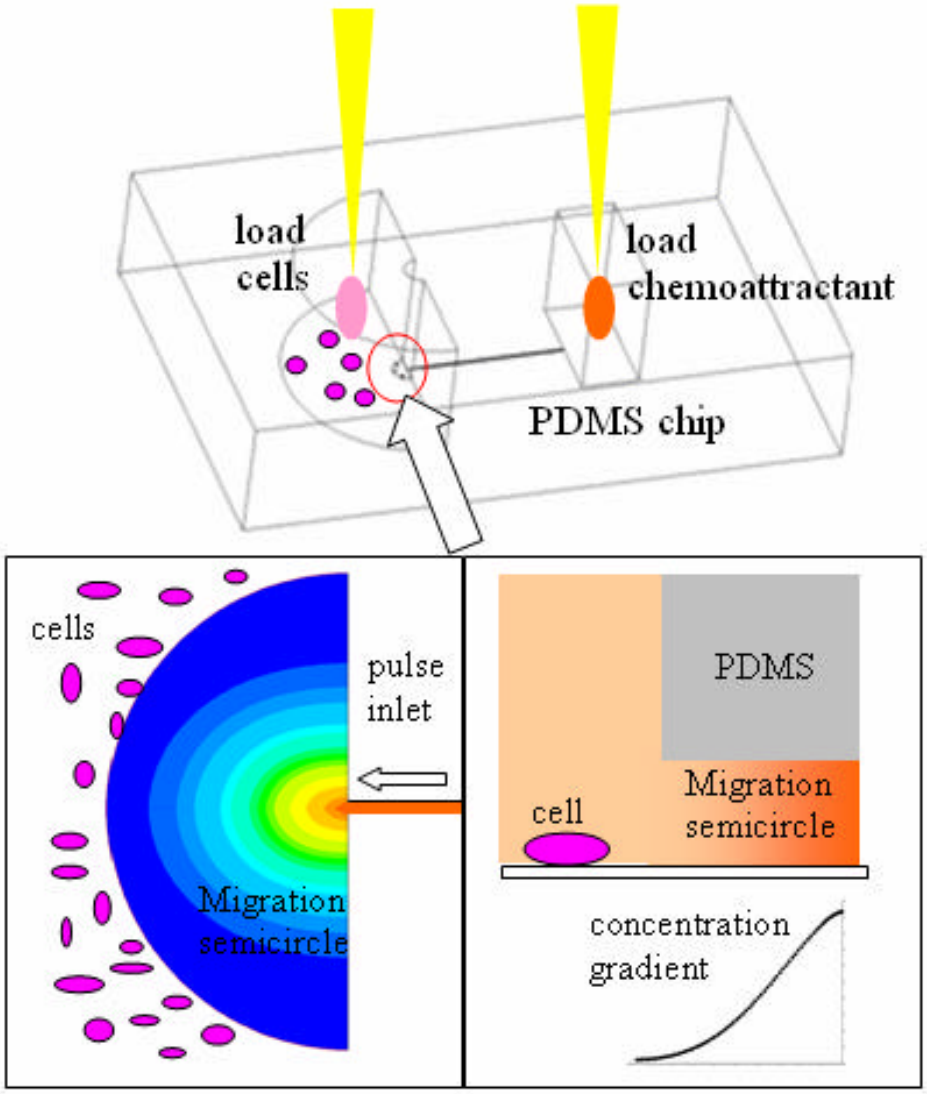

Figure 2 Images of MPGS.
(Left) An actual top view of a chemotaxis chip attached to and operating on a Braille actuator module. (1) four 2 * 4-pin Braille display modules, (2) a machined aluminum monolithic fingerplate with two hold-down clamps, (3) PDMS microfluidic chip, (4) a transparent heater unit. (Right) A schematic figure of a side view of a microfluidic chemotaxis chip attached to the Braille actuator module.

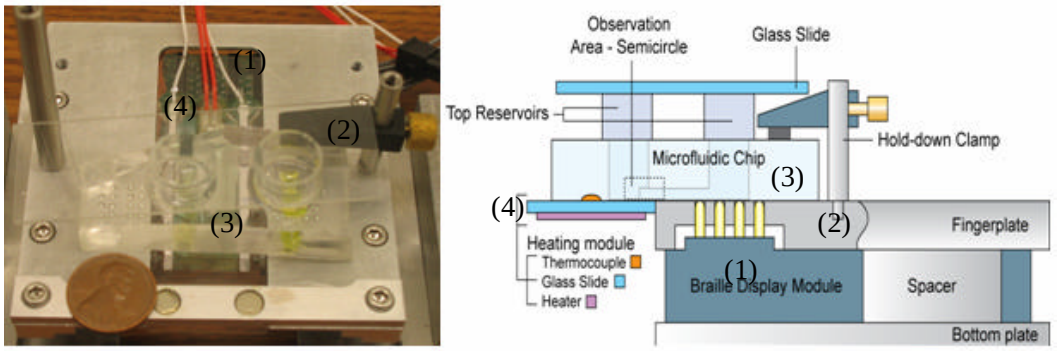

Figure 3 Simulation results of the concentration gradient.
Concentration gradient along the symmetry line of migration semicircle after 12 hours under the chemoattractant with diffusivity 4.3×10-11 m2/s: (1) pumping condition 1; (2) pumping condition 2; (3) pumping condition 3; (4) pumping condition 4.

(1) pumping condition 1

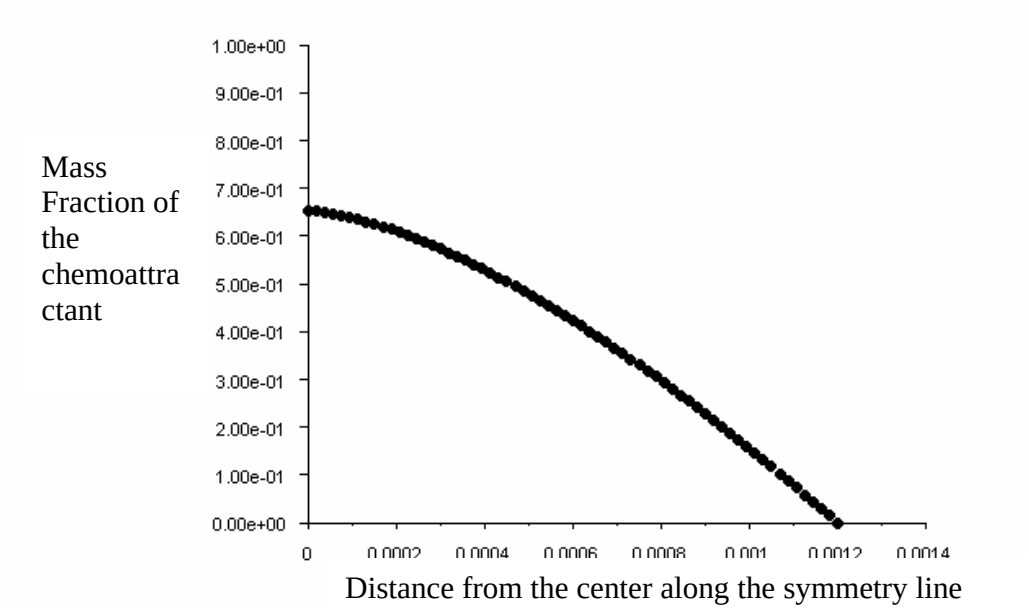

(2) pumping condition 2

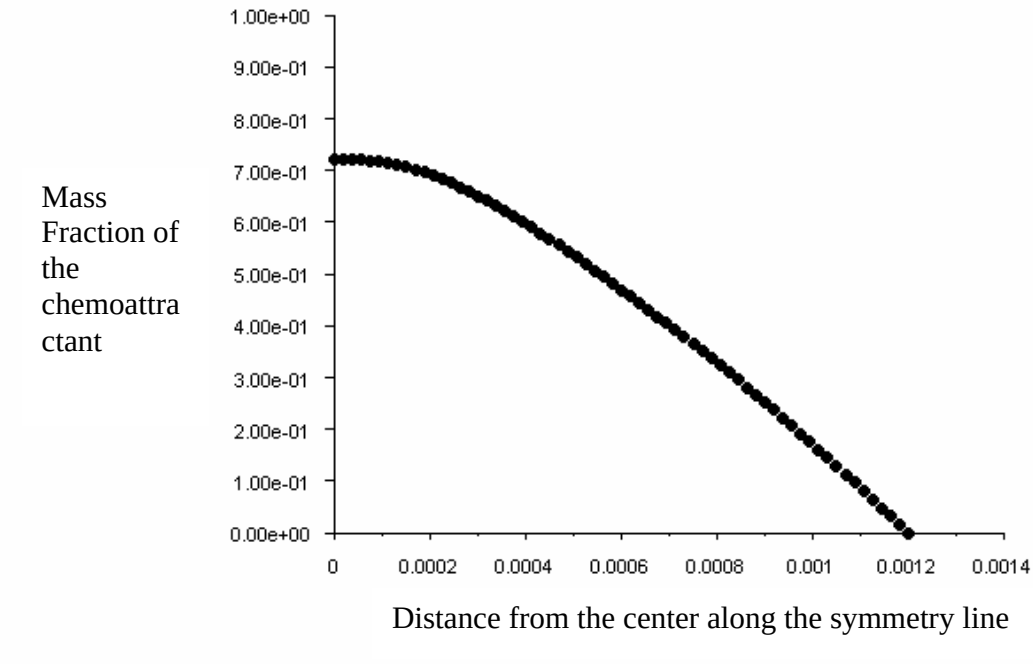

(3) pumping condition 3

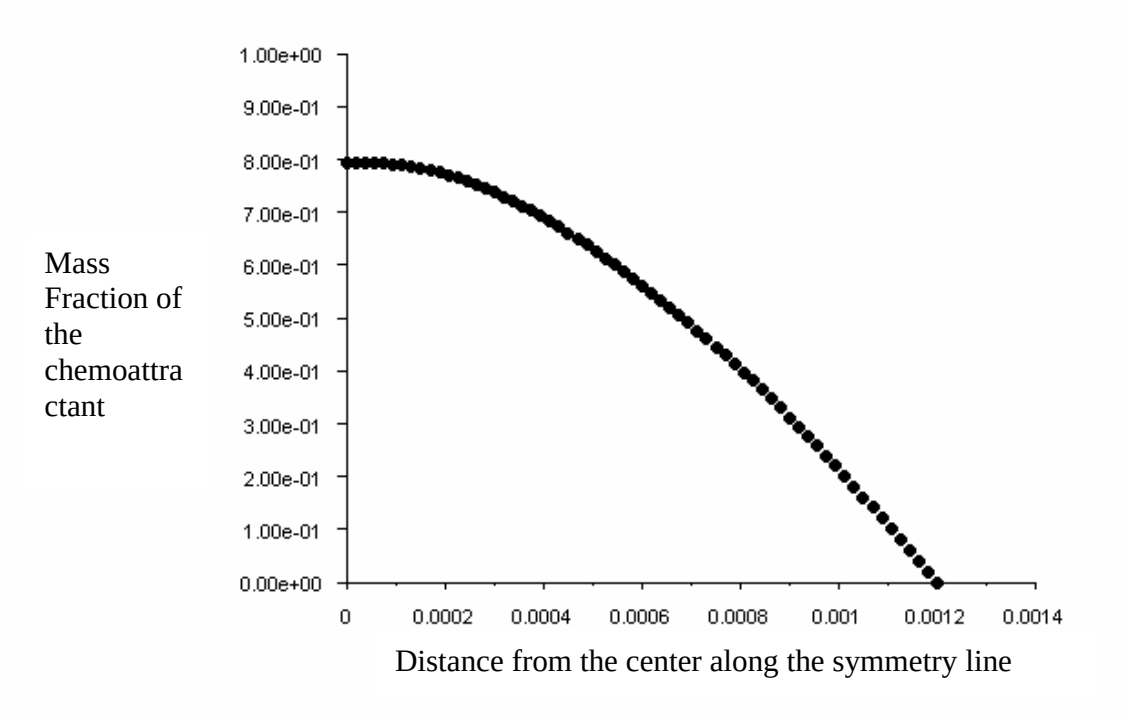

(4) pumping condition 4

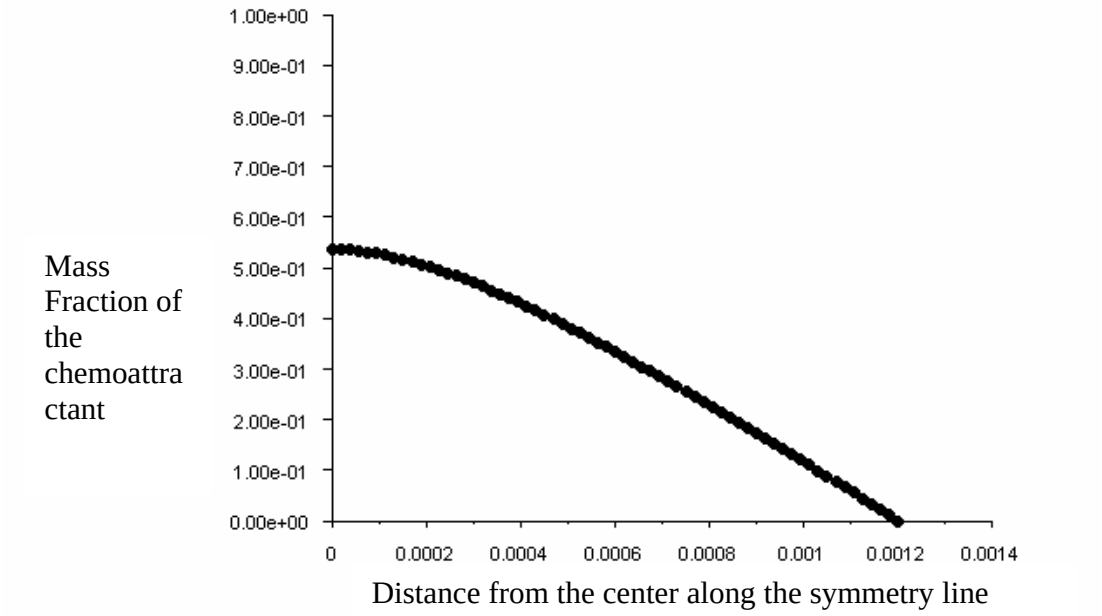

Figure 4 Cell migration images.
(left) cell image before pumping CXCL12, (right) cell image after pumping CXCL12 for 24 hours by condition 1 in table 1 with 500 ng/ml CXCL12.

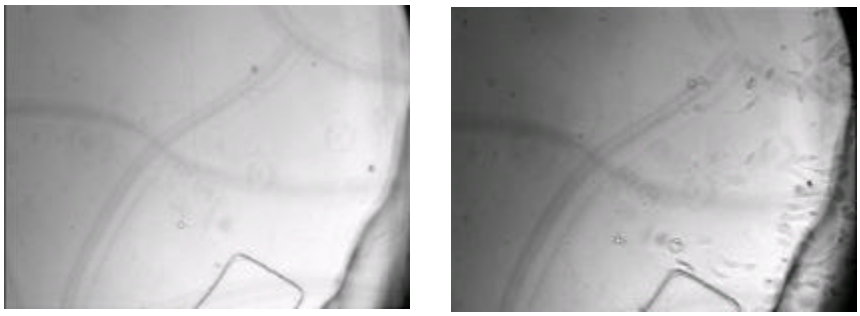

Chapter III

Fluid shear stress mediated inhibition of prostate cancer cell migration is modulated by flow and CXCR4

Abstract

This paper evaluates prostate cancer cell migration under different magnitudes and patterns of fluid flow in a microfluidic channel. Under continuous steady laminar flow conditions at a fluid flow rate of 0.67 µl/min which, in the device being studied, corresponds to a shear stress of 0.44 dynes/cm^2, PC-3 prostate cancer cells have a tendency to migrate with a reduced speed and with a significant portion of cells undergoing cell detachment. When the PC-3 cells are exposed to a similar average flow rate but in periodic pulsatile flow patterns the PC-3 cells are not inhibited from migrating and have minimal detachment. Furthermore, we show that fluid shear stress mediated inhibition of PC-3 cell migration is modulated by expression and signalling by the chemokine receptor CXCR4. PC-3 cells exposed to 2000 ng/mL of the CXCR4 ligand, CXCL12, show normal migration and reduced cell detachment under steady laminar flow at a fluid flow rate of 0.7 µl/min whereas PC-3 cells with CXCR4 knocked down showed

reduced adhesion and migration even at a lower flow rate of 0.10μL/min. These flow and CXCR4-dependent differences in cell migration are important given the physiological relevance of fluid flow, common use of flows in microfluidic systems, and importance of CXCR4 in determination of cancer cell invasiveness.

Introduction

Cell migration is a key factor in tumor cell spreading and invasion. Here, we evaluate the migratory behavior of a prostate cancer cell line (PC-3 cells) in microfluidic devices under a range of flow rates and flow patterns. This type of basic cellular analysis is

important for two reasons: (i) tumor cells are exposed to fluid flow conditions physiologically and (ii) there are an increasing number of studies on cell migration using microfluidic devices where cells are exposed to flow.

Tumors often have a high internal pressure which generates interstitial flows [51, 52]. Using a mathematical model of interstitial pressure-fluid flow, Jain et al [53], further showed that the interstitial fluid velocity is nearly zero within the tumor mass but is high at the periphery where there is a large pressure drop. Fluid flow and shear stress created by interstitial flow at common sites for prostate cancer metastasis such as the bone may even be as high as 8–30 dynes/cm^2 *in vivo* during mechanical loading [54]. Recently, several reports of *in vitro* systems that mimic interstitial flow have been reported. For example, Ng and Swartz (2003) applied a steady flow at a shear stress of 1.135 to 0.324 dyn/cm^2 and demonstrated fibroblast alignment [55]. In experiments described here, fluid flow velocities of 215 and 30 μm/sec representing shear stress of 0.43 and 0.07 dynes/cm^2 respectively were applied to PC3 cells in microfluidic devices and cell adhesion and migration behavior investigated.

In addition to systems that aim to recreate physiological flow conditions, a considerable number of *in vitro* studies culture cells under flowing conditions as a consequence of using fluid flow to create chemical gradients in order to study chemotaxis [56-63]. Walker et al., 2005 [64] studied the effect fluid flow, rather than the chemical gradient, exerted on cells by these premixer gradient generators commonly used for chemotaxis studies. They found that a constant shear stress of 0.687 dynes/cm^2, commonly generated in these devices, was able to induce HL60 promyelocytic leukemia cell to migrate downstream. For comparison, we note that these shear stress levels are much lower than

typical level of fluid shear stress in the arteries 10–20 dyn/cm^2 for shearing endothelial cells [60, 65] . Overall, despite the critical importance of cell migration in cancer, there are still relatively few detailed studies on the effect of fluid flow on cancer cell migration. In this paper we ask the question, how is prostate cancer cell (PC3 cells) migration affected by different flow rates? We also evaluate how the cytokine receptor CXCR4 modulates these effects. Expression of CXCR4 is correlated with the ability of prostate cancer cells to metastasize and access cellular niches, such as bone marrow, and promote tumor cell survival and growth [15]. And CXCL12 concentrations range from 125 to 625 nM in biological fluids including bone marrow [66]. CXCL12 actions in vivo microenvironment are potentiated by their very high local release levels and strong affinity for both cell surface heparin sulfate proteoglycans and extracellular matrix that further enable CXCL12 local concentration increase to μM [67]. How CXCR4 may modulate that ability of tumor cells to withstand fluid shear stress, however, is an understudied area.

Material and methods

Microfluidic Device Fabrication

The microfluidic device was fabricated with poly(dimethysiloxane) (PDMS) using soft lithography and rapid prototyping on copper boards. PDMS (Sylgard 184, Dow Corning, Midland, MI) is optically transparent, gas permeable, non-toxic, mechanically compliant, and proven to be compatible with embryo culture. Instead of making molds of microchannels on silicon wafers with traditional time-consuming lithography methods,

we constructed molds by etching copper boards [46]. Copper mold fabrication is faster and easier with a minimum feature size of ~100μm.

Braille pumping system

In this research, we applied an integrated microfluidic pumping and valving system powered by computer-controlled and individually actuated Braille pins on a portable Braille display[47]. The system takes advantage of resilience and elasticity of PDMS microchannels and bottom thin films. Fluid in the microchannel can be pumped when Braille pins go up, “squeezing” the bottom thin film, pushing fluid to move forward (see Fig. 5).

Characterization of Fluid Flows by the Braille pumping system.

The travel distance of 6 μm diameter beads were tracked using a digital CCD camera (Hamamatsu ORCA-ER) and an inverted microscope (Nikon Eclipse TS100) with 10X objective. Image sequences were acquired at 5 frames/s to determine the average travel speed of the beads which also represents the average flow speed. Then the average flow rate and shear stress can be calculated.

Temperature control system

Temperature control is essential for long term cell culture outside of an incubator. Under our PDMS chip, we placed a transparent indium tin oxide (ITO) heater connected to a PID temperature controller (E5GN; Omron; Schaumburg, IL). The heaters are fabricated by depositing a thin layer of Indium-Tin-Oxide (ITO) onto a glass substrate using

electron-beam evaporation. ITO is a transparent, conducting material and therefore can form a resistive heater distributed over the surface of the substrate while still allowing light to pass through[48].

Modified media for CO_2 independent culture

RPMI Medium 1640 with GLUTAMAX™-I (61870; Gibco) was buffered with NaHCO3 and 3-(N-morpholino) propanesulfonic acid (MOPS). The concentrations of the added NaHCO3 and MOPS were 10mM each. In addition, bovine serum albumin (BSA) was added at 0.1% by volume. The pH was adjusted using HCl to 7.2 before use on the microscope stage as recommended by Futai et al, 2006 [45]. I will refer to this media subsequently as "modified media".

PC3 cell culture in the incubator

PC3 prostate cancer cells were obtained from ATCC (Manassas, VA) and passaged under appropriate growth conditions. PC-3 cells were maintained in RPMI 1640 + 10% fetal calf serum (Invitrogen Corp., Carisbad, CA). Cell were passaged by trypsinization using 1×trypsin + EDTA (Invitrogen Corp.) and resuspended in appropriate growth media.

PC3 cell culture on microscope stage

In order to conduct cell experiments outside the incubator, we must provide means to regulate osmolality, temperature, and pH values which play pivotal roles in basic cellular functions and reactions. Thus, I overlay the top reservoirs with mineral oil to decrease evaporation from the top. Also, the membrane that comprises the floor of the device

consists of three layers: PDMS-parylene-PDMS[48]. The parylene layer helps decrease evaporation through the bottom. An ITO heater and temperature control system regulates culture temperature. Finally, to maintain similar CO2 condition as in a cell incubator, modified cell culture media was utilized.

siRNA knockdown of CXCR4

The pSUPER vector that express short hairpin small interfering RNAs (siRNA) under the control of polymeraseQ OH1-RNA promoter was used after inserting pairs of annealed DNA oligonucleotides between the Bgl II and HindIII restriction sites according to the manufacturer protocol (Oligoengine, Seattle, WA) [68]. After transfecting and culturing, PC3-CXCR4-si cells showed significant reduction of CXCR4 protein expression as measured by using Western Blot Analysis [69].

Cell experiment protocol

Before the cell migration experiments, PDMS microfluidic chips were sterilized by ultraviolet light. Then the microfluidic channel and cell inlet reservoir were coated with 100 ng/ml collagen type I, the major component of the bone matrix, and incubated for at least an hour. Finally, the microfluidic chip was rinsed with Dulbecco's Phosphate-Buffered Saline (DPBS) and then with modified culture media.

Preparation of the cells was as follow. PC3 cells were first starved for 12 hours in the incubator with serum free media (RPMI 1640 + antibiotic/antimicotic + 0.1% BSA) and then rinsed with a few mL of sterile DPBS. Next, the cells were removed from the culture flask using cell dissociation buffer enzyme free Hanks'- based (Invitrogen),

centrifuged to a pellet, resuspended in the modified cell culture media, and then counted by a hemocytometer. Finally, cells were loaded and seeded in the microfluidic chips for six hours before flow exposure. Coupled with a syringe pump, we were able to generate continuous/steady flow. Cell migration was investigated by real-time imaging with digital CCD camera (Hamamatsu ORCA-ER), inverted microscope (Nikon Eclipse TS-100), and 10X objective. Images were taken every 10 minutes for at least 12 hours.

And for comparison of CXCL12 effects, PC3 cell adhesion on Collagen I was tested after 6 hour of CXCL12 activation. CXCL12 has been added into modified serum free media for this experiment. Starved PC3 cells were seeded under modified serum free media with 2000 ng/ml CXCL12 for 6 hour before applying flow.

Data Analysis

Time-lapse cell images were tracked by using Metamorph and analyzed by ImageJ. Several cell migration parameters were calculated: (1) migration distance (sum of straight-line segments that a cell travels between consecutive images) (2) cell migration speed (migration distance over time).

Statistical Analysis

Each experimental condition was performed in duplicate and 50 or more cells were analyzed for each condition (see Table 2). For migration speed and DI data, analysis of variance (one-way ANOVA) was applied to examine statistical significance, followed by a posthoc Tukey method for multiple comparisons. Results were considered to be significant at $P<0.05$.

Results

Microfluidic Device Design

We used a flat wide channel similar to parallel plate flow chambers commonly used to expose cells to defined fluid shear stresses (see Fig. 5). In this design, steady laminar flow can be generated by using syringe pumps and pulsatile flow can be generated by Braille pumps.

Continuous steady laminar flow with flow rates of 0.67 µL/min inhibits PC3 cells migration

PC3 cells were pumped from the outlet reservoir into the closed laminar flow microchannel chamber coated with collagen I then the flow stopped to allow cells to attach. After 6 hours, cells were exposed to steady laminar flow generated by a syringe pump at an average flow rate of 0.67 µl/min, which in my device generates an estimated shear stress of 0.44 dynes/cm^2. Experimental results showed that under this flow condition, PC3 cells expressed decreased migration, started to detach and about 24% of cells were washed out by the flow over 12 hours (see Fig. 6,7). Average migration speed of PC3 cells under steady laminar flow was significantly lower than that under pulsatile flow with similar average flow rate or that under same laminar flow but with CXCL12 activation (see Fig. 8).

Pulsatile flow patterns do not inhibit PC3 cells migration

Interstitial flow pattern is expected to vary according to different sites in the body. For example, outward flow at periphery of tumors with high interstitial pressure may be fast,

steady and constant [3]. Interstitial pressure in normal tissues, in contrast, is closer to zero. Thus, the interstitial flow at normal tissue is expected to be relatively slower and any high velocity flows more pulsatile rather than steady and constant [4].

To evaluate effects of fluid flow pattern on cancer cell migration, I evaluated the effect flow with the same time-averaged flow rate but using a pulsed flow profile. This was performed using a computerized microfluidic actuation system that utilizes refreshable Braille displays rather than a syringe pump. Flow rates and patterns are controlled by using different pumping frequencies and patterns. In the microchannel devices used, a 5Hz actuations frequency (because the pumping is performed using a 4 pattern pin sequence, this leads to a net forward surge at a rate of 1.25Hz) generates an average flow rate of 0.66 µl/min. Unlike in the case of exposure to a continuous steady laminar flow, Most PC3 cells under pulsatile flow migrated without detaching or shrinking at this same average flow rate (see fig. 7(a)).

CXCR4 enhances PC3 cell adhesion and reduces migration inhibitory effect of fluid shear stress

To test the effect of CXCR4 signaling on adhesion and migration, PC-3 cells were treated with CXCL12 for 6 hours [22] during seeding and then tested for response to flow Interestingly, PC3 cells with CXCL12 activation survived and spread well at the steady 0.67µL/min flow rate where 16 over 66 non-CXCL12-treated cells (~24% cells) detached and were washed away (see fig. 6 and 7(b)). Moreover, PC3-CXCR4-si cells with the receptor CXCR4 knocked down showed reduced adhesion and migration even at a much lower flow rate of 0.10 µl/min. Therefore, CXCL12 signaling through the receptor

CXCR4 enhances PC3 cell adhesion and confers resistance to fluid shear stress mediated decrease in cell migration.

Discussion

Flow affects cell migration behavior through mechanotaxis whereby cells sense shear stress [58, 59, 63] and autologuous chemotaxis whereby flow-induced uneven distribution of autocrine factors triggers migration [56, 70]. Cells have been proposed to possess mechano-sensor such as integrin [71] or chemical receptors for sensing of extracullar stimuli. Since different flow rate and flow patterns generate various shear stresses as well as autocrine distribution, cells may have different responses under different flow conditions. In this research, PC-3 cells presented different adhesion and migration behavior under different flow rates.

Cancer cells traffic and spread under blood and interstitial flow. So flow may regulate cancer metastasis through mechanotaxis and chemotaxis. My experiment results showed that when average flow rate was 0.67 μl/min representing a shear stress of 0.44 dyn/cm^2, PC-3 cells exhibited reduced adhesion and migration. However, with activation of CXCL12, PC-3 cells showed enhanced adhesion and migration under the same laminar flow condition. Finally, PC3-CXCR4-si cells showed reduced migration phenomenon under lower average flow rate 0.10 μL/min. To sum up, flow effects and importance of CXCR4 on PC-3 adhesion and migration are clarified through results in this research.

Conclusion

A practical, multifunctional, and efficient cell migration assay has been developed for the characterization of cell migration under different flow patterns. The research demonstrates crucial effects of flow as well as CXCR4 on prostate cancer cell PC-3 adhesion and migration.

Table 2 Pulsatile and steady flow conditions for PC3 cell migration studies.

The average flow rate was measured by fluorescence bead tracking experiments. All conditions were duplicated and total cells that were analyzed are also listed in Table 1.

Pulsatile flow by Braille System				Steady laminar flow by syringe		
Pumping Frequency	Average flow rate µl/min	# of cells analyzed	Calculated average shear stress dyn/cm^2	Average flow rate µl/min	# of cells analyzed	Average shear stress dyn/cm^2
5Hz	0.66 ± 0.02	126	0.43 ± 0.01	0.67	50	0.44

Figure 5 The microfluidic System.
(a) The picture of the microfluidic device

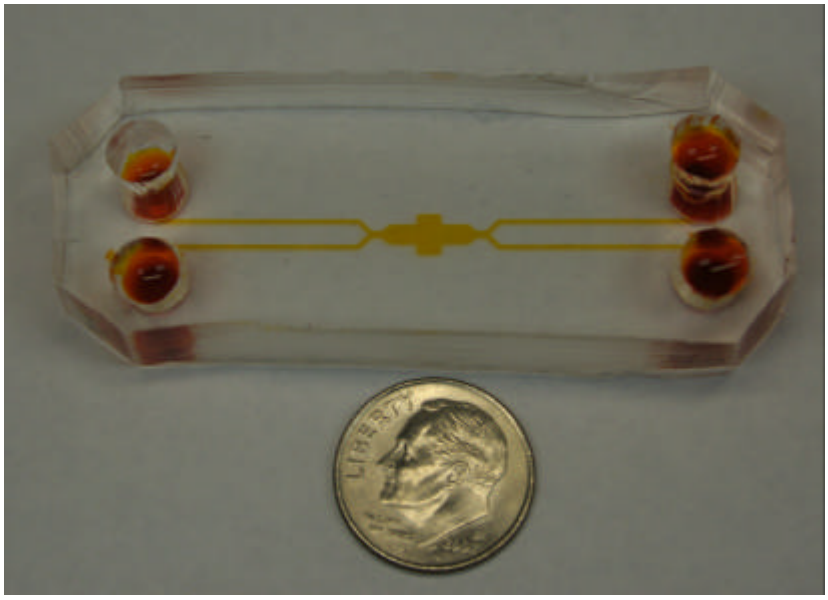

(b) A schematic figure of the microfluidic device aligned on the Braille module
The PDMS microfluidic device can be aligned on the Braille module (pins). When Braille pins go up, “squeezing” the bottom PDMS thin film, fluid in the microchannel can be pumped and move forward.

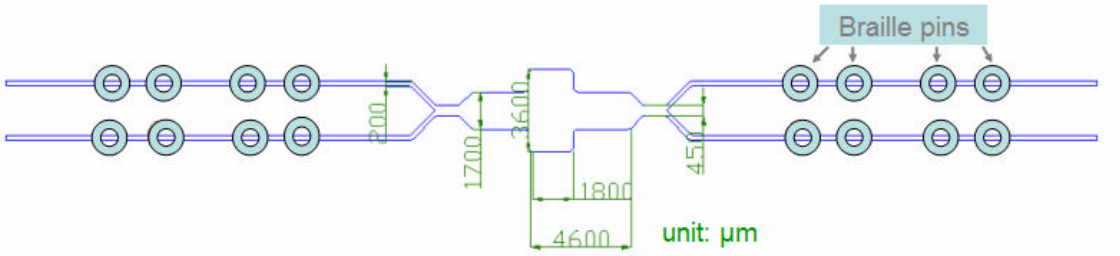

(c) A schematic figure of a side view of a microfluidic chemotaxis chip attached to the Braille actuator module. The whole system includes: (1) four 2 * 4-pin Braille display modules, (2) a machined aluminum monolithic fingerplate, (3) two hold down clamps, (4) PDMS microfluidic chip, (5) a transparent ITO heater unit, (6) the syringe pump. The PDMS microfluidic system can be aligned on the Braille module or connected to the syringe pump. Therefore, fluid in the channel can be either pumped by Braille system (1) or by the syringe pump (6).

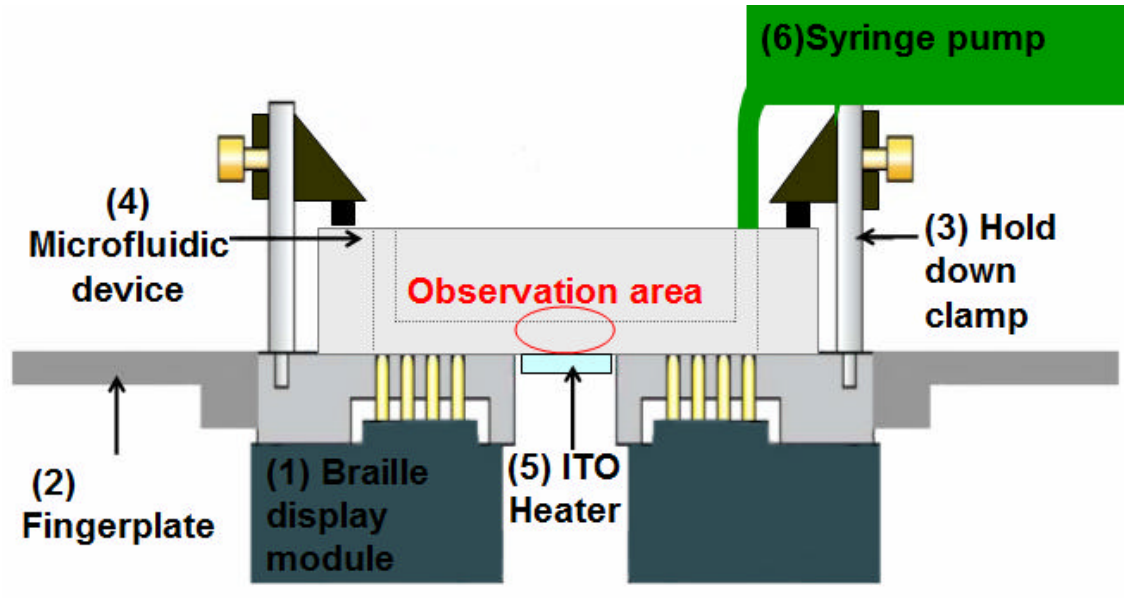

Figure 6 PC3 cell images under steady laminar flow with average flow rate 0.67 µl/min by the syringe pump.
Compared with cell image at 0 hour and at 12 hour, PC3 cells labeled with red circles detached and were washed away by steady laminar flow.

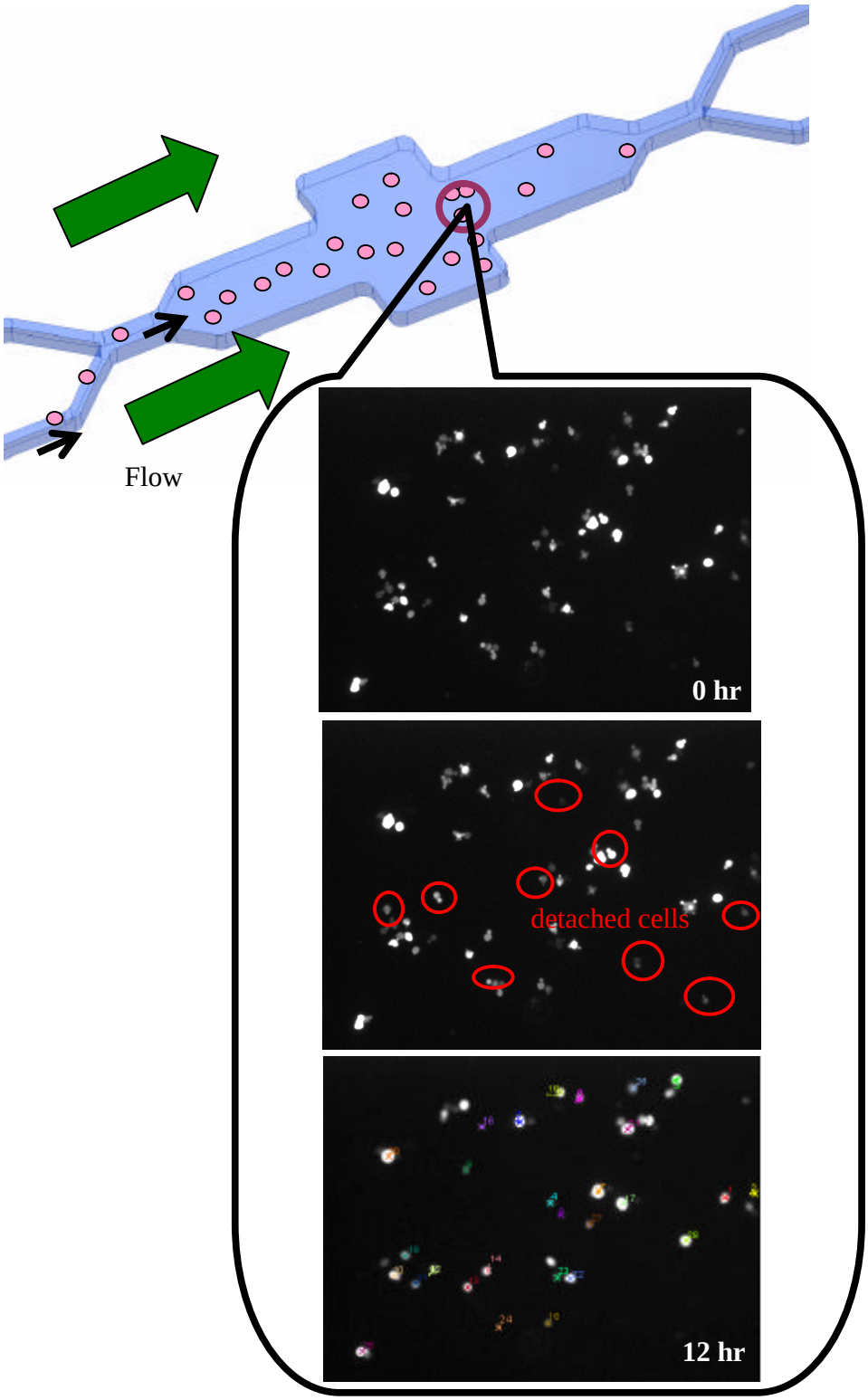

Figure 7 PC3 cell images at the similar location in the microchannel
(a) under pulsatile flow with average flow rate ~0.66 µl/min by the syringe pump, (b) under the same steady laminar flow but with CXCL12 activation
In (a), only 1~2% of PC3 cells were detached and washed by pulsatile flow. In (b), with CXCL12 activation, PC3 cells seemed attach and spread better and no cell was detached and washed away by steady laminar flow with average flow rate 0.67 µl/min

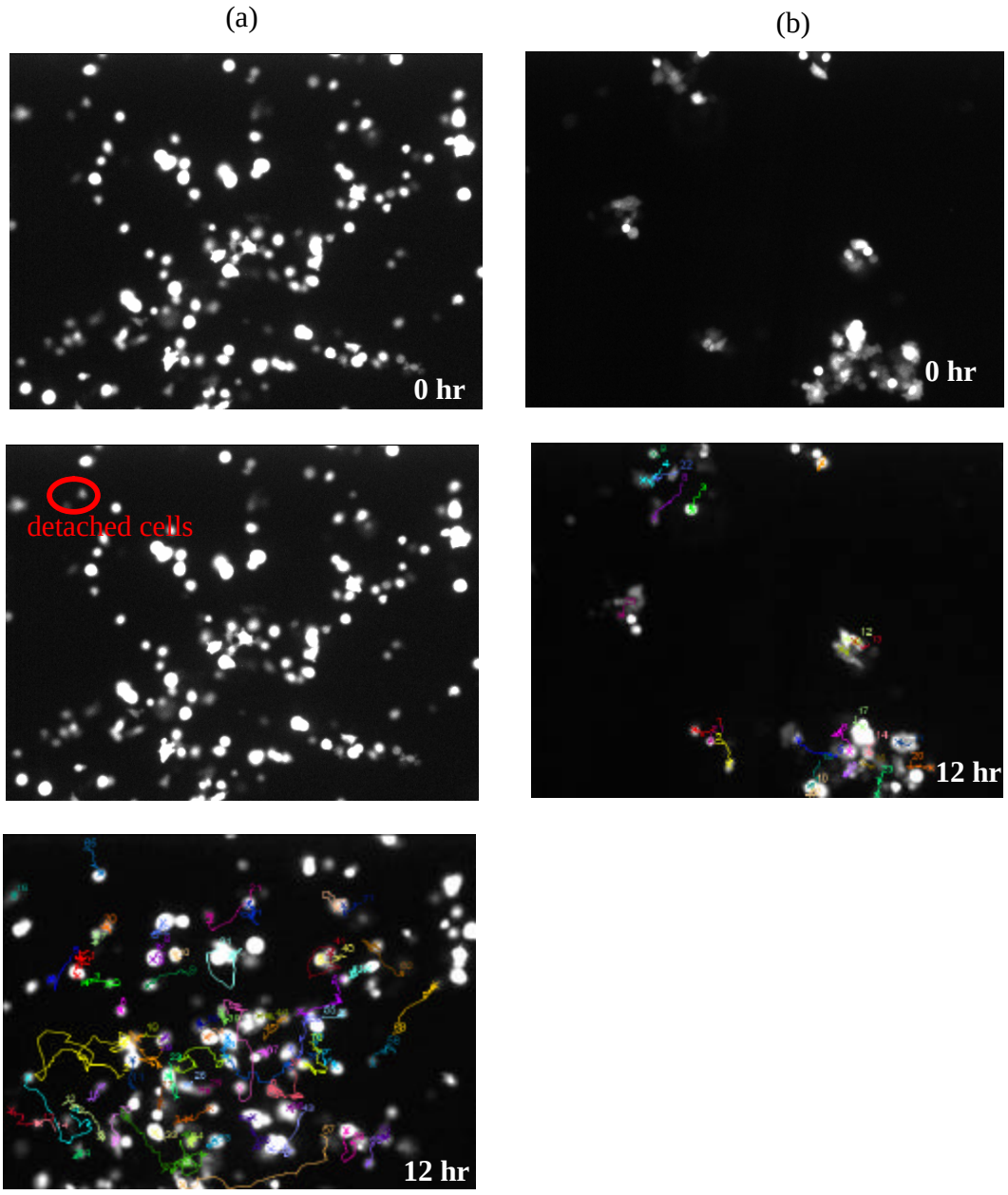

Figure 8 Comparison of PC-3 cell migration speed for six hours under different conditions

Average migration speed of PC3 cells under steady laminar flow was significantly lower than that under pulsatile flow with similar average flow rate or that under same laminar flow but with CXCL12 activation.

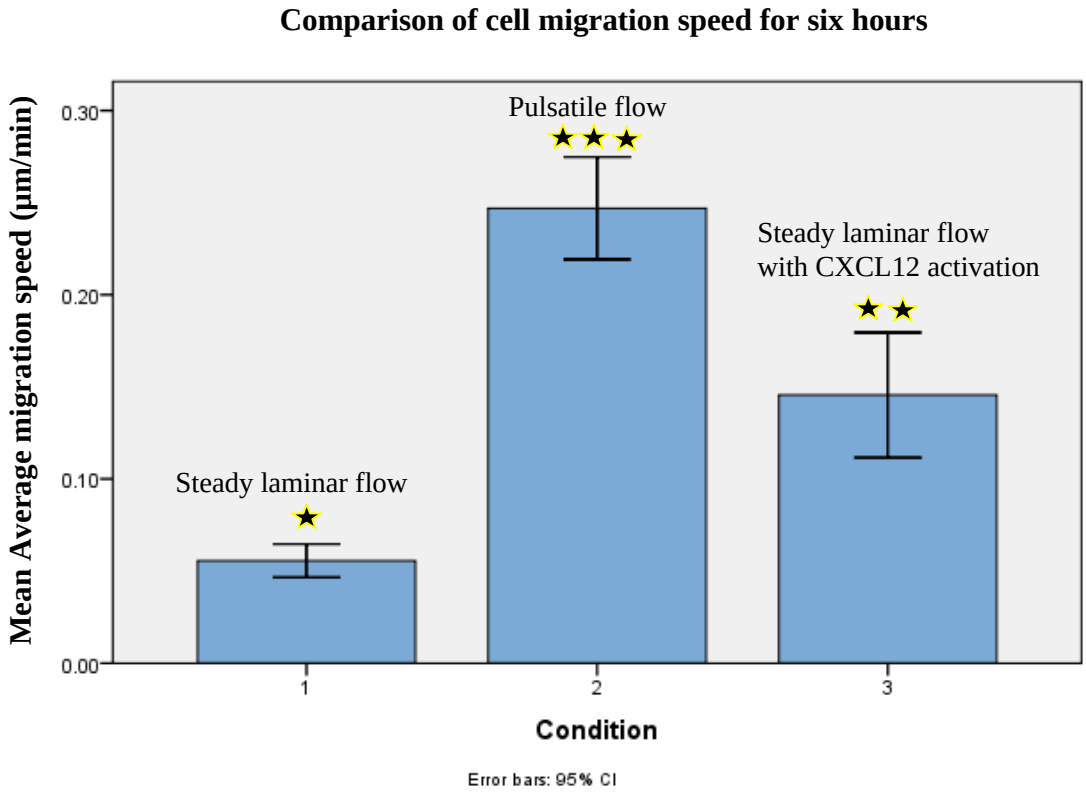

Chapter IV

Pulsatile CXCL12 stimulation induces PC3 cells to migrate with high directionality

Abstract

This chapter describes a microfluidic device to investigate PC3 cell migration under pulsatile CXCL12 stimuli. PC3 cells migrate with high directionality under a pattern of stimulation where 2 min exposure of CXCL12 is applied every 10 min interval. PC3 cells show relatively reduced directed migration with 5 min exposure every 10 min interval despite being exposed to larger quantity of CXCL12 overall. These results are particularly interesting when contrasted with the observation that there is no directed migration under exposure of the cells to a steady CXCL12 gradient. PC3 cells with CXCR4 knockdown showed reduced migration under all stimulation conditions demonstrating the importance of CXCR4 signaling in the CXCL12 mediated directed migration process. The chapter further discusses physiological relevance and mechanistic implications of the observations.

Introduction

Chemotaxis, the directed movement of cells under the effect of chemicals, plays a key role in embryogenesis, angiogenesis, immunity, and metastasis. Several chemokines, growth factors, and extracellular matrix components are reported to be crucial factors in chemotaxis. CXCL12 through its G-protein-coupled receptor CXCR4 is pivotal for modulating the trafficking of stem cells and cancer cells by inducing G-protein-coupled signaling and reactions. CXCR4, one of the most important receptor in human cancer malignancy, allows tumor cells to access cellular niches, such as bone marrow, that favor tumor cell survival and growth[15]. The most common way to study CXCL12 induced directed migration of cancer cells is to use end-point transwell assays[23]. However, those assays lack the ability to visualize the cell migration process. With the development of microfluidics, several devices such as the T-sensor [27] and the premixer gradient generator [28] have shown the abilities to generate stable chemical gradients and to analyze cell trajectories. Interestingly, there have not been demonstrations to date of chemotaxis of cancer cell in gradients of CXCL12 alone using microfluidic gradient generators. Mosadegh et al., 2008[18], for example, demonstrated that steady CXCL12 gradient alone did not induced chemotaxis of breast cancer cell MDA-MB-231. I also performed experiments using the same premixer gradient generator to test chemotaxis of PC3 cells with a steady nonlinear CXCL12 gradient and also similarly found that the cells do not migrate with directionality. How could these negative results be reconciled with the demonstrated in vivo significance of CXCL12 and positive chemotaxis results from transwell assays?

There are several possible reasons why cancer cells do not show chemotaxis within the microfluidic premixer gradient generators; I discuss three here. First, as proposed by Mosadegh et al.[18], the microfluidic device may have detrimental effect on chemotaxis because they constantly wash away autocrine factors necessary for cell to be sensitized to CXCL12 gradients. Second, as shown by Walker et al, [64], microfluidic devices, such as T-sensors and premixers with steady gradient, apply continuous shear stress on cells, which may effect cell migration due to shear stress perpendicular to the chemical gradient direction. I also propose a third possibility, that steady gradients of CXCL12 have limited ability to trigger directed cell migration because such gradients are not physiological and further because they are mechanistically disadvantageous.

Biologically, there are several lines of evidence to suggest temporally patterned stimulation of cells to CXCL12 *in vivo*. To begin with, cells release chemokines in a pulsatile manner and it takes several minutes for the recycling pathway of excytosis to recover [49]. Next, a chemical gradient may be difficult to maintain steadily in the body due to pulsatile blood and interstitial flow. And for CXCL12, its half life is less than 1 minute under the effect of dipeptidyl peptidase (DPP) IV equivalent to the activity in normal human plasma [50]. Furthermore, extracellular matrix (ECM) structures such as glycosaminoglycans (GAG)s- heparin sulfate (HS) immobilizes and localize CXCL12 [72]. When cells migrate through such environments CXCL12 encounters would be periodic and thus more pulsatile. Recently, it has also been reported that a critical role of CXCR7 in vivo is to actively scavenge CXCL12 from the extracellular space [24]. This would lead to rapid decrease in available CXCL12 in the vicinity generating, in essence, a pulsatile exposure of cells to CXCL12. Steady gradients generated in microfluidic

devices may also be disadvantageous mechanistically because the concentration gradient would be shallower compared to transwells. This may decrease the difference in receptor occupancy between the front and back of cells. Furthermore for G-protein couple receptors (GPCRs), such as CXCR4, continuous exposure may not be cost effective for instructing cells since there is rapid receptor desensitization[25]. Temporally patterned exposure of chemicals rather than a steady gradient, therefore, may be mechanistically more efficient by providing time for the signaling system to recover from desensitization. Despite the physiological relevance and mechanistic prudence of using temporally patterned stimulation for cancer cell chemotaxis, there is a lack of study of this topic. This paucity of experiments is due, at least in part, to lack of convenient tools to study cancer cell chemotaxis in response to temporally patterned stimulations. Here, I use the microfluidic device developed and described in Chapter 2 to perform such studies.

Material and methods

The microfluidic chip is composed of PDMS and fabricated by using multilayer soft lithography. (Fig. 9)

a. Device fabrication

The microfluidic device was fabricated in poly(dimethysiloxane) (PDMS) using soft lithography and rapid prototyping on copper boards. PDMS (Sylgard 184, Dow Corning, Midland, MI) is optically transparent, gas permeable, non-toxic, mechanically compliant, and proven to be non-toxic as assessed by the mouse embryo assay [48]. Instead of making molds of microchannels on silicon wafers with traditional time-consuming

lithography methods, we constructed molds by etching copper boards [46]. Copper mold fabrication is faster, easier, and the minimum feature size is ~100μm.

b. Braille Pumping system

Microfluidics is a relatively new field where complex fluid control is exerted through microscale pumps, valves, sensors, and actuators. A major limitation of current state-of-the-art microfluidic cell culture and chemotaxis system, however, is the lack of an integrated cell-compatible microfluidic system that incorporates multiple, miniaturized pumps and valves. In this research, we used a new computer-controlled, integrated microfluidic control system with up to hundreds of on-chip pumps and valves, powered by individually actuated Braille pins on a portable, refreshable Braille display[47]. The system takes advantage of the resilient yet elastic nature of PDMS microchannels fabricated with soft lithography, together with the movement of Braille pins to "squeeze" fluid through channels. Each stroke of a Braille pin can be used to generate a forward or backward flow of liquid through the microchannel when synchronized to various valving patterns. The volume of flow generated per stroke can be controlled by adjusting the volume of liquid displaced by the pin. This method of fluidic control is portable, versatile, and cost-effective. Braille displays are commercially available, and can be battery-powered, have embedded computer control in devices the size of a laptop computer or a person's hand [15].

c. Temperature control system

Temperature control is essential for long term cell culture outside of an incubator. Under our PDMS chip, we placed a transparent indium tin oxide (ITO) heater connected to a PID temperature controller (E5GN; Omron; Schaumburg, IL). The heaters are fabricated by depositing a thin layer of Indium-Tin-Oxide (ITO) onto a glass substrate using electron-beam evaporation. ITO is a transparent, conducting material and therefore can form a resistive heater distributed over the surface of the substrate while still allowing light to pass through[48].

d. Modified culture media with higher stability in atmospheric gas conditions

RPMI Medium 1640 with GLUTAMAX™-I (61870; Gibco) was buffered with $NaHCO_3$ and 3-(N-morpholino) propanesulfonic acid (MOPS). The concentrations of the added $NaHCO_3$ and MOPS were 10mM each. In addition, bovine serum albumin was added to 0.1% by volume. The pH was adjusted using HCl to 7.2 before using outside the incubator on the microscope stage as recommended by Futai et. al, 2006 [45].

e. PC3 cell culture in the incubator

PC3 prostate cancer was obtained from ATCC (Manassas, VA) and passaged under appropriate growth conditions. PC-3 cells were maintained in RPMI 1640 + 10% fetal cell serum (Invitrogen Corp., Carisbad, CA). Cell were passaged by trypsinization using 1×trypsin + EDTA (Invitrogen Corp.) and resuspended in appropriate growth media.

f. Microenvironment for PC3 cell culture on chip outside of an incubator

A cell line is usually grown and maintained in the favorable conditions (typically, 37°C, 5% CO_2) of a cell incubator. In order to conduct cell experiments outside the incubator, adjustments are needed. It must be noted that osmolarity, pH value, and temperature play pivotal roles in basic cellular functions and reactions. First, evaporation problem can be lethal to cells by changing osmolarity and pH value. Mineral oil is overlayed to minimize evaporation from the top. Also, the bottom membrane consists of three layers: PDMS-parylene-PDMS layers. The purpose of adding the parylene layer is to decrease evaporation from the bottom through the thin membrane. Second, temperature is essential for maintaining normal cellular processes. Therefore, an ITO heater and temperature control system is provided in this experiment. Third, to maintain similar pH condition as cell incubator, modified cell culture media was applied. The modified media contain RPMI Medium 1640 with GLUTAMAX™-I, sodium bicarbonate, and MOPS. Sufficiently high sodium bicarbonate can satisfy immediate cellular needs for carbonate. One may notice that sodium bicarbonate is an important nutrient for many cell types but may cause shift of pH, which is harmful to cells. However, MOPS, an organic chemical buffer that is widely used in cell culture, can help increase pH stability.

g. siRNA knockdown of CXCR4

The pSUPER vector that express short hairpin small interfering RNAs (siRNA) under the control the polymeraseQ OH1-RNA promoter was used after inserting pairs of annealed DNA oligonucleotides between the Bgl II and HindIII restriction sites according to the manufacturer protocol (Oligoengine, Seattle, WA) [68]. After transfecting and culturing,

PC3-CXCR4-si cells showed significant reduction of CXCR4 protein expression by using Western Blot Analysis. [69]

h. Cell experiment protocol

Before the cell migration experiments, PDMS microfluidic chips were sterilized by ultraviolet light. Then microfluidic channel and cell inlet reservoir were coated with 100 ng/ml collagen type I, the major component of the bone matrix, inside the incubator for at least an hour. Finally, the microfluidic chip was washed by Dulbecco's Phosphate-Buffered Saline (DPBS) and then the modified culture media.

For cell migration assays, cells were first starved for 12 hours in the incubator with serum free media (RPMI 1640 + antibiotic/antimicotic + 0.1% BSA) and then rinsed with a few mL of sterile DPBS. Next, cells were removed from the culture flask using cell dissociation buffer, centrifuged down, resuspended in modified cell culture media, and then counted by a hemocytometer. Finally, cells were loaded and seeded in microfluidic chips for six hours before pumping chemoattractant.

CXCL12 concentration used in this research was 250 nM. CXCL12 concentrations range from 125 to 625 nM in biological fluids including bone marrow[66]. CXCL12 actions under in vivo microenvironment are potentiated by their very high local release levels and strong affinity for both cell surface heparin sulfate proteoglycans and extracellular marix that further enable CXCL12 local concentration increase to μM[67].

i. Data Analysis

Time-lapse cell images were tracked by using Metamorph and analyzed by ImageJ. Several cell migration parameters were calculated by image analysis: (1) migration distance (sum of straight-line segments that a cell migrate between consecutive images) (2) cell migration speed (migration distance over time) (3) net displacement toward pulses (straight length of cell displacement between starting and final positions, x displacement in our images), (4) cell velocity toward pulses (net displacement toward pulses over time) (5) migration angle (angle of the net displacement vector, measured clockwise from the positive y direction), and (6) directionality index (DI), net displacement towards pulses divided by migration distance. DI is a measure of how much of the total movement of a cell is directed towards a certain direction, ranging from -1 (cell moves completely opposite of pulse direction) through 0 (cell moves perpendicular to pulse direction) to 1 (cell moves completely in pulse direction).

j. Statistical Analysis

Each experimental condition was performed in duplicate and approximately 60 or more cells were analyzed for each condition. For migration speed, velocity, and DI data, analysis of variance (one-way ANOVA) was applied to examine statistical significance, followed by a posthoc Tukey method for multiple comparisons. Results were considered to be significant at $P<0.05$. Statistical analysis of migration angles was performed by Oriana for Windows (Kovach Computing Services, Wales, UK) to display the directionality of the chemotactic response. Migration angles were summarized in a rose diagram, showing the distribution of angles between cell migration and flow direction. Also, the radius in the rose diagram indicates cell number.

Results

Table 1 shows the pulsatile patterns that I used. The pulsatile chemical exposure profile in the cell migration experiment region of the microfluidic channel was characterized experimentally using fluorescein conjugated dextran (FITC-dextran) (500kDa) as an approximate fluorescent surrogate of CXCL12 (Figure 10). I varied the duration of chemokine stimulation per set interval of 10 minutes, as well as the average fluid flow rate. The timings to be tested were chosen based on generally known G protein-coupled receptor dynamics. With many G protein-coupled receptors, receptor desensitization and internalization occur within seconds to minutes [25]. Also, Dinauer in 1980 showed that Amebas washed free of 10 nM cAMP require about 10 min to recover full sensitivity to a pulse of the same concentration.[73] Although the cell type and chemoattractant used are totally different, it provides a starting point for choosing a time interval to study GPCR mediated chemotaxis events. Moreover, preliminary experiments with 20 min intervals of stimulation showed less directed migration.

Pulsatile CXCL12 stimuli induced PC3 directed migration (chemotaxis)

Table 3 lists the experimental conditions and number of cells tracked and analyzed for each condition. Fig. 11(a) shows that PC3 cells migrate with high directionality under pulsatile CXCL12 stimuli. The average directional index (DI) under conditions with pulsatile CXCL12 stimuli is significantly higher than that under other conditions. Average DI was 0.08 under static conditions, 0.18 under pulsatile flow without any CXCL12 exposure and 0.20 with continuous exposure. The DI jumped to 0.44 under pulsatile exposure of 2 min pumping of CXCL12 for every 10 min interval. CXCL12 did

not induce chemokinesis of PC3 cells (Fig. 11(b)) but simply increased directionality. I note that the directed migration of cells in these assays has two components: a chemotactic component and a component due to cells migrating towards a less dense region. Thus the purely chemotactic component of the observed DI of 0.44 is expected to be lower. Nonetheless, the significant difference in DI between continuous CXCL12 exposure and no exposure is noteworthy. Interestingly, although not statistically significant, a trend is observed that shorter exposure (2 minutes rather than 5 minutes) to CXCL12 is not only sufficient but may even be preferred to induce directed migration of PC3 cells.

The difference in directional preference can also be clearly seen by the distribution of migration angles (Fig. 12). Most PC3 cells under pulsatile CXCL12 stimuli showed significant preference to migrate toward the stimuli, whereas more PC3 cells under flow only or in static control migrated more randomly and with much lower directional preference.

PC3-CXCR4-si cells did not show directed migration towards CXCL12

The average DI of PC3-CXCR4-si cells exposed to CXCL12 stimulation was similar to that of wild type PC3 cells under static conditions (no flow and no CXCL12 stimuli) (Fig. 11(a)). This result supports the mechanism that the directed migration of PC3 cells in response to CXCL12 pulses is mediated by CXCR4 signaling. Fig. 11(b) further shows that PC3-CXCR4-si cells have significantly lower speed than wild type PC3 cells.

CXCL12 gradients estimated experimentally using FITC-dextran as a fluorescent surrogate

To estimate CXCL12 concentration gradients and pulses generated in this research, I used FITC-dextran (500kDa) as a molecular surrogate for CXCL12 (8kDa) and performed fluorescence video microscopy. Based on Stokes-Einstein equation, the diffusivity of CXCL12 will be about 3 times higher than that of FITC-dextran. However, the gradient should be similar because convection by flow dominated in this experiment (Peclet number = 510 for CXCL12). First of all, dues to dead volumes within microchannels, we noticed that the concentration at the cell migration chamber does not immediately reach the full concentration of the solution added to the chemoattractant reservoir (Fig 10a). After 2-3 cycles of 2 minute pumping the chemoattractant concentration reaches approximately 60%. Reaching the 95% concentration level, however, required an additional 50 to 60 cycles. Within each cycles, there is also a pattern of rapid increase in concentration, a leveling off, and rapid decrease in concentration of CXCL12 as shown in Fig. 10(b). At the cellular level, this temporal stimulation pattern would result in exposure of cells for a brief period to a very steep chemoattractant gradient, followed by exposure to a uniform high concentration of chemoattractant, followed by a brief exposure of the cell to a steep gradient again but in the opposite direction. From the FITC-dextran experiments, we plot the slope, G, of the concentration gradient (nM/40μm) at one reference point within the cell migration chamber over time to depict this change in chemical gradients as felt by the cell (Figure 10c). Since the length of the cell is on average is 40μm, G is effectively ? C.

Fractional difference in chemoattractant concentration

Recent experiments on yeast cells[74], neurons[75], and D. discoideum[76] and neutrophils[77] suggest that these cells sense fractional differences in concentration (? C /C) rather than absolute differences in concentration. Thus, I also plot ? C /C as a function of time in our microfluidic devices (Figure 10(d)).

Estimate of the difference in receptors occupied by chemoattractant

In addition to differences in concentration gradients between the front and back of a cell, once can also estimate the difference in number of bound receptors between the front and back. From Hachet-Hass 08 [78], the dissociation constant K_d of CXCL12 for the CXCR4 receptor is 55 ±15 nM. The concentration of CXCL12 pipetted into the chemoattractant reservoir is 250nM. Based on basic thermodynamic equilibrium assumptions, the fraction of receptor occupied, B, equals to $C / (C + K_d)$, where C is the concentration of chemoattractant and K_d is the dissociation constant. In directed migration of mammalian cells, it is generally assumed that cells sense spatial gradients based on differences in receptor occupancy between the front and the back (? B).

$$\Delta B = B_f - B_r = \frac{C + \Delta C}{C + \Delta C + K_d} - \frac{C}{C + K_d} = \frac{K_d \Delta C}{(C + \Delta C + K_d)(C + K_d)}$$

Since K_d is 55 nM, and based on measured C and ? C, ? B can then be plotted as a function of time (Fig. 10(e)).

Estimate of the fractional difference in receptors occupied by chemoattractant

Furthermore, for a given ? B, it is also commonly observed that CI decreases with increasing B[79]. Although the exact nature of how B affects CI for a given ? B is not clear, a simple model would be to assume CI depends on fractional difference in receptors occupied, ? B/B, rather than simply ? B. How ? B/B changes over time for our system is plotted in Fig. 10(f).

Discussion

PC3 cells respond with directed migration more efficiently when exposed to sharp gradients of CXCL12 periodically rather than when exposed to a steady constant gradient. How can this be understood mechanistically? I propose a mechanism that considers fractional difference in receptor occupancy between the front and back of a cell (? B/B) together with a time dependent receptor desensitization and time dependent receptor resensitization.

That directed cell migration depends on fractional difference in receptor occupancy between the front and back a cell (? B/B) makes intuitive sense and is at least qualitatively supported from reported experimental studies of chemotaxis [28, 79]. Time dependent receptor desensitization is also a well known phenomena for GPCRs. With many G protein-coupled receptors, receptor internalization and desensitization occur within seconds to minutes [25]. Finally, it is also well known that the desensitized GPCR signaling pathways will recover over time. For example, Dinauer in 1980 showed that Amebas washed free of 10 nM cAMP require about 10 min to recover full sensitivity to a pulse of the same concentration.[73] Although the cell type and chemoattractant used are

totally different, it provides a starting point for choosing a time interval to study GPCR mediated chemotaxis events.

Based on these observations, I propose a simple qualitative model to compare and explain the dramatic difference in the effect of steady versus pulsatile exposure of cancer cells with CXCL12. In this model, the chemoataxis index (CI) is considered to be a function of effective ? B/B (? B/B_{eff}) integrated over time ($\int$? $B/B_{eff}dt$). In turn, ? B/B_{eff} is modeled as ? B/B multiplied by sensitivity of the signaling pathway. Based on known phenomena of receptor desensitization and resensitization, and based on the simple stimulation patterns used in our pulsatile studies, I model desensitization as a simple step decrease of sensitivity from 1 to 0 after 1 minute followed by a steady constant sensitivity at 0 during the rest of the stimulation. Receptor resensitization which is typically slower is modeled as a linear function, where the slope is such that sensitivity will recover from 0 to 1 over an 8 min time course.

Based on Fig. 10(f), the condition of 2 min pumping of CXCL12 and 8 min pumping of media has positive ? B/B that starts with a maximum value of ~0.7 then decreases during the first 40 seconds of stimulation, after which it becomes zero for 2 min, then takes a negative value for another 40 seconds. Because of rapid desensitization and slow resensitization, the 40 second exposure to a negative ? B/B that occurs after 2 min 40 seconds would not contribute significantly to the directionality of cell migration (? B/B_{eff} is 0 due to densitization). The 40 second (2/3 minute) exposure to the positive ? B/B at the beginning, however, gives a calculated value for $\int$? $B/B_{eff}dt$ of 14 (sec) repeated every 10 minutes cycle. Over the course of a 6 hour cell migration experiment that total $\int$? $B/B_{eff}dt$ would reach 14*6*6=504. In contrast, exposure of cells to a constant gradient

of the type generated in the common premixer gradient generators would result in a constant ? B/B but with a value of 0.4 or lower leading to a $\int ? B/B_{eff} dt$ value of 16 or less for the first minute but only once not repeated every 10 minutes. Over a 6 hr cell migration experiment, the total $\int ? B/B_{eff} dt$ for a static gradient study would thus still only be 16 (rather than 504 for the pulsed gradient generator). If we assume a positive correlation between $? B/B_{eff}$ and CI, we see that the pulsatile exposure would give rise to a much higher CI than constant exposure to a static chemical gradient.

Prostate carcinoma (PCa), the most frequently diagnosed cancer in men and the second leading cause of cancer death in American males. Skeletal metastases occur in approximately 90% of patients with advanced prostate carcinoma. Metastasis is the highly organized and nonrandom movement of cancer cells from one organ or tissue to another. Over the past few years a considerable number of studies have shown that chemotaxis plays a pivotal role in metastasis. Several chemokines, growth factors, and extracellular matrix components are reported to be crucial factors in prostate cancer cell chemotaxis[80, 81]. Prostate cancer cells were observed migrating across bone marrow endothelial cell monolayer in response to CXCL12 [23]. Positive correlations were established between CXCL12 levels and tumor metastasis. A confusing result in the field of CXCL12 chemotaxis has been that CXCR4 expressing tumor cells do not always show efficient directed migration towards high concentrations of CXCL12 in vitro studies. Particularly, study of breast cancer cell chemotaxis in microfluidic devices with steady gradients generated by continuous flow of different premixed concentrations has shown that a CXCL12 gradient is not sufficient to trigger directed migration [18]. The authors demonstrated that an additional sensitization factor, in this case EGF or other autocrine

factors produced by the breast cancer cells, was necessary to induce directed migration. In this chapter, similar chemotaxis experiments using a similar premixer gradient device were performed with PC3 prostate cancer cells. Again, no directed migration could be observed in gradients of CXCL12 alone. Considering the physiological relevance of pulsatile chemical exposure of cells, I designed a new microfluidic device to expose PC3 cells to pulses of CXCL12 rather than a static gradient. Experiments demonstrated that temporal CXCL12 stimuli induced significant directed migration of PC3 cells. Here, the use of temporal patterns in and of itself seems to serve as a sensitization trigger to allow PC3 cells to respond to CXCL12 signals and undergo directed migration. The results add to evidence of the importance of pulsatile chemical stimulation physiologically and in nature. For example, many hormones are released in a pulsatile manner and directed migration of Dictyostelium occur under pulsatile cyclic AMP (cAMP) exposure [82]. The microfluidic device described also contributes to the range of available tools to study cellular responses to pulsatile chemical exposure even if the conditions are not physiological. For example, the effect of pulsatile tumor necrosis factor-a (TNFa) stimulation on NF-?B nuclear translocations [83] have been used to reveal chemical signaling pathways. From their result, lower frequency of TNFa stimulation gave full-amplitude translocations, whereas higher frequency pulses gave reduced translocation, which indicates that pulsatile stimulation (lower frequency) may induce better cell response than continuous stimulation.

Conclusion

Directed migration of tumor cells towards sources of CXCL12 often require a sensitization factor such as EGF or other autocrine factors. Here, we show that temporally patterned pulsatile exposure is sufficient to sensitize PC3 cells to migrate towards a CXCL12 source in the absence of any other chemical stimuli. The results provide fresh perspectives on the importance of temporal stimulation patterns in biochemical cell sensing and directed migration. Although this chapter only focused on prostate cancer cells and CXCL12 exposure, the microfluidic device developed is broadly applicable to the study of a wide range of cell types and their response to temporally patterned stimulation to cytokines and chemoattractants.

Table 3 Experimental conditions and number of cells analyzed for each condition

Condition #	Description	# cells analyzed
1	PC3 cells were exposed to SDF-1 stimuli 2min for every 10 min interval	81
2	PC3 cells were exposed to SDF-1 stimuli 5min for every 10 min interval	84
3	PC3 cells were exposed to SDF-1 stimuli continuously	82
4	Same as condition1 but using PC3-CXCR4-si cells	69
5	PC3 cells were exposed to only flow but no SDF-1	75
6	PC3 cells under no flow and no SDF-1 condition	74

Figure 9 The image and schematic design of the microfluidic system.
(a)The PDMS microfluidic devices, (b) A schematic figure of the microfluidic system includes (1) Braille display modules, (2) a machined aluminum monolithic fingerplate, (3) four hold-down clamps, (4) the PDMS microfluidic device, (5) top reservoirs, and (6) a transparent heater unit. Pulsatile flow can be easily generated and controlled in a microchannel using Braille system and pumping frequency can be controlled precisely by computer program as fast as 10Hz.

9(a) The PDMS microfluidic devices

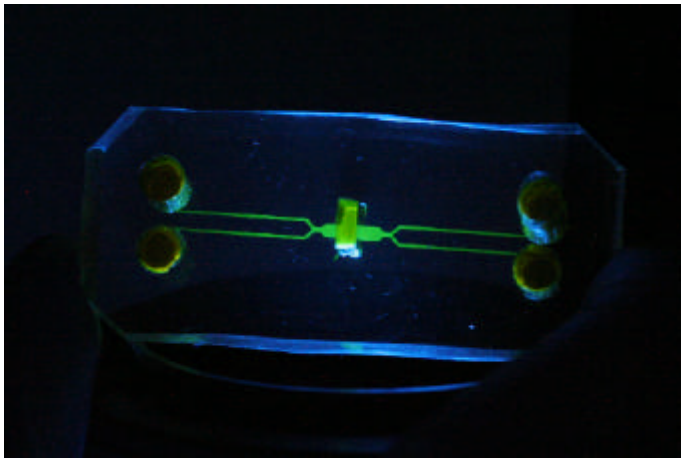

9(b) A schematic figure of the microfluidic system

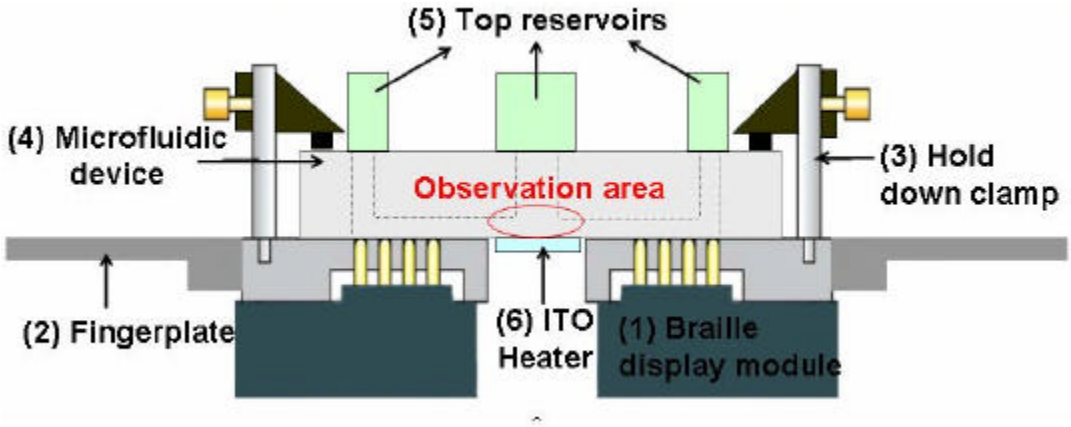

Figure 10 Gradient and model analysis by FITC-dextran.
Assessing the shapes of the sequential pulses generated close to the edge of cell migration area using FITC-dextran with pumping condition: pump 2 min of FITC-dextran and then 8 min of media for every 10 min interval at average flow rate 0.1 µl/min: (a) peak concentration of a single pulse over time; (b) the concentration of a spot within the cell migration chamber over time; (c) G, the concentration gradient (nM/40µm) at one reference point within the cell migration chamber over time; (d) ? C /C over time; (e) ? B over time; (f) ? B/B over time.
10(a) peak concentration of a single pulse over time: peak concentration increases slowly with time

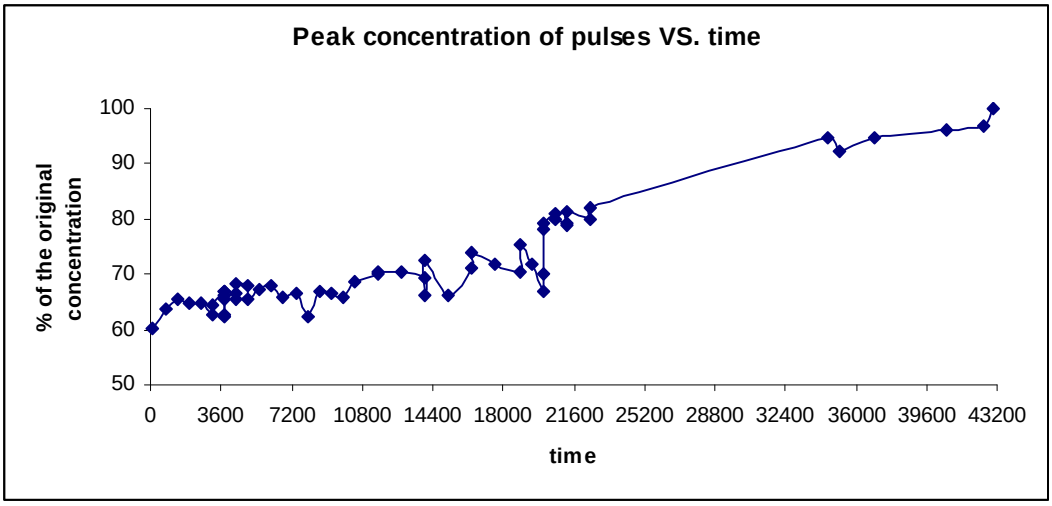

10(b) the concentration of a spot in the microchannel over time: to show the shape of a pulse

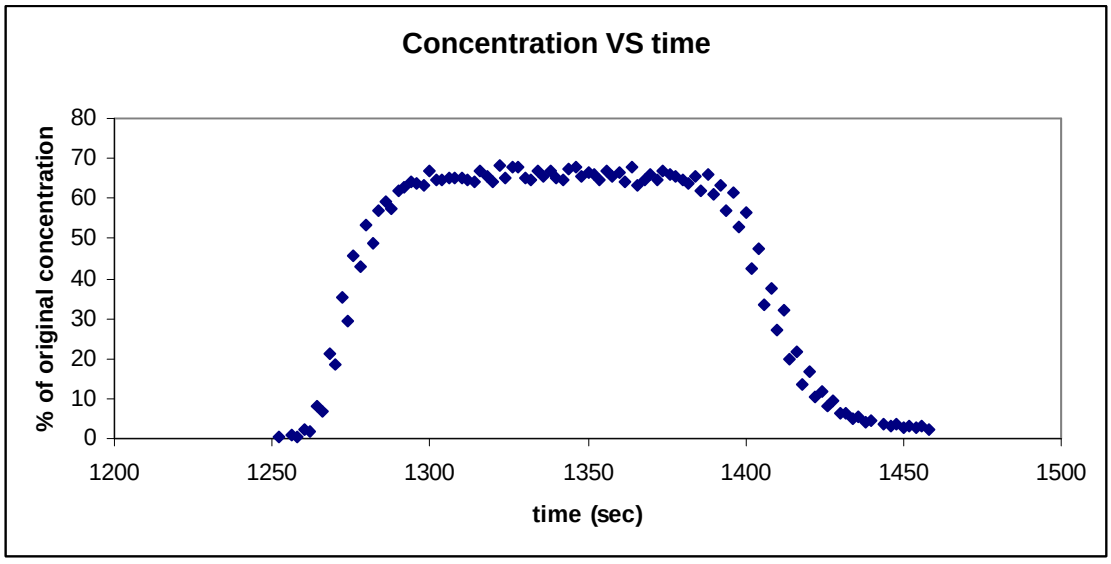

10(c) G, the concentration gradient (nM/40μm) at one reference point within the cell migration chamber over time: G increased when the pulse came in, then decreasing when the concentration reaches maximum (see 10(b)). And later G became negative as the pulse passed and finally went back to 0 when CXCL12 was washed away and the main concentration became close to 0.

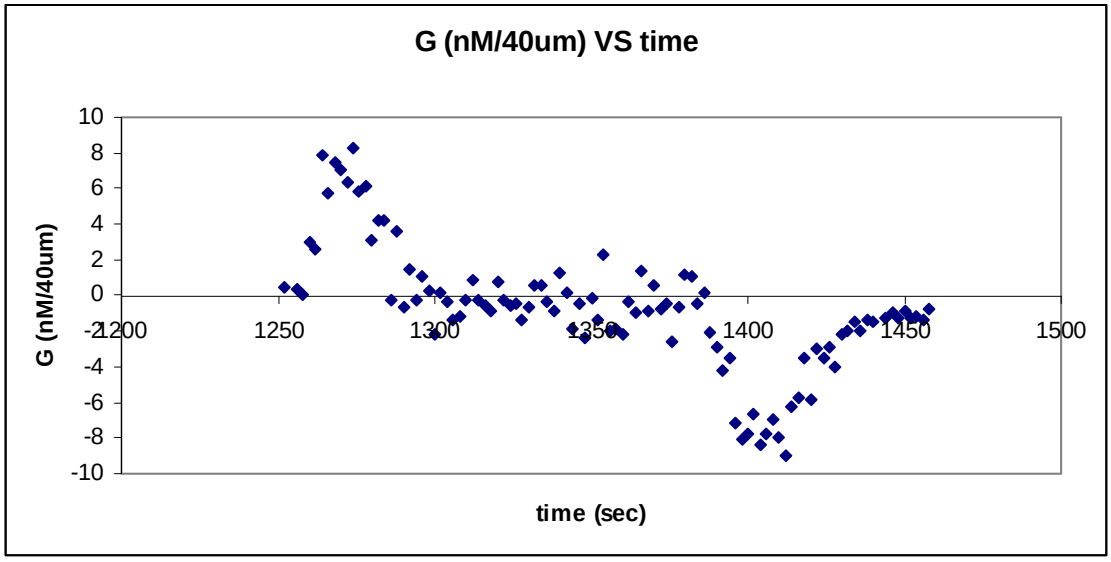

10(d) ? C /C over time

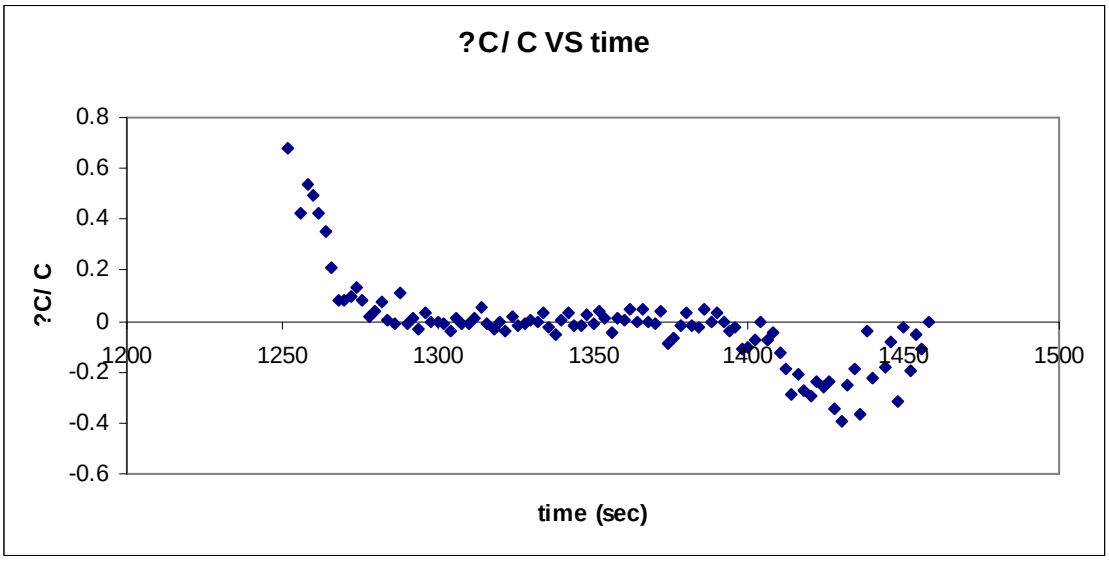

10(e) ? B over time

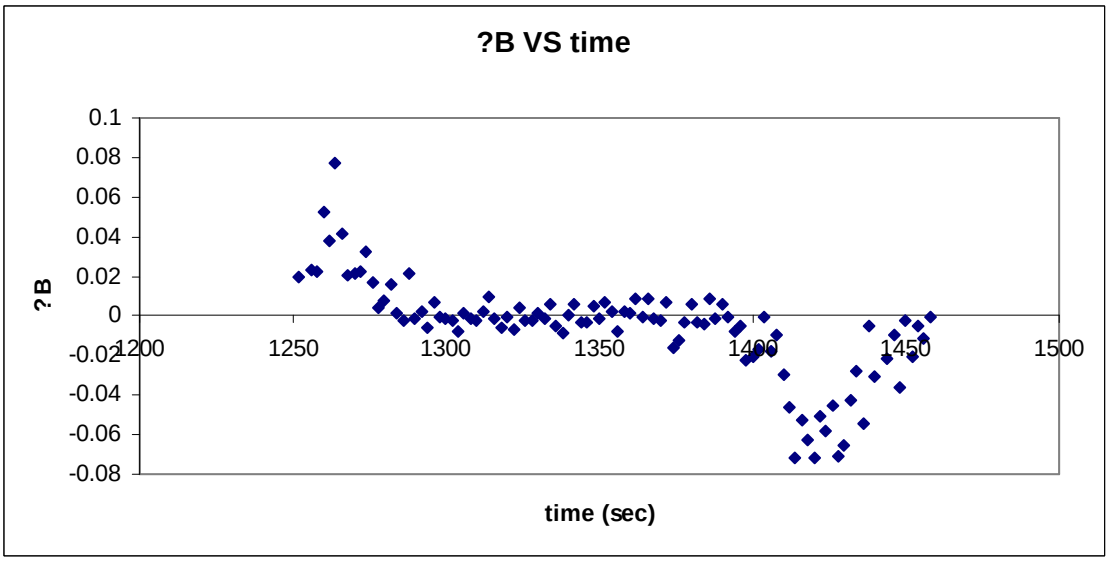

10(f) ? B/B over time

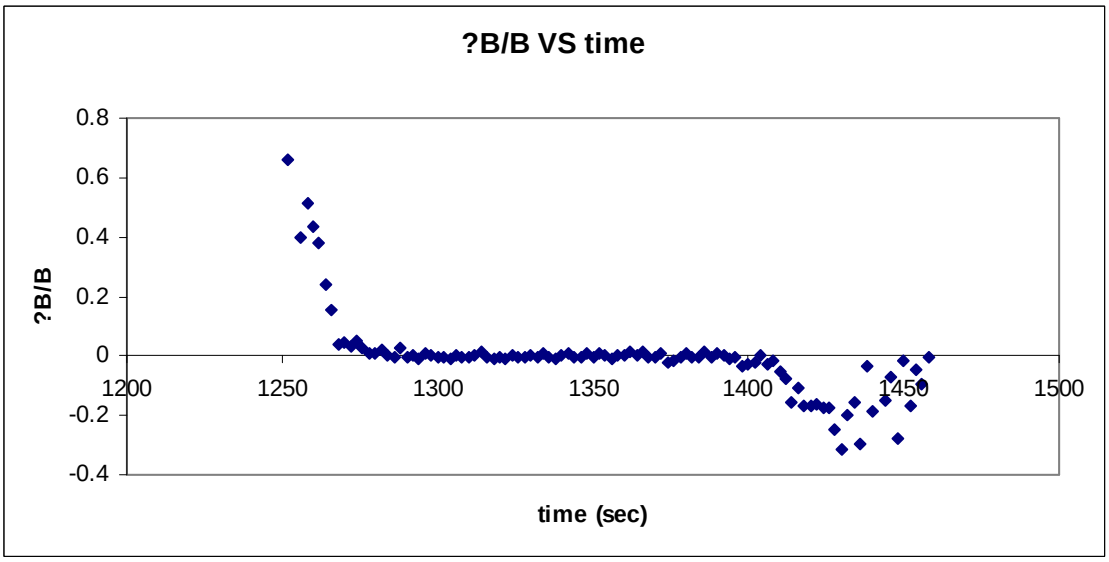

Figure 11 PC3 cells reactions under different pulsatile conditions from 6 to 12 hour. (a) average Directionality Index (DI); (b) average migration speed (μm/min); (c) average migration velocity toward CXCL12 stimuli (μm/min).

11(a) Average DI from 6 to 12 hr

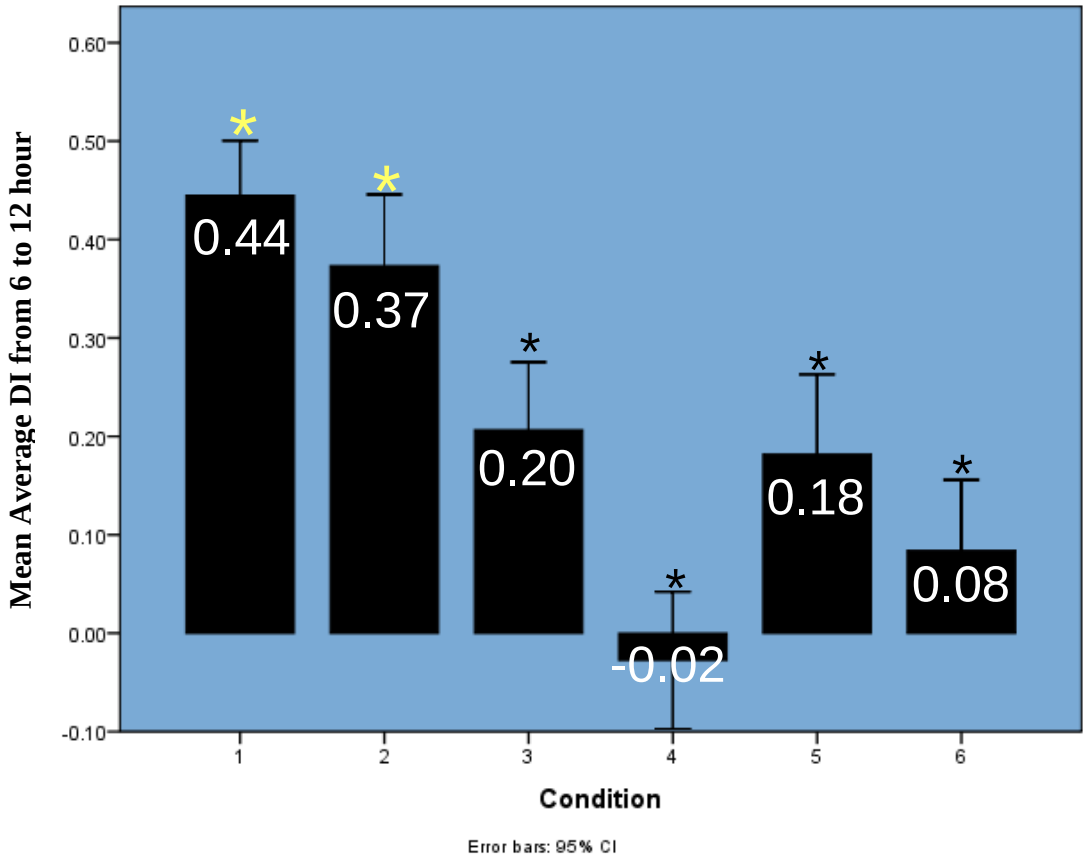

11(b) Average migration speed from 6 to 12 hr

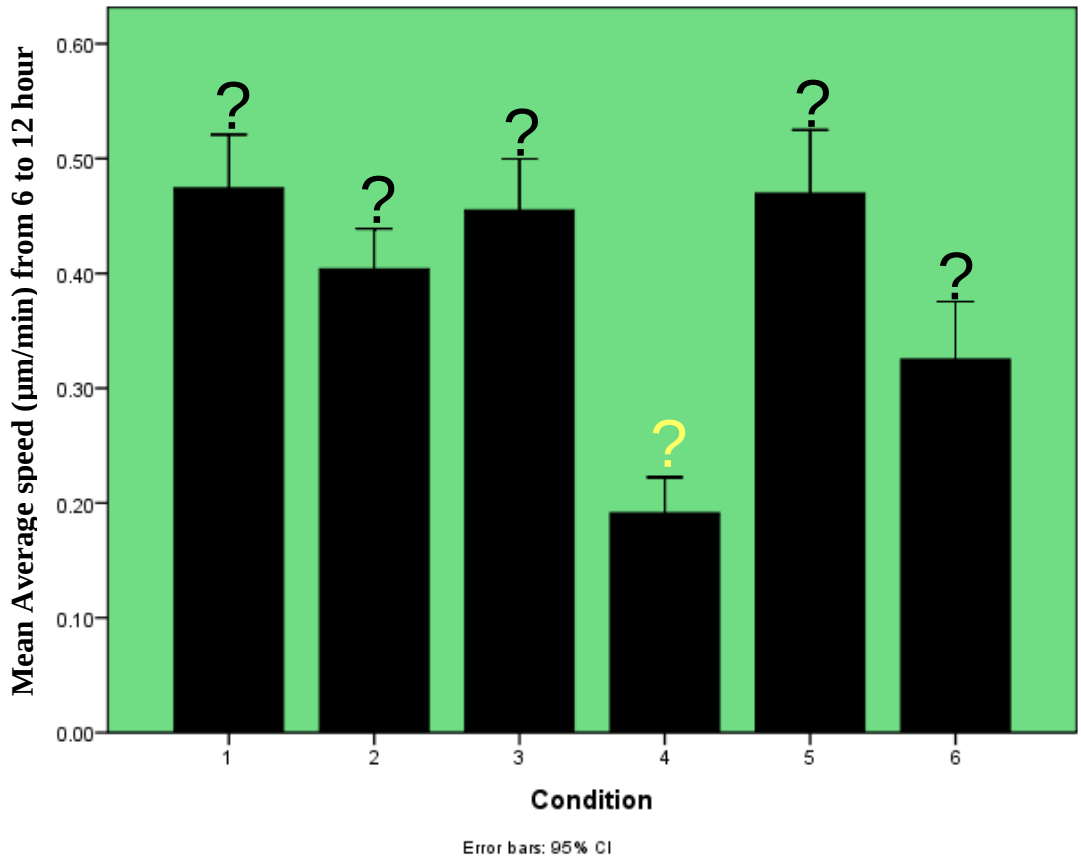

11(c) Average migration velocity toward CXCL12 stimuli from 6 to 12 hr

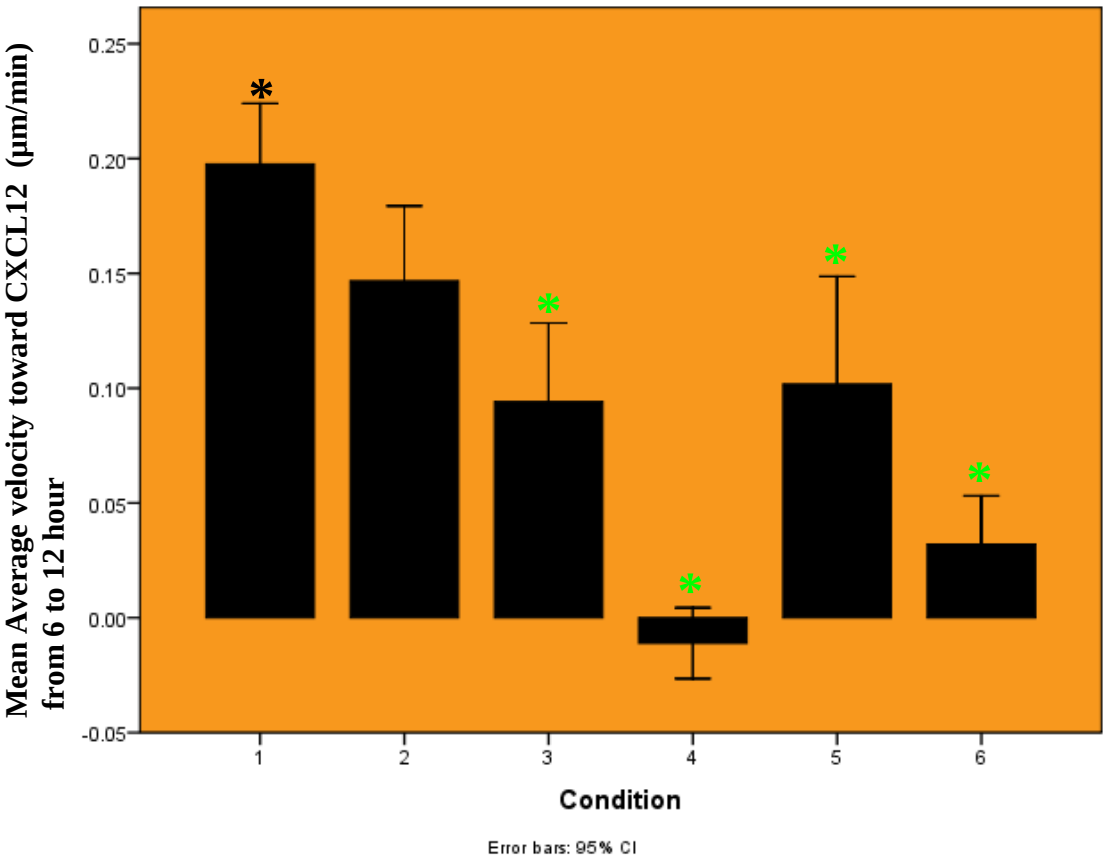

Figure 12 Migration angles of PC3 cells under different pulsatile patterns.
Direction plots show the distribution of migration angles, grouped in 20 degree intervals (wedges). The radius of each wedge indicates the number of cells that migrated in a particular direction. From 6-12 hour, migration angle of PC3 cells under (a) no pumping condition; (b) pump media at average flow rate 0.10 µl/min; (c) pump 2 min of SDF-1 and 8 min of media for every 10 min at average flow rate 0.10 µl/min; 5(d) pump 5 min of SDF-1 and 5 min of media for every 10 min at average flow rate 0.10 µl/min

12(a) static condition (no pumping)

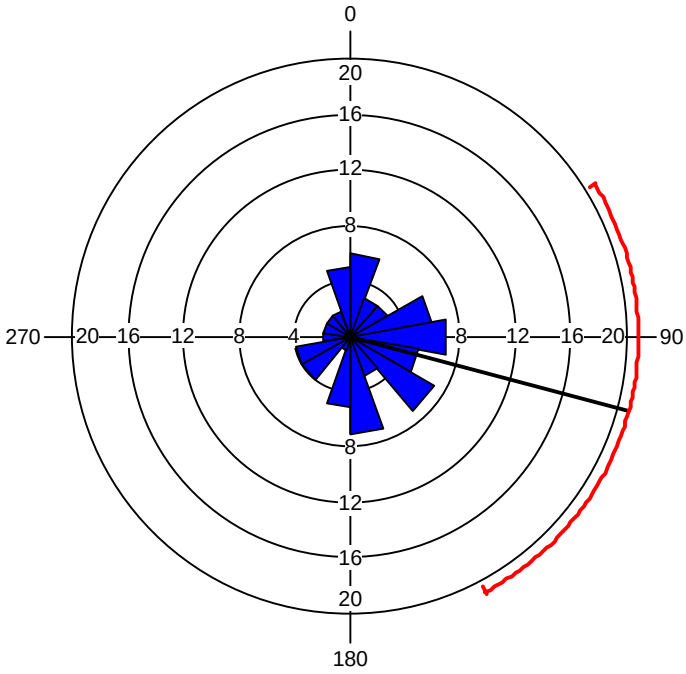

12(b) pump media at average flow rate 0.10 µl/min

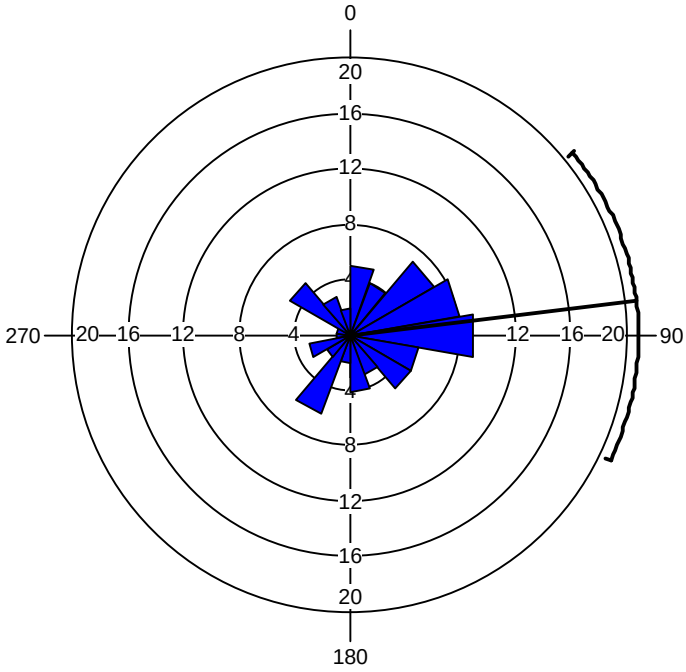

12(c) pump 2 min of CXCL12 and 8 min of media for every 10 min interval at average flow rate 0.10 µl/min

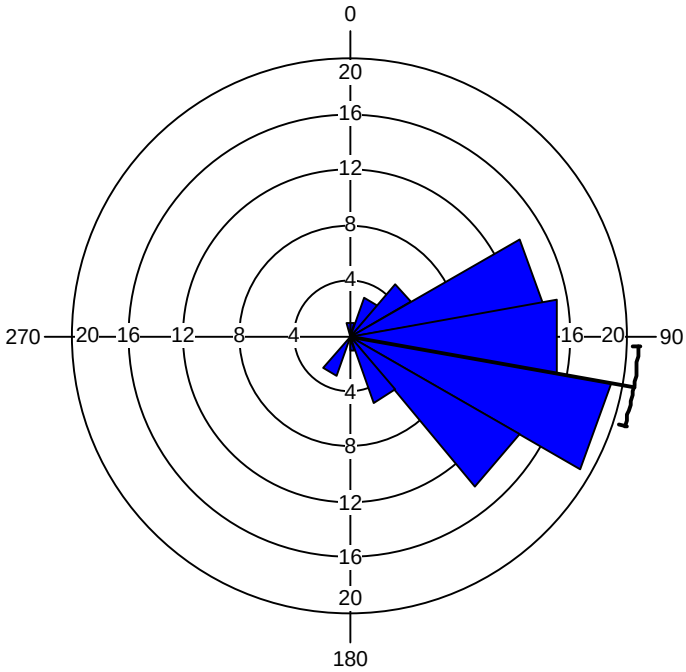

12(d) pump 5 min of CXCL12 and 5 min of media for every 10 min interval at average flow rate 0.10 µl/min

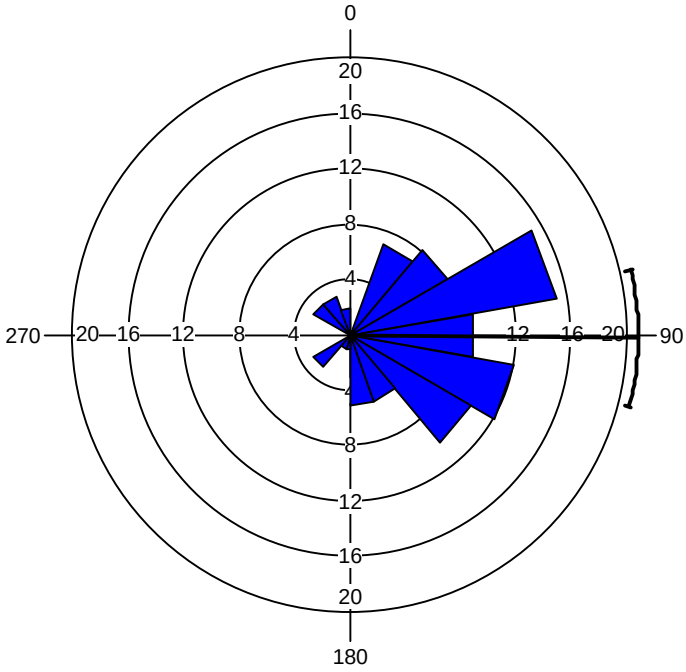

Chapter V

Future Application

Future Applications

Besides effects of and CXCL12 on PC3 cell adhesion and migration, there are other important future applications following this study. For example, many interesting cell adhesion and migration mechanisms affected by shear stress or different chemicals can be further investigated by using this microfluidic system as well as high throughput drug testing and possible sorting of cancer stem cells.

Application 1: Investigate effects of epidermal growth factor (EGF) on PC3 cell adhesion and migration

Besides CXCL12, EGF is another important chemoattractant for study of prostate cancer metastasis. To begin with, EGFR is overexpressed in several solid tumors including those of the breast, prostate, brain, bladder, and lung, with this increased signaling correlating with tumor progression to invasion and metastasis [84]. Next, on stimulation with EGF, nonmuscle myosin heavy chain II-B (NMHC-IIB), a molecular motor and an important component of the cytoskeleton, undergoes a transient phosphorylation correlation with its cellular localization [85]. Therefore, EGF may play an important role in directed cell migration. Furthermore, disruption of EGF-dependent myosin II-B heavy chains phosphorylation in cell affected its cellular localization and chemotaxis [86]. To sum up, it is important and helpful to investigate EGF effects on adhesion and migration of PC3 cells and then to further understand prostate cancer metastasis. And similar to CXCL12, different patterns of EGF stimuli can be applied to see if PC3 cells were activated by EGF and react with better adhesion and directed or even faster migration. Besides EGF, many potential chemoattractants, drugs, or even conditioned media can be tested by using this microfluidic system.

Application 2: Investigate synergistic effects of CXCR4 and EGFR on PC3 cells

For prostate cancer metastasis, PC3 cells do not just sense individual chemical signal at one time but react under the integrated effect of different signals. Among all possible interactive signal effects of chemicals on PC3 cells, the synergistic effects of CXCR4 and EGFR are the most notable to figure out. There are several biology evidences for possible

“cross-talk” between CXCR4 and EGFR. To begin with, Phillips in 2005 [87] demonstrated that activation of the EGFR by EGF increases CXCR4 expression and the migration of non-small cell lung cancer (NSCLC). Overexpression of EGFR within the primary tumor may provide the microenvironmnetal signals necessary to upregulate CXCR4 expression and promote metastasis. Then Mosadegh in 2008 [18] also showed that EGF promotes breast cancer cell chemotaxis in CXCL12 gradients. Steady CXCL12 gradient alone failed to induce MDA-MB-231 breast cancer cell chemotaxis in their premixers. However, with certain concentration of EGF, MDA-MB-231 breast cancer cell showed significant improvement on directed migration under CXCL12 gradients. Moreover, Procile in 2004 [19] showed that CXCL12 dependent proliferation correlates to the phosphorylation and activation of extracellular signal-regulated kinases (ERK)1/2, which in turn are correlated to epidermal growth factor (EGF) receptor transactivation. Finally, AG1478, a specific EGFR inhibitor, strongly diminished the CXCL12- and EGF-induced cell proliferation and ERK1/2 activation [20]. Evidences above suggest a possible important “cross-talk” between CXCR4 and EGFR intracellular pathways that can link signals of cell chemotaxis in cancers with high CXCR4 expression. Though a large number of studies have been made on synergistic effects of CXCR4 and EGFR, what seem to be lacking, however, are their roles in prostate cancer. The purpose of this application is to investigate synergistic effects of EGF on SDF-1 on PC3 cell adhesion and migration which is essential for further understanding prostate cancer metastasis.

Studies of synergistic effects of CXCR4 and EGFR can be also done using by the microfluidic system. Since the result of directed migration of PC3 cells under pulsatile CXCL12 stimuli was analyzed in this research, the next step is to activate PC3 cells with

EGF and see if PC3 cells increase migration directionality or speed under pulsatile CXCL12 stimuli after activation of EGF. And PC3 cells with CXCR4 knockdown can be used as comparison. Moreover, different concentration of EGF can be applied to verify if there is a dose-dependent manner. Finally, combined with the results of effects on pulsatile EGF stimuli on PC3 cell migration, different concentration of CXCL12 can be used to fin out its effects on PC3 cells migration phenomenon under EGF stimuli.

Application 3: Isolation of cancer stem cells

In recent years, there have been numerous hypotheses and researches on existence cancer stem cells. For clinical treatment of prostate cancer, although existing therapies for prostate carcinoma eradicate the bulk of cells within a tumor, most patients go on to develop androgen-independent disease that remains incurable by current treatment strategies. And there is now increasing evidence in some malignancies that the tumor cells are organized as a hierarchy originating from rare stem cells that are responsible for maintaining the tumor. Prostate cancer stem cells are reported to possess a significant capacity for self-renewal, proliferation, and also able to regenerate the phenotypically mixed populations of nonclonogenic cells, which express differentiated cell products, such as androgen receptor and prostatic acid phosphatase. Current research showed that the prostate cancer stem cells have a $CD44^{+}$/a2ß1^{hi}/$CD133^{+}$ phenotype and approximately 0.1% of cells in any tumor express this phenotype [88]. Understanding the properties of cancer stem cells can be beneficial for future cancer treatments.

Over the past decades, a considerable number of studies have been made on CXCL12 and stem cells. CXCL12 has been demonstrated to play a pivotal role in the regulation of

trafficking of normal hematoietic stem cells (HSC) and their homing and retention in bone marrow. Also, functional CXCR4 is also expressed on nonhematopoietic tissue-committed stem/progenitor cells (TCSCs) [89, 90]. From several biology evidences, we postulate cancer stem cells have higher CXCR4 expression than normal cancer cells. Also, primary results already showed that few cells did migrate much faster with higher directionality than other cells under CXCL12 stimuli. Therefore, the hypothesis of this application is that cancer stem cells which have more CXCR4 will migrate better than normal cancer cells under CXCL12 stimuli. And it will be interesting to compare migration phenomenon of PC3 stem cells versus PC3 cells under CXCL12 stimuli or even isolate cancer stem cells by migration in the microfluidc system.

The protocol of this application is similar to application 1 and 2. However, prostate cancer stem cells can be first transfected with different fluorescent color such as GFP and then seeded with normal PC3 cells with ds-Red transfection. Then the best patterns of CXCL12 stimuli can be applied and see if prostate cancer stem cells migrate better than normal prostate cancer cells.

Appendices

17

Microscale Integrated Sperm Sorter

Yaokuang Chung, Xiaoyue Zhu, Wei Gu, Gary D. Smith, and Shuichi Takayama

Summary

This chapter describes the design and fabrication of a passively driven microfluidic sperm sorter using soft lithographic microfabrication techniques. This self-contained device can separate motile sperm from nonmotile sperm and other cellular debris. The sorting system is small (coin sized) and structurally simple. It comprises two inlets; two outlets; a sorting channel; and arrays of horizontally oriented reservoirs that function as passively driven, constant-flow-rate pumps. Sperm with higher motility are sorted out from the rest of the semen samples based on their ability to swim through interfaces between adjacent laminar streams into separate streamlines, whereas the nonmotile sperm and debris remain in their initial streamlines. The device, which we call a microscale integrated sperm sorter, does not rely on any external power sources or controllers and incorporates all sample loading and sorting functions necessary to prepare high-quality sperm for in vitro fertilization. This self-contained, inexpensive, and portable device may also be useful for developing convenient sperm motility assays that can be used at the point of care or at home.

Key Words: Sperm sorter; passively driven pump; motility; microfluidics; soft lithography; bioassay.

1. Introduction

This chapter introduces the mechanism, materials, and fabrication of a microscale integrated sperm sorter (MISS), which is small, simple, and disposable and can sort out small amounts of healthy sperm needed in clinical settings. It not only provides an efficient, quick, and nondamaging way to sort motile sperm, but also an interesting example of designing structurally simple, yet fully functional, integrated, and self-contained microfluidic devices.

From: *Methods in Molecular Biology, vol. 321: Microfluidic Techniques: Reviews and Protocols*
Edited by: S. D. Minteer © Humana Press Inc., Totowa, NJ

1.1. Biological Significance

1.1.1. Importance of Sperm Sorting

Approximately 5% of infertility problems are the result of abnormal or lack of sperm *(1)*. Currently, one of the most advanced techniques to treat such sperm-related infertility is an in vitro fertilization (IVF) method called intracytoplasmic sperm injection (ICSI), in which a single sperm is directly injected into an oocyte with a tiny pipet *(2)*. Although this method drastically reduces the number of viable sperm required for fertilization, it bypasses all natural sperm selection processes. It is, therefore, important to have an efficient, artificial, but biomimetic selection process to maximize the probability of fertilizing oocytes with high-quality sperm that will lead to successful pregnancies and healthy offspring *(3)*.

1.1.2. Current Sperm-Sorting Techniques and Limitations

The human ejaculate contains a mixture of seminal plasma, sperm, nonreproductive cells, microorganisms, and nonspecific debris. For ICSI and other IVF procedures, the motile sperm population needs to be separated from the rest of the semen samples because the motile sperm are the most fertilizable and the nonmotile ones are not only inferior in their capability to fertilize, but can also damage the motile sperm. Primary methods commonly used for isolating motile sperm from semen samples are centrifugation, sperm migration into culture medium (swim-up), density gradient separation, or a combination of these techniques. Recovery rates, motility, morphology, and degrees of DNA integrity may vary among these methods *(4)*.

1.1.2.1. Centrifugation

The centrifugation method uses centrifugal force generated by high-speed spinning to obtain a compact pellet of all sperm and debris and, thus, separation from the seminal plasma. Although this method is quite effective, it is reported that sperm can be damaged during centrifugation, either by physical damage of the sperm or owing to significant release of reactive oxygen species (ROS) from sperm and semen leukocytes *(5)*. Furthermore, the extraction rates of motile sperm from initial samples can be very low *(6)*.

1.1.2.2. Swim-up

To avoid damage caused by ROS in the centrifugation method, a direct swim-up separation technique has been developed. In this method, a semen sample is covered with media so that motile sperm can swim toward this top layer *(4)*. This technique can be performed using either washed (quickly centrifuged and resuspended) or unwashed (direct) semen samples. Although this

simple technique results in good recovery with minimal sperm dysfunction, it can be time-consuming and not efficient enough to recover sperm from low-motility semen samples or patient samples that include large amounts of cellular debris.

1.1.2.3. Density Gradient Separation

Density gradient separation separates cells or particles based on their differing intrinsic densities. There is a well-referenced medium for density gradient separation, which is composed of colloidal silica coated with polyvinylpyrrolidone. Because of the heterogeneity of particle sizes, centrifugation of the medium will spontaneously form a density gradient. For sperm separations, liquefied seminal plasma is layered on an isotonic discontinuous gradient and centrifuged. Subsequent separation relies on the percentage of active sperm in the ejaculate and added force of centrifugation to isolate motile sperm from other cells. Even though this technique can selectively isolate motile sperm from debris and neutrophils, the occurrence of lower DNA integrity after density gradient separation *(7)* makes this method less desirable.

1.1.3. Microfluidic Sperm Sorting

The described sperm sorting is based on microfluidics, the flow of fluids through small channels. An interesting feature of microfludics is the ability to flow different streams adjacent to each other with no turbulent mixing between the streams. Such laminar flows occur when viscous force dominates over inertial force or when the Reynolds number (*Re*) is small *(8)*. Because microchannels have small dimensions, the *Re* in microfluidic systems is typically low (<1 for the MISS), and the flows are laminar.

1.2. Design and Fabrication of Device

The main challenge of designing a practical microfluidic sperm sorter is to integrate all components necessary for sorting while keeping the device inexpensive, easy to fabricate, simple to use, and overall compact in size. The sperm sorter described in this chapter satisfies these needs with a K-shaped channel that connects four horizontally oriented reservoirs: two for loading sperm sample and media, and another two for collecting separated motile and nonmotile sperm (*see* **Fig. 1**).

The combined reservoir arrays also serve as a passively driven pumping system that maintains a steady flow rate regardless of fluid volume in the reservoirs *(9,10)*. Although a variety of materials may be potentially used, this chapter describes fabrication of the sperm sorter in polydimethylsiloxane (PDMS) through soft lithography *(11)*.

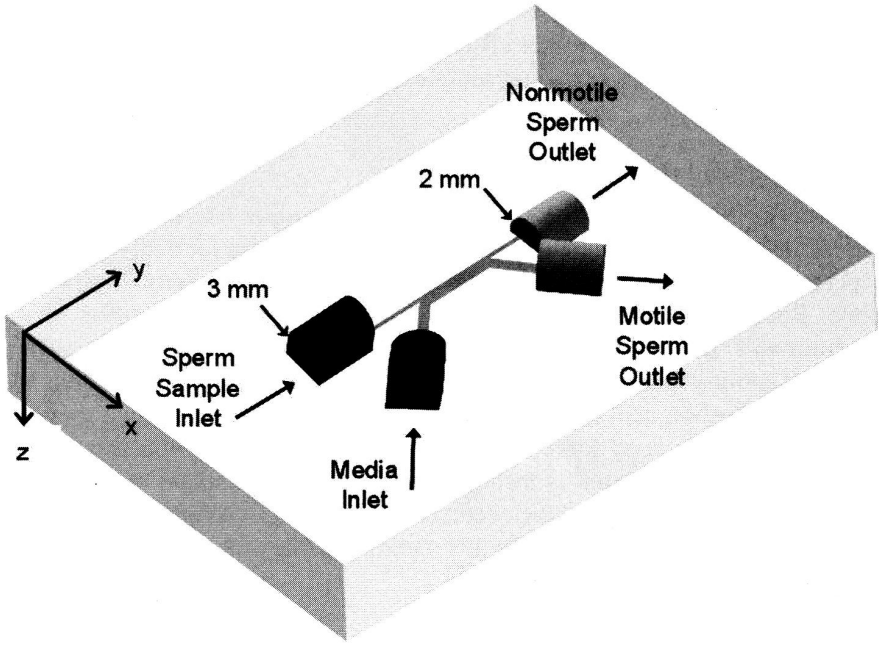

Fig. 1. Structure of MISS. (Reproduced with permission from **ref. *9***.)

1.2.1. Sorting Mechanism

MISS takes advantage of laminar flows in microfluidic channels together with differences in the swim velocity of motile vs nonmotile sperm. As mentioned earlier, flow in small channels is often laminar. The Re_D for flow in a tube is defined as follows:

$$\mathrm{Re}_D = \frac{\rho \times u_m \times D_h}{\mu}$$

in which ρ is the fluid density; μ is the fluid dynamic viscosity; u_m is the mean fluid velocity over the tube cross-section; and D_h is the hydraulic diameter defined as

$$D_h = \frac{4 \times A_c}{P}$$

in which A_c and P are the flow cross-section area and the wetted perimeter, respectively. Turbulent flow occurs when the Re_D is above approx 2000 ***(12)***. For the MISS design described here,

$$\mathrm{Re}_D \approx \frac{10^3\left(kg/m^3\right) \times 1.6 \times 10^{-3}\left(m/s\right) \times 6.67 \times 10^{-5}\left(m\right)}{855 \times 10^{-6}\left(N \cdot s/m^2\right)}$$

Owing to this small *Re*, flow is laminar and allows two streams to flow adjacent to each other without turbulent mixing.

From the Stokes-Einstein equation, diffusivity is defined as

$$D = \frac{k_B \times T}{\bar{f}}$$

in which k_B is the Boltzmann's constant, which is approx 1.38×10^{-23} J/K; T is the absolute temperature; and $\bar{f}$ is the frictional drag coefficient, which is related to the dimension of the particle and the fluid properties such as viscosity. For a spherical particle, the friction drag coefficient is defined as $\bar{f} = 6 \times \pi \times \mu \times R$, in which R is the sphere radius. Nonmotile human sperm, approximated to be a spherical particle with a diameter of 6 μm, have a diffusivity of 1.5×10^{-13} m²/s in water at room temperature. Such a particle or nonmotile sperm would need 690 s to diffuse just 10 μm. By contrast, motile human sperm swim faster than 20 μm/s at room temperature ***(13)***.

In the multiple laminar flow system of the MISS, a media stream intersects with a sample stream and creates an interface. Nonmotile sperm and miscellaneous cellular debris remain in the initial streamline, owing to their low diffusivity, and, finally, exit into a waste outlet. Unlike nonmotile particles, high-motility sperm can actively swim across the interface and be sorted into a separate, motile sperm outlet. This mechanism allows the MISS to sort motile sperm away from nonmotile sperm and debris efficiently and without harm in a gentle biomimetic manner.

1.2.2. Flow Control

A key factor for successful sorting with the MISS is to control flow rates. The absolute flow rate of the fluid is crucial for determining the total time that sperm spend to sort themselves out by motility. A longer residence time may allow an increasing number of sperm with low forward motility to enter the collecting stream; a shorter residence time may allow selection of sperm with higher motility. The relative flow rates between the sample stream and the collecting stream are important for determining the position of the fluid interfaces, as well as the purity and recovery rate of the motile sperm. If the sperm sample stream is too thin, the throughput decreases. If the sperm sample stream is too wide, then even nonmotile sperm and debris may collect in the motile sperm outlet. The MISS is designed to give sperm a residence time of approx 20 s in the main separation channel, and the width of the sample stream is approximately equal to or a little smaller than the sample inlet and nonmotile sperm outlet ***(9,10)***.

The key to achieving the desired flow control in the MISS is to use horizontally oriented fluid reservoirs. In this reservoir design, a constant pressure drop is maintained regardless of the volumes of fluid in the reservoirs, enabling

constant fluid flow rates and a stable laminar flow interface for sorting (**Fig. 1**). In a typical design, the inlet and outlet reservoirs are 3 and 2 mm in height, respectively. The combination of hydrostatic force produced from the 1-mm height difference between inlets and outlets and a net capillary force imbalance resulting from the differences in reservoir size provides the pressure drop across the reservoirs needed to drive the flow through this microchannel system. Because of the relatively small size of the reservoirs, surface tension keeps fluids and sperm suspensions within the horizontally oriented reservoirs and prevents the liquid from spilling out. The horizontal reservoir configuration causes the fluid meniscus to move horizontally rather than vertically, thus keeping the height difference and, hence, the hydraulic pressure between the inlet and outlet reservoirs constant. This contrasts with conventional gravity-driven pumping mechanisms, in which flow rate decreases over time owing to changes in fluid levels associated with the use of vertically oriented reservoirs open to the atmospheric pressure. In a typical MISS design, the sperm inlet and non-motile sperm outlet have a width of 100 μm and a length of 5000 μm. The width and length of the media inlet and motile sperm outlet is 300 and 5000 μm, respectively. The main separation channel's width is 500 μm, and its length is 5000 μm. All channel heights are 50 μm.

1.2.3. Sorting Procedure and Results

In a typical sorting test, semen samples from human subjects are obtained with institutional review board (IRB) approval. To begin, the channels and reservoirs of the MISS are filled with media. When the channel walls are made hydrophilic, the fluid will spontaneously wick into the channels. Once the channels are filled with liquid, the fluids in the outlet reservoirs are emptied, except for a small amount of liquid sufficient to form a concave meniscus. Finally, a sperm sample is loaded into the sperm sorter inlet, while taking precautions not to overfill the reservoirs.

Typical experiments have shown an increase in motile sperm purity from 10 to >98% after a single passage though the device using washed human semen. The gentle and reliable microfluidic sorting mechanism and the steady fluid flows generated by the passively driven pumping system provide a simple yet generally consistent sorting capability. The main problem that one encounters is channel clogging, which can occur when the sample is too highly concentrated or includes an excess of large debris. This device also works well with unwashed human semen ***(10)***. In a typical experiment, sperm motility increased from 44 ± 4.5 to 98 ± 0.4% following processing. However, it is important to note that if unwashed semen is of high viscosity, the isolation is less efficient for the design described owing to slower flow rates.

1.2.4. Soft Lithography

The fabrication procedures used for constructing the MISS takes advantage of a set of microfabrication methods called "soft lithography," which uses molding to replicate microfeatures into elastomers. These patterned elastomers are then used as masks, stamps, molds, or microchannels. Soft lithography is advantageous for many microfluidic applications because it allows fabrication of microchannel structures more rapidly and with low equipment costs compared to surface/bulk micromachining ***(14)***. Soft lithography has been used extensively in microfluidic applications to fabricate components such as sensors, mixers, sorters, and cell culture chambers ***(11)***. This chapter specifically describes the use of soft lithographic methods to fabricate the MISS.

2. Materials

1. SU-8 (MicroChem, Newton, MA): this is a negative, near-ultraviolet (UV), epoxy photoresist. Compared with other photoresists, SU-8 is distinguished for its ability to produce thicker and/or higher-aspect-ratio structures while using standard contact lithography equipment. This feature is owing to SU-8's low optical absorption in the UV range as opposed to the higher absorptions of other sensitive photoresists. SU-8 fills the need for fabricating the relatively thick microchannels required for the MISS ***(15–17)***.
2. PDMS: this is a transparent, thermosetting polymer that consists of a base and a curing agent component. This class of materials (silicon rubber) has been thoroughly used for specific clinical applications such as contact lenses and various implanted devices. PDMS (Sylgard 184) is obtained from Dow Corning. The curing agent is normally added to the base in a 1:10 weight ratio. The weighted components are mixed with an electric mixer or by hand and degassed under vacuum until no bubbles remain in the mixture. After degassing, the PDMS can be cast against photoresist patterned silicon (Si) wafers. Detachment of the cured PDMS from the Si wafer gives a PDMS slab with open-channel features that can then be sealed against PDMS, glass, plastic, or other flat surfaces.

   For microfluidic applications, PDMS is useful because of several important properties, including mechanical flexibility, gas permeability, and optical transparency. Its elasticity and hermetic self-sealing properties make multilayer construction of PDMS-based devices relatively straightforward. Although the surface of PDMS is inherently hydrophobic, it can be made hydrophilic through a plasma oxidation treatment, surface coating, or surface grafting. Plasma treatment will also allow permanent bonding of PDMS to other treated PDMS, Si, or glass.
3. Epotek epoxy: Epotek UVO-114 (Epoxy Technology, Billerica, MA) is a viscous epoxy that cures into a stiff solid once exposed to sufficient UV light. This material can be used to create a rigid replica of microfeatures present in elastomeric PDMS. In a typical procedure, a piece of PDMS is placed with microfeatures facing down on prepoured Epotek in a Petri dish. After degassing

and eliminating bubbles underneath the PDMS, the Epotek and PDMS structure are exposed for 90 min to strong UV from a UV chamber (3D Systems) to form a solid mold.

4. Semen samples: the semen samples that we tested were obtained with IRB approval from men undergoing evaluation for infertility after a minimum of 3 d of abstinence. Before sorting experiments, a semen sample analysis was performed to assess semen volume, pH, viscosity, liquefaction, sperm count, sperm motility, sperm agglutination, strict sperm morphology, and cell contamination. Semen samples with forward progression spermatozoa were selected for experimental use.
5. Bovine serum albumin (BSA) fraction V (Sigma, St. Louis, MO).
6. Phosphate-buffered saline (PBS) (Invitrogen, Carlsbad, CA).
7. HEPES-buffered human tubal fluid with 0.2% BSA (processing medium) (Irvine Scientific).
8. Propidium iodide (PI) (Molecular Probes).
9. (Tridecafluoro-1,1,2,2-tetrahydrooctyl)-1-trichlorosilane (United Chemical Technologies).

3. Methods

This section describes the details of the MISS microfabrication along with the procedure for using the MISS for sperm sorting. The simple structure of the device makes it suitable for fabrication through a variety of techniques using various materials. Here, we describe a typical procedure used in our laboratory.

3.1. Fabrication of Microfluidic Sperm Sorter

Although the structure of the MISS is simple, the coexistence of defined structures with both micrometer- and millimeter-length scales makes fabrication a challenge. Procedures such as photolithography are excellent for making micrometer features but are limited in making features with millimeter height. On the other hand, methods for milling and machining millimeter-sized objects are often not well suited for precise fabrication of microchannels. It is because of this challenge of making multiscale structures that the fabrication procedures described next are rather lengthy. Once a good master mold with all the structures is obtained, subsequent MISS devices can be more readily fabricated simply through casting.

3.1.1. Fabrication of a Mask

The first step is to prepare a photomask with channel features for further microfabrication. Although chrome masks are generally used in conventional photolithography, they are expensive and often require long lag times to obtain. In rapid prototyping with contact photolithography, it is convenient to use transparency film masks, which are lower yet sufficient in resolution and much

cheaper and quicker to obtain than chrome ones. A typical mask would be 5 × 7 in. and is drawn with readily available software such as AutoCAD. The AutoCAD dxf files are converted to gbr files by conversion software such as LinkCAD. Finally, the gbr files are printed at 20,000 dpi by CAD/Art Services (www.outputcity.com). A resolution of 20,000 dpi is sufficient to fabricate microchannels with widths as low as 1.25 μm. This resolution is more than sufficient since the minimum width of the sperm sorter is 100 μm.

3.1.2. Fabrication of an Si Master With Channel Features

Once the transparency mask is obtained (a K-shaped channel in the case of the MISS), contact photolithography is used to fabricate a master mold of the K-shaped microchannel features. PDMS prepolymer can then be cast against this master to generate a PDMS replica.

1. Spin hexamethyldisilazane (HMDS) primer over a Si wafer to help promote adhesion of SU-8. SU-8 is a typical epoxy-based negative photoresist that cures or hardens with UV exposure. Then spin coat SU-8 (MicroChem) photoresist onto the Si wafer. A high-resolution transparency mask defines the eventual channel architecture. The mask selectively permits UV light through to induce or prevent curing of spin-coated photoresist on a wafer. The detailed procedure is as follows:

Precoat HMDS primer	Step 1: 500 rpm	10 s
	Step 2: 1000 rpm	10 s
	Step 3: 3000 rpm	30 s
Coat SU-8	Step 1: 750 rpm	60 s
	Step 2: 1500 rpm	30 s
	Step 3: 2000 rpm	30 s
Soft bake	Step 1: 65°C	10 min
	Step 2: 95°C	15 min
Exposure		4 min, 30 s
Postexposure bake	Step 1: 65°C	3 min
	Step 2: 95°C	9 min
Develop	Immerse the wafer under and spray with MicroChem SU-8 Developer until the unpolymerized substrate is gone; then dry with a gentle stream of nitrogen.	

2. To prevent PDMS from bonding to the wafer, silanize the wafer using $C_8H_4Cl_3F_3Si$, TFS. Perform silanization by chemical vapor deposition of silane in an evacuated desiccator for 10 min, with the substrates hung upside down above a cover glass coated with a 1:1 ratio mixture of mineral oil and silane.

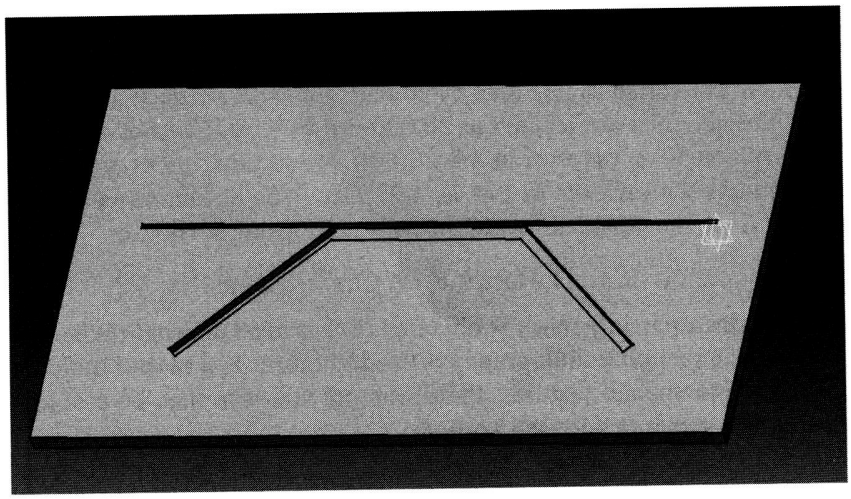

Fig. 2. First PDMS mold cast against pattern fabricated by photolithography.

3.1.3. Fabrication of an Epoxy Mold

Because of to the fragility of Si wafers, we often prepare an epoxy replica, which is stronger and easier to manipulate.

1. Make a PDMS mold of the Si wafer with photoresist channel features (**Fig. 2**). Pour degassed PDMS on the wafer to form a flat PDMS sheet approx 4 to 5 mm thick. If the PDMS is too thin, it will easily bend and deform in the epoxy molding step.
2. Cure and remove the PDMS mold from the silanized wafer, and put it on the epoxy prepolymer. To avoid bubbles trapped underneath the PDMS, precoat the PDMS surface with channel features with copious epoxy prepolymer, and then swiftly flip the channel feature side down onto a Petri dish prefilled with epoxy prepolymer from one end to the other, pushing potentially trapped air to one side.
3. Remove any residual bubbles from the epoxy with a needle, and then further degas it under vacuum until all bubbles are gone. It regularly takes 2 h for the degassing process.
4. Expose the epoxy in a UV chamber for 90 min to harden. The wavelength ranges from 280 to 400 nm.
5. Peel off the PDMS slab after the expoxy mold is cured.

3.1.4. Fabrication of a Master Mold With Both Microchannel Features and Millimeter-Sized Reservoirs

1. Glue small metal (typically steel or copper) cuboids or cylinders (2- to 3-mm radius) onto the solid epoxy surface using Superglue to form horizontally oriented fluid reservoirs that serve as steady-flow, passively driven pumps (**Fig. 3**).

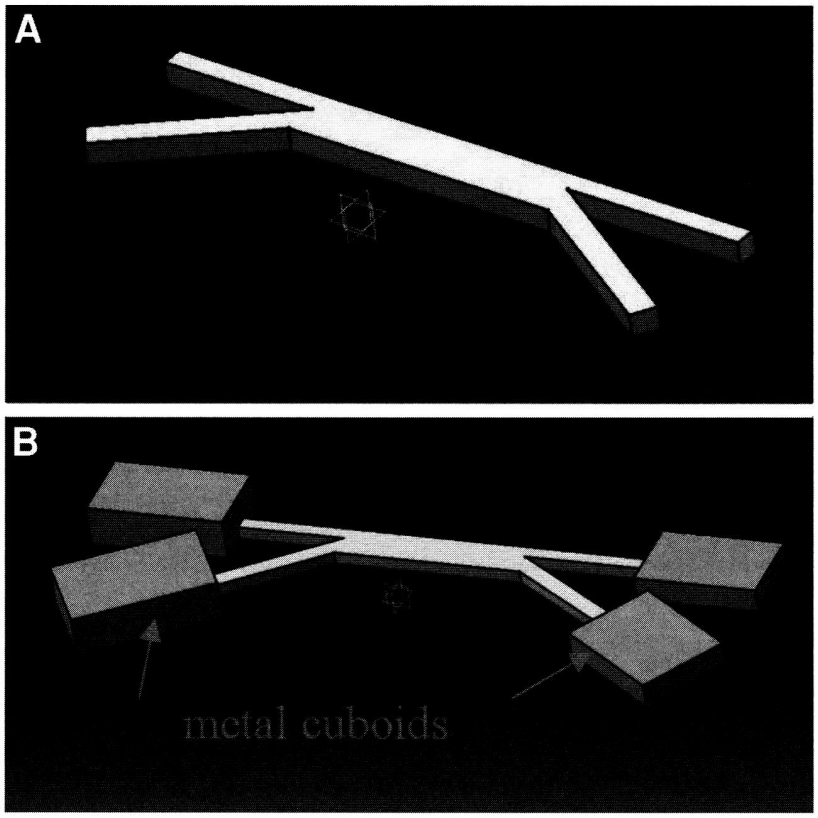

Fig. 3. (**A**) Epoxy mold without metal cuboids; (**B**) epoxy mold with cuboids glued to the wafer.

The cuboid or cylinder can be of any material as long as it is not chemically reactive or does not inhibit PDMS crosslinking. Low-viscosity glue is desirable, so that it can be dispensed accurately with a narrowed tip using a micropipettor (*see* **Note 1**). Overdispensing glue will change the desired shape of the reservoirs, which serve as passively driven pumps.

2. Pour degassed PDMS on this epoxy mold.
3. Cure the PDMS at 60°C for at least 60 min.
4. Remove the cured PDMS slab from the epoxy mold with the metal reservoirs still glued to it. This slab provides a second PDMS structure (**Fig. 4**).
5. Make a second epoxy mold by casting against the second PDMS structure. This second epoxy mold, which has the combined microchannel and millimeter-sized reservoir features (*see* **Fig. 5**), is made by repeating **steps 2–4** in **Subheading 3.1.3.** This will be the master mold used for subsequent fabrication of the PDMS-based MISS (**Fig. 5**).

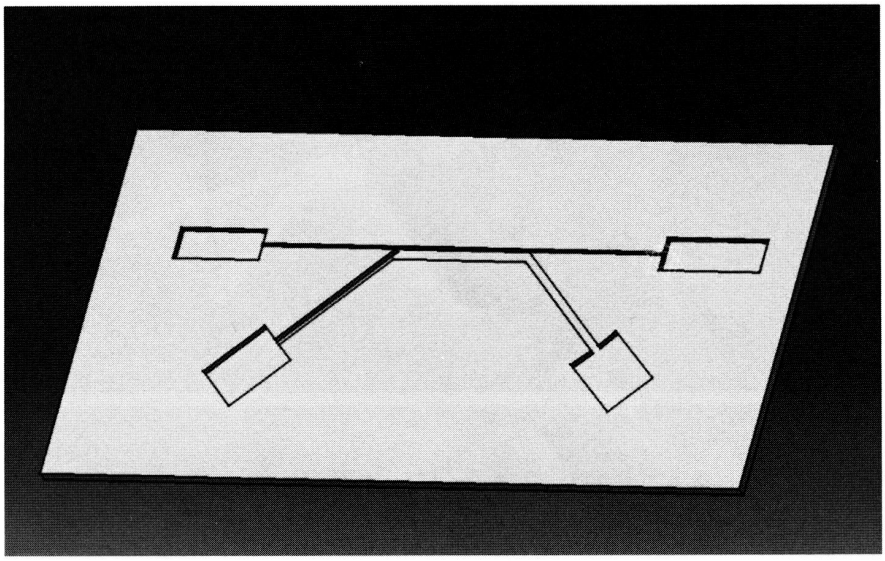

Fig. 4. The second PDMS structure.

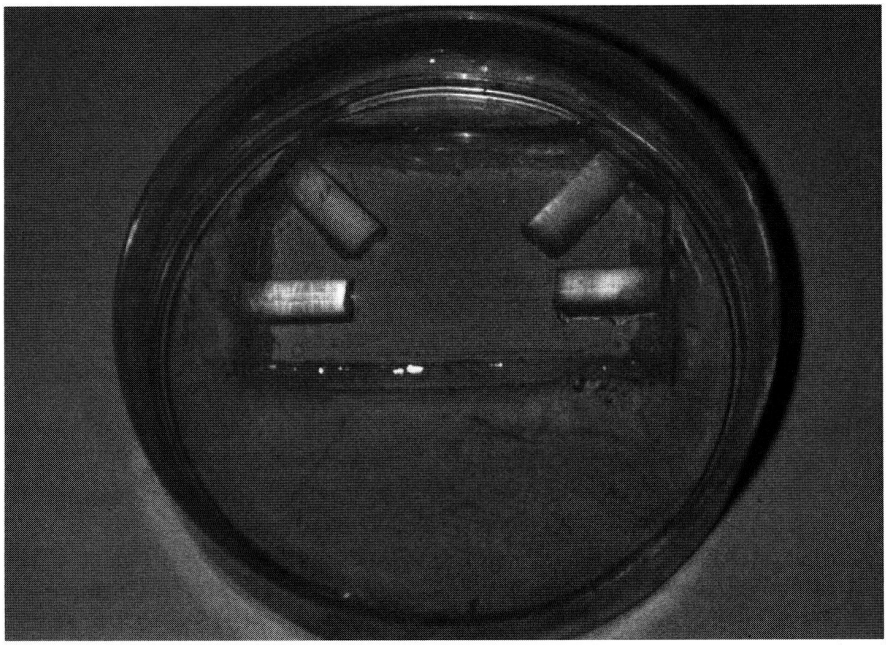

Fig. 5. The final epoxy mold.

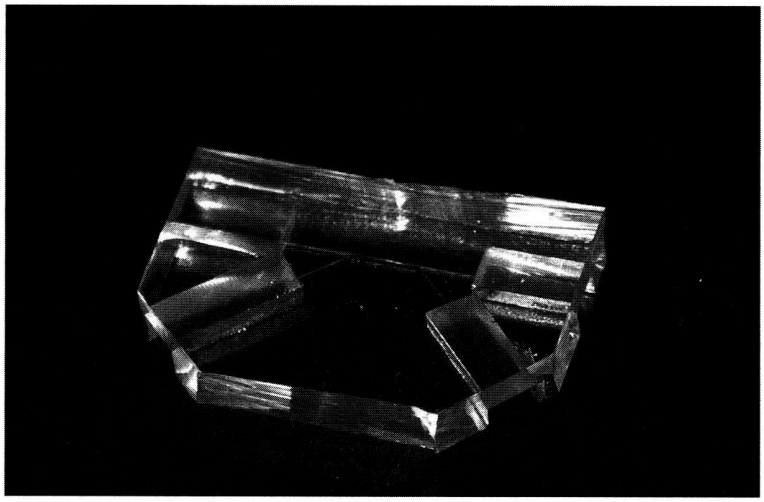

Fig. 6. Top layer of MISS.

3.1.5. Final Assembly

The final step of the fabrication involves bonding of the PDMS mold with a flat substrate (typically PDMS or glass) to obtain an enclosed channel system.

1. Pour degassed PDMS on the epoxy mold to a thickness of 4 mm to form microfluidic channels with horizontally oriented reservoirs. This piece will be the top layer of the final device (**Fig. 6**).
2. Pour degassed PDMS on flat Petri dishes to form the bottom part of the MISS to a thickness of 2 mm (**Fig. 7**).
3. Partially cure both PDMS layers by leaving them at room temperature overnight or at 60°C for 20 min.
4. Put the two partially cured PDMS layers together and cure the combined structure at 60°C for an additional 60 minutes to obtain the closed channel structure (**Fig. 8**) (*see* **Notes 2** and **3**).

3.2. Plasma Oxidation of Sperm Sorters

The purpose of plasma oxidation of sperm sorters is to make the channel hydrophilic to facilitate introduction of fluids into the channels. PDMS is inherently hydrophobic and aqueous solutions are difficult to introduce into channels. Furthermore, nonspecific adsorption causes sperm to stick to the surfaces of the channels and reservoirs, thus reducing the yield. To change the surface property of PDMS devices from hydrophobic to hydrophilic, we use plasma oxidation to activate the surface and make the surface transiently hydrophilic for a few hours. We typically plasma oxidize the whole device in a plasma

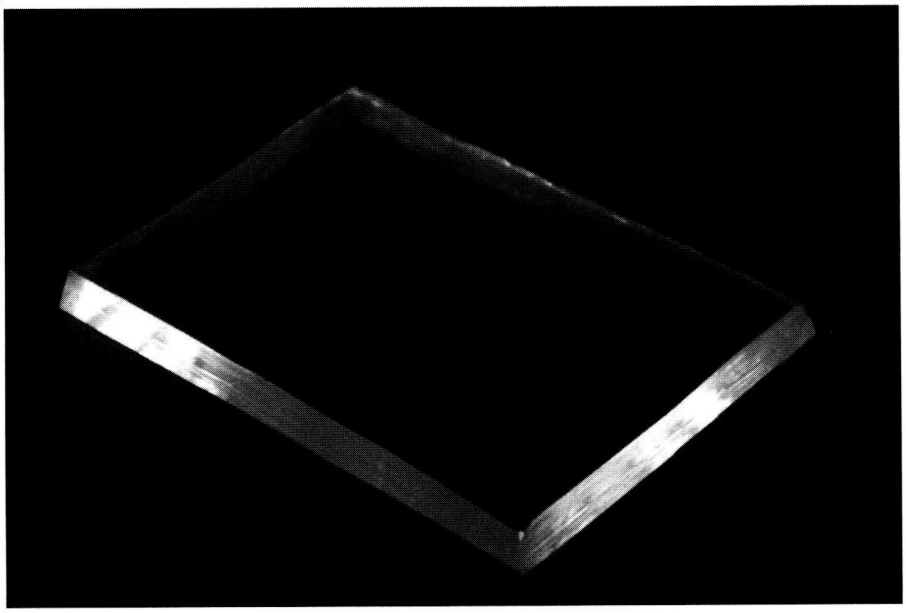

Fig. 7. Bottom layer of MISS.

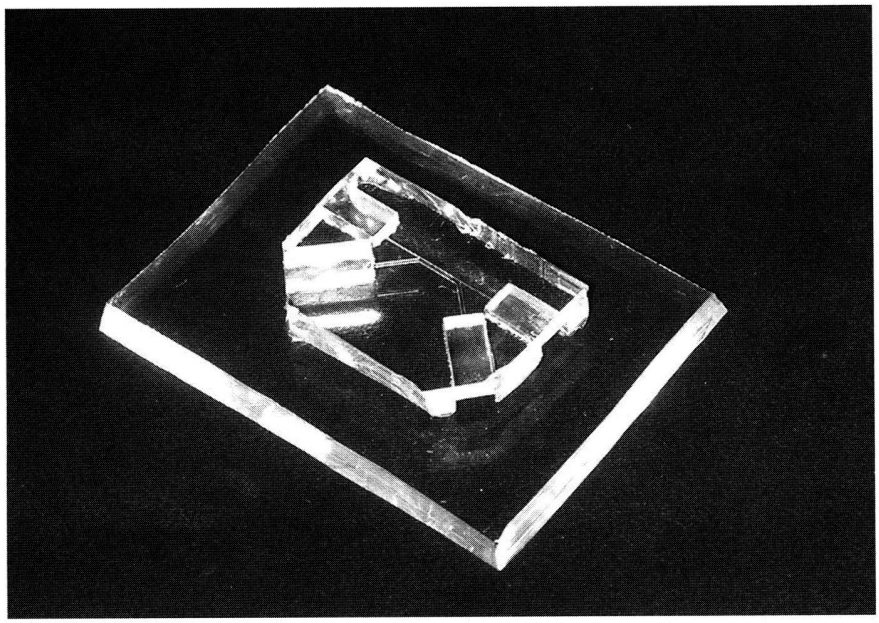

Fig. 8. The bonded structue.

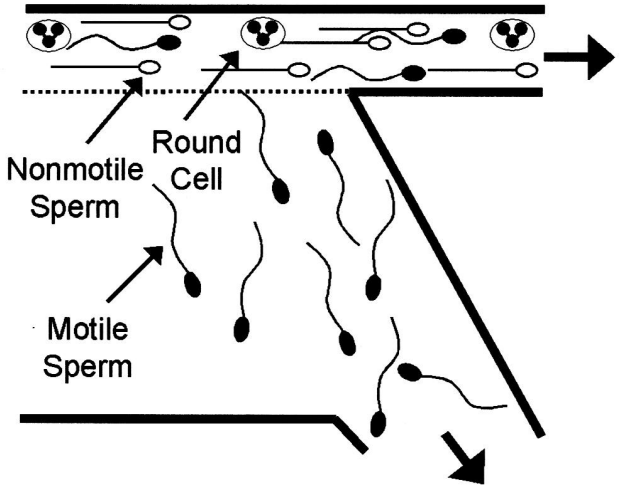

Fig. 9. Schematic illustration of sperm-sorting process. (Reproduced with permission from **ref. *9***.)

chamber for 10 min to make the surface transiently hydrophilic. If the device is hydrated and stored in a humid environment immediately after plasma treatment, channel surfaces can remain hydrophilic indefinitely (*see* **Notes 4** and **5**). Following plasma oxidation, channels and reservoirs are further coated with a 1% BSA solution (dissolved in PBS) to minimize nonspecific adsorption of cells to channel walls (*see* **Notes 6** and **7**).

3.3. Sorting Sperm With a MISS

A typical sorting experiment would be as follows:

1. Add 60 µL of processing medium to the media inlet.
2. After media wicks through the channel to the outlets, add 2 µL of medium to each of the outlet reservoirs.
3. Add a 50-µL semen sample to the sample inlet. All positions can be seen in **Fig. 1**. The semen and media flow at a constant flow rate from the inlet to the outlet (*see* **Notes 8** and **9**). Owing to the laminar flows and motility differences between sperm, most nonmotile sperm exit the upper outlet, whereas a significant portion of the motile sperm will exit out the lower outlet (**Fig. 9**).
4. Analyze the number of motile sperm using a Makler counting chamber (Sefi-Medical, Haifi, Israel) while taking dilution factors into account.
5. Visualize nonmotile sperm (more precisely, membrane-compromised sperm) by adding 3 µL of PI (60 m*M* dissolved in processing medium; Molecular Probes) to sperm samples prior to sorting and using a Texas Red filter set (577-nm excitation, 620-nm emission) to view red fluorescence.

6. Record images and movies on an inverted microscope (Nikon TE 330) with a charge-coupled device camera (Hamamatsu ORCA-100).

The MISS system enables straightforward, gentle, and reliable sorting of motile, morphologically normal spermatozoa from a mixture using microfluidics. The MISS is structurally simple, straightforward to fabricate, cost-effective, and a stand-alone device that is fully functional without any external power sources or controls ***(9)***. It is ideal for sorting small volumes of samples and can provide high-quality (motile and of good morphology) sperm even from debris-laden samples ***(10)***.

4. Notes

1. It is possible to glue metal reservoirs directly on the Si wafer with channel features without making the first epoxy mold. However, the wafers are fragile and can break easily owing to cutting and peeling of PDMS on the wafer. It is also not necessary to make the second epoxy mold; the PDMS can be cast directly against the first epoxy mold with metal cuboids glued on it.
2. Occasional leaks occur at the reservoir's edges (i.e., at the interface between the main PDMS device, the substrate, and air) owing to capillary action and result in cross-contamination between reservoirs. To solve this problem, we dabbled and cured small amounts of PDMS at the PDMS-substrate interface between reservoirs. The amount of PDMS dabbled should be limited to prevent the risk of it being wicked into the channels.
3. Alternatively, glass cover slides can be used as the bottom layer whenever the bonding performed is through plasma oxidation treatment ***(17)***. A glass bottom is originally hydrophilic; however, the bonding technique using plasma oxidation is sensitive to experimental conditions and can sometimes be difficult to reproduce reliably.
4. Plasma oxidation can be used to bond permanently a flat PDMS surface to unsilanized glass, silicon, or PDMS. A typical procedure would involve facing two surfaces (to be bonded) up in the oxidation chamber, and oxidizing for 30 s with 40 mA at 200–800 mtorr under oxygen plasma. The two sides would then be immediately brought into contact after oxidization (within minutes) and hermetically sealed, followed by incubating in a 60°C oven or baking on a heating plate for 1.5 h to ensure full, irreversible bonding. Plasma oxidization only temporarily changes the PDMS surface to hydrophilic. For bonding purposes, it is important that the PDMS surface be oxidized only briefly, and that oxidized surfaces be brought into contact with each other immediately thereafter. Short oxidizations activate functional groups (hydroxyl) on the PDMS surface. The functional groups from each surface will form chemical bonds and, hence, make bonding irreversible. If the oxidization is long (>10 min), the surface will be degraded and will not be able to form chemical bonds between surfaces. Plasma oxidization keeps the PDMS surface hydrophilic only transiently if the surface is kept dry. To elongate the device's hydrophilicity, an aqueous solution

should be introduced into the channel within 10 min after oxidation. Incubation with 1–5% BSA solution also helps to maintain the hydrophilicity. It is also possible to dry and save the device after bonding; oxidize again for 10 min immediately before the introduction of liquid.

5. Devices can be entirely UV sterilized after their production, because all components are transparent. Autoclaves can also be used.
6. The channel surface can be coated with BSA and then dried for storage. The channel may be receptive for the introduction of liquid later without using plasma oxidization. This will allow users without a plasma oxidizer to use the device. BSA is a common blocking protein with negative charges that can make surfaces hydrophilic. However, it will not create a channel surface as hydrophilic as plasma oxidization would, and often liquid needs to be aspirated for the channel to be air/bubble free.
7. After plasma oxidation, devices can also be immersed in a water-filled ziplock bag (or other tight-sealing container) for long-term storage to keep the channels hydrophilic.
8. Clogging is an issue that often occurs in the sperm sample inlet. Although it is relatively desirable that clogging occur at the sperm inlet (rather than outlets or media inlet) since purity is not compromised, clogging is still a challenge. Most clogs are eliminated by pushing on the channel from the top with a pipet tip or finger.
9. Along with channels, reservoirs also need to be as hydrophilic as possible. Lower contact angles result in less contact angle hysteresis and more stable flows. Reservoirs should not be overfilled so that the liquid meniscus is bulging outward and, thus, changes the surface tension. In addition, it is preferable to add sperm sample after filling other inlet and outlet reservoirs.

References

1. Mosher, W. D. and Pratt, W. F. (1991) Fecundity and infertility in the United States: incidence and trends. *Fertil. Steril.* **56,** 192–193.
2. Palermo, G., Joris, H., Devroey, P., and Van Steirteghem, A. C. (1992) Pregnancies after intracytoplasmic injection of single spermatozoon into an oocyte. *Lancet* **340,** 17–18.
3. Schultz, R. M. and Williams, C. J. (2002) *Science* **296,** 2188–2190.
4. Tuker, K. E. and Jansen C. M. A. (2003) Sperm separation techniques: comparison and evolution of gradient products, in: *The Art and Science of Assisted Reproductive Technique + Art).* (Allahbadia, G. N. and Basuray-Das, R., eds.) Jaypee Medical Publishers, New Delhi, India, pp. 218–221.
5. Aitken, R. J. and Clarkson, J. S. (1988) Significance of reactive oxygen species and antioxidants in defining the efficacy of sperm preparation techniques. *J. Androl.* **6,** 367–376.
6. Englert, Y., Van de Bergh, M., Rodesch, C., Bertrand, E., Biramane, J., and Legreve, A.(1992) Comparative auto-controlled study between swim-up and Percoll preparation of fresh semen samples for in-tro fertilization. *Hum. Reprod.* **3,** 399–402.

7. Zini, A., Finelli, A., Phang, D., et al. (2000) Influence of semen processing technique on human sperm DNA integrity. *Urology* **6,** 1081–1084.
8. Weigl, B. H., Bardell, R. L., and Cabrera, C. R. (2003) Lab-on-a-chip for drug development. *Adv. Drug Deliv. Rev.* **55,** 349–377.
9. Cho, B. S., Schuster, T. G., Zhu, X., Chang, D., Smith, G. D., and Takayama, S. (2003) Passively driven integrated microfluidic system for separation of motile sperm. *Anal. Chem.* **75,** 4671–1675.
10. Schuster, T. G., Cho, B. S., Keller, L. M., Takayama, S., and Smith, G. D. (2003) Isolation of motile spermatozoa from semen samples using microfluidics. *Reprod. BioMed. Online* **7(1),** 75–81.
11. Whitesides, G. M., Ostuni, E., Takayama, S., Jiang, X., and Ingber, D. E. (2003) Soft lithography in biology and biochemistry. *Annu. Rev. Biomed. Eng.* **3,** 335–373.
12. White, F. M. (1999) *Fluid Mechanics*, 4th ed., McGraw Hill, Columbus, OH.
13. World Health Organization. (1999) *WHO Laboratory Manual for the Examination of Human Semen and Sperm–Cervical Mucus Interaction*, 4th ed., Cambridge University Press, Cambridge, UK.
14. Xia, Y. and Whitesides, G. M. (1998) Soft lithography reviews. Angew. *Chem. Int. Ed.* **37,** 550–575.
15. Gadre, A., Kastantin, M., Li, S., and Ghodssi, R. (2001) An integrated BioMEMS fabrication technology. *Intl. Semiconductor Device Res. Symp.* 1–4.
16. Carlier, J., Arscottl, S., Thomy, V., et al. (2004) Integrated microfluidics based on multi-layered SU-8 for mass spectrometry analysis. *Micromech. Microeng.* **14,** 619–624.
17. Duffy, D. C., McDonald, J. C., Schueller, O. T. A., and Whiteside, G. M. (1998) Rapid prototyping of microfluidic systems in poly(dimethylsiloxane). *Anal. Chem.* **70,** 4974–4984.

Appendices 2 A Surface-modified sperm sorting device with long-term stability

Biomed Microdevices (2006) 8: 99–107
DOI 10.1007/s10544-006-7705-7

A surface-modified sperm sorting device with long-term stability

Jason M. Wu · Yaokuang Chung · Kimberly J. Belford · Gary D. Smith · Shuichi Takayama · Joerg Lahann

We report on a PDMS-based sperm sorting device, which has been surface-modified via graft-*co*-polymerization to create moderately hydrophilic and non-fouling surfaces with long-term stability. The applicability of our method to PDMS-based sperm sorting devices was demonstrated by successfully sorting human semen samples.

Abstract Microfluidic devices fabricated from poly (dimethylsiloxane) (PDMS) offer the ability to improve our biological and medical capabilities. Although PDMS offers a range of intriguing benefits for biomedical applications, the intrinsically hydrophobic nature of PDMS may impede with the tremendous potential of these devices. Here, we describe a PDMS-based sperm sorting device, which has been surface-modified via graft-*co*-polymerization of poly(ethylene glycol) methyl ether methacrylate to create a moderately hydrophilic and non-fouling surface. This process involves the exposure of PDMS to UV/ozone, which activates the PDMS surface to bond to the substrate and, at the same time, initiates the graft-*co*-polymerization from the PDMS surface. In this study, we confirmed long-term stability of surface-modified PDMS for up to 56 days based on Fourier transformation infrared spectroscopy (FTIR), contact angle measurements, and protein adsorption studies. Moreover, the applicability of our method to PDMS-based sperm sorting devices was demonstrated by successfully sorting human sperm.

J. M. Wu
Department of Chemical Engineering, University of Michigan, Ann Arbor, MI 48109, USA

Y. Chung
Department of Biomedical Engineering, University of Michigan, Ann Arbor, MI 48109, USA

K. J. Belford
Department of Chemical Engineering; Department of Biomedical Engineering, University of Michigan, Ann Arbor, MI 48109, USA

G. D. Smith
Department of Obstetrics & Gynecology; Department of Urology; Department of Molecular & Integrated Physiology, University of Michigan, Ann Arbor, MI 48109, USA

S. Takayama
Department of Biomedical Engineering; Department of Macromolecular Science and Engineering, University of Michigan, Ann Arbor, MI 48109, USA

J. Lahann (✉)
Department of Chemical Engineering; Department of Macromolecular Science and Engineering; Department of Materials Science and Engineering, University of Michigan, Ann Arbor, MI 48109, USA
e-mail: lahann@umich.edu

Introduction

In the foreseeable future, the public will be able to address an increasing number of their health concerns with "lab on chip" devices (Sia and Whitesides, 2003). Specifically, the area of reproductive medicine is prone to improvements that involve miniaturized systems, such as microfluidic sperm sorters (Cho et al., 2003; Suh et al., 2003). For this vision to occur, it is critical that these instruments not only function as designed, but also be easy to attain, simple to operate, and available on a need to use basis (Cho et al., 2003; Ng et al., 2002; Belder and Ludwig, 2003). Precursors to these tools are currently in development and may include autonomous polydimethylsiloxane (PDMS) made microfluidic systems that have already demonstrated to greatly improve our biological analysis capabilities (Sia and Whitesides, 2003; Suh et al., 2003; Hu et al., 2002). PDMS offers many advantages, such as being inexpensive, harmless to cells, transparent, easy to fabricate, and having the capability to bond other surfaces

to form watertight seals (Sia and Whitesides, 2003; Ng et al., 2002; Hu et al., 2002; Olah et al., 2005; Berdichevsky et al., 2004). However, one of the drawbacks of PDMS is its hydrophobic nature, which leads to a surface with poor wettability and a tendency to allow nonspecific adsorption of material such as proteins and cells (Sia and Whitesides, 2003; Ng et al., 2002; Hu et al., 2002). This is a significant problem for devices designed to use natural sources such as hydrostatic pressure to force fluid through their system to be processed. Solutions to this obstacle include surface treatments, such as plasma oxidation and UV/ozone treatment that can alter PDMS to become hydrophilic (Sia and Whitesides, 2003; Cho et al., 2003; Ng et al., 2002; Hu et al., 2002; Olah et al., 2005; Berdichevsky et al., 2004). Unfortunately, PDMS will quickly undergo hydrophobic recovery thereby reverting back to its hydrophobic state when left under ambient conditions (Olah et al., 2005). In addition, treating PDMS repeatedly by these methods leads to permanent cracking on the surface, which may affect fluid flow so that the device no longer functions properly (Olah et al., 2005). Some alternative methods have been proposed to modify PDMS-based devices, such as vapor-deposition of reactive coatings (Lahann et al., 2003) or graft-*co*-polymerization (Hu et al., 2002; Hu et al., 2004).

Herein, we report on a process that uses surface-initiated graft-co-polymerization of poly(ethylene glycol) methyl ether methacrylate (PEG-MA) to modify the luminal channel surface of PDMS-based cell sorting devices. PEG-MA was chosen because it has been previously applied to create hydrophilic and non-fouling surfaces (Zou et al., 2002; Jeong et al., 1996; Zou et al., 2002; Zhang et al., 2001). The PEG-MA reacts with radicals on the PDMS surface that are formed by exposure to UV/ozone (Hu et al., 2002; Jeong et al., 1996; Zou et al., 2002). For surface activation, a UV/ozone cleaner is used, which utilizes two short-wavelengths of UV radiation (184.9 nm and 253.7 nm) (Efimenko et al., 2002). The UV light dissociates molecular oxygen at 184.9 nm and ozone at 253.7 nm to generate atomic oxygen (Efimenko et al., 2002). In addition, the 253.7 nm wavelength activates the PDMS to react with the atomic oxygen (Efimenko et al., 2002). The molecules created under these conditions include oxidation products and (latent) radicals (Efimenko et al., 2002). When immersed in a solution containing PEG-MA, the radicals react with the carbon-carbon double bond of the PEG-MA molecule to initiate the grafting process. Further propagation of the chain of PEG-MA is driven by the heat of the reaction solution and leads to the formation of more hydrophilic and anti-fouling coatings on PDMS microfluidic channels. Along with the alteration of surface properties, the radicals generated by UV/ozone exposure allow also for irreversible bonding of the PDMS microfluidic channel system to the substrate. This results in an enclosed watertight system that is suitable for processing biological fluids, such as semen.

In order to demonstrate the feasibility of this grafting process for surface modification of PDMS-based sperm sorting devices, a previously described microscale integrated sperm sorter (Fig. 1) was used as the test platform (Cho et al., 2003; Suh et al., 2003). This device is an enclosed PDMS based microfluidic system and has been shown to enable isolation of motile sperm from semen samples for use in infertility analysis and treatments (Cho et al., 2003; Suh et al., 2003). It essentially consists of a piece of PDMS containing the microfluidic channel system and reservoirs used for sperm sorting bonded to a flat piece of PDMS that serves as a base. Two characteristics of the sperm sorter design are noteworthy. First, fluid moves naturally through the system with only the aid of hydrostatic pressure, capillary forces, and surface tension (Cho et al., 2003; Suh et al., 2003). Secondly, the flow of fluid in the microfluidic channels is laminar (Cho et al., 2003; Suh et al., 2003). When fluid containing sperm and the medium meet in the main channel of the device, each stream flows side by side without mixing and exits through its respective outlet (Cho et al., 2003). The basis of sperm sorting is the ability of motile (and thus desirable) sperm to swim,

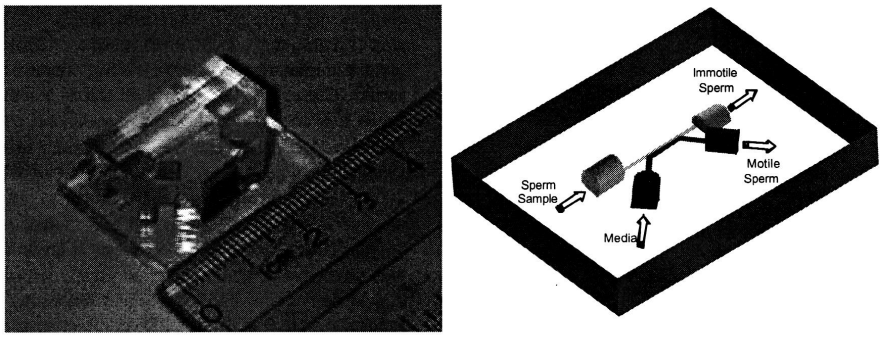

Fig. 1 The micrograph shows a microscale-integrated sperm sorting device used in this study. Laminar flows of semen sample (light) and medium (dark) enter from the left. At the outlet, motile and immotile sperm are separated and can be isolated

which allows sperm to move from the semen stream into the second stream containing the medium for recovery (Cho et al., 2003; Suh et al., 2003). In our approach, it is imperative that the channel surface has sufficient hydrophilicity to not resist flow through the device and that the surface be resistant to adsorption of unwanted cellular debris which can clog the channels and hinder fluid flow.

Materials and methods

Materials and reagents

For grafting, poly(ethylene glycol) methyl ether methacrylate (PEG-MA) (average M_n ~475 g/mol) was obtained from Aldrich, ethanol (anhydrous) from Fisher Chemical, deionized water (DI water), packed inhibitor-removal columns to remove hydroquinone (HQ) and hydroquinone monomethyl ether (MEHQ) from Aldrich. For fabrication of microfluidic devices, poly(dimethylsiloxane) (PDMS) was obtained from Dow Corning (Sylgard 184). For protein adsorption test, Tween 20 was obtained from Fluka, phosphate buffered saline (PBS) (pH: 7.4) from Sigma, albumin bovine serum from Sigma, and Alexa Fluoro 546-conjugated fibrinogen from Molecular Probes. For sperm sorting tests, phosphate-buffered saline (PBS) was obtained from Invitrogen, bovine serum albumin (BSA) fraction V from Sigma, HEPES-buffered human tubal fluid with 0.2% BSA (Processing medium: PM) from Irvine Scientific, and propidium iodide (PI) from Molecular Probes.

Bonding of the microfluidic sperm sorting devices

The PDMS microfluidic channel system of the sperm sorter with the desired reservoir and channel features was fabricated using a soft lithography technique as described previously (Suh et al., 2003). The microfluidic channel was sealed against a flat slab of PDMS.

Grafting process

Prior to grafting, PEG-MA was passed through a packed inhibitor-removal column to remove the inhibitor, MEHQ. Both the glass bottle used to collect the PEG-MA and the column were wrapped in aluminum foil to prevent exposure to light. PDMS sperm sorter and base components of the sperm sorter were rinsed and scrubbed with ethanol to clean their surfaces. Each piece was then dried with argon. DI water and ethanol in a ratio of 4:1 (DI water/ethanol) were added to a reaction vessel and stirred. The solution was degassed by applying vacuum to the reactor followed by flowing argon gas to the system. This process was repeated for a total of 3 times before allowing the argon to continuously flow through the system until the end of the reaction. PEG-MA was then added to the reaction vessel to create a 0.25 M PEG-MA solution. While the grafting solution was heated to 65°C, the components of the sperm sorter were placed on the loading tray of a Jelight 342 UVO Cleaner. Surfaces to be activated were placed 5 mm below the UV lamp to maximize exposure to UV/ozone and activated for 15 min. Next, the PDMS sperm sorter channel system was placed on top of the PDMS base so that the activated surfaces were in contact. If the two pieces did not seal completely, they were pressed together to achieve bonding. Once the sperm sorting devices were assembled, grafting solution was loaded into the reservoirs to ensure that fluid easily moved through the entire channel system. This step also helped to minimize the formation of air bubbles, which could have interfered with the grafting process. The devices were gently submerged into the liquid and then the grafting solution was heated to the reaction temperature of 80°C. Grafting was allowed to proceed for 3 hours. Once the reaction was complete, the heat source was turned off to let the solution cool down for 30 min. The sperm sorters were removed from the reaction vessel and sonicated in DI water in a Bransonic 52 Ultrasonic Cleaner (50/60 Hz). Argon gas was blown through the microfluidic channel system to remove any obstructions. This technique was repeated until the channel was cleared. Samples were stored exposed to air in Petri dishes at ambient conditions. If polymerization was not excessive, the grafting solution was reused. The liquid lost to evaporation was replaced with a 4:1 DI water to ethanol solution and the grafting procedure was repeated.

Contact angle measurements

PDMS pieces were grafted and sonicated alongside the sperm sorters. These samples were dried with argon and then stored exposed to air in a covered Petri dish at ambient conditions. Three drops of 50 μL of DI water were placed on different locations on each grafted PDMS sample using a syringe. An image of each drop was captured using a Nikon Coolpix 990 digital camera. Each image was printed and the contact angle of each drop was measured on both sides using a protractor with the smallest units of measurement being 1°. The reported contact angle was calculated by averaging the angle measurements for the three drops on each piece.

ATR-FTIR spectroscopy

Sections from the grafted PDMS pieces used to obtain contact angle measurements were also analyzed using attenuated total reflectance Fourier transformed infrared spectroscopy (ATR-FTIR). The UV/ozone activated side of each piece of PDMS was examined using a Nicolet 6700 FTIR (KBR

beamsplitter and MCT-High D* detector) with SMART ARK Accessory containing a ZnSe 45° crystal. Each spectrum was obtained through 256 scans at a resolution setting of 4.

Protein adsorption testing

Portions of the grafted PDMS pieces were incubated with fibrinogen to demonstrate the non-fouling capabilities of the grafted surface. A PDMS sheet containing a matrix of circular wells of 1 mm in diameter and 2 mm deep was conformally bonded to the grafted PDMS. 30 μg/ml of fibrinogen was deposited into each well and allowed to remain there for 10 min. Each sample was then allowed to sit in a solution consisting of 500 ml of PBS, 0.5 g of BSA (0.11% wt/vol), and 0.1 ml of Tween 20 (0.2% vol/vol) for 10 min to wash away excess protein. Each piece was rinsed off with DI water and dried with air. The surfaces were examined by fluorescence microscopy using a Nikon Eclipse TE 300 at a magnification of 4× and images were captured using a Hamamatsu ORCA-100 CCD camera. The intensity of each image was obtained using the Plot Profile tool available on Image J 1.34s software (http://rsb.info.nih.gov/ij/download.html).

Testing of surface-modified sperm sorting devices

For the sperm sorting experiments, semen samples were obtained with University of Michigan Medical School Institution Review Board approval from men undergoing infertility evaluation. The procedure for sorting semen samples for motile sperm and the ensuing analysis to determine the success of device was described previously (Cho et al., 2003). The dimensions of the microfluidic channel system used in the testing are as follow: sperm inlet and outlet channels were 120 μm wide, 5000 μm long, and 150 μm deep, media inlet and outlet channels were 360 μm wide, 5000 μm long, and 150 μm deep, and the main channel was 500 μm wide, 5000 μm long, and 150 μm deep.

The fluid flow test was essentially analogue to the method used for sorting motile sperm. DI water was colored with enough food coloring so that it was visible within the microfluidic channel. 60 μl of DI water of one color was loaded into the medium inlet reservoir. 50 μl of DI water of another color was loaded into the sample inlet. 2 μl of DI water was loaded at each outlet reservoir. Fluid placed at the medium inlet reservoir was observed to flow out into the medium outlet reservoir. Fluid placed at the sample inlet reservoir was observed to flow out into the sample outlet reservoir. When the inlet channels merge into a single channel, the fluids moved parallel to each other and colors were not observed to mix. In some instances, fluid did not automatically enter the microfluidic channel system; in these cases, it was necessary to first flow DI water through the system in order to pre-wet the PEG-MA hydrogel.

Results and discussion

Fabrication of the sperm sorting devices

In a series of grafting studies, we found that PEG-MA can be reliably grafted to PDMS if the PDMS was previously exposed to UV/ozone for 20 min. From a process development point, it would add additional attractiveness if the UV/ozone activation would not only support grafting of PEG-MA, but also to bond PDMS microfluidic systems together. For this reason, initial work focused on bonding pieces of PDMS to each other immediately after treating them with UV/ozone at different distances from the UV source and exposure times. This step was followed by placing the samples into an oven between 60 and 80°C for 30 min to stabilize the seal thermally. Key findings from these experiments were: (i) UV/ozone activation times between 30 sec to 20 min are sufficient to seal PDMS together; (ii) attachment between the PDMS pieces was reduced as the samples were moved further from the UV source; (iii) PDMS used beyond the expiration date of the material showed reduced surface adhesion; and (iv) cleaning PDMS with ethanol prior to UV/ozone treatment improves bonding.

Surface modification of the sperm sorting devices

Once the bonding of two pieces of PDMS was demonstrated using the same duration of exposure to UV/ozone necessary for graft-co-polymerization, we shifted our focus to the surface modification of sperm sorting devices. As initial grafting conditions, we used an UV/ozone exposure of 20 min at a distance of 5mm from the UV source followed by thermal bonding for 30 min at 65°C. Over the course of the project, the results from fluid flow tests from PEG-MA grafted devices resulted in further optimization of these process conditions. To assess whether or not the PEG-MA solution freely flowed through the sperm sorting device, solutions were labeled using food coloring. It was observed that in some of the devices, fluid flow was prevented due to the formation of air bubbles either in the microfluidic channel system or in the reservoirs. The formation of air bubbles was prevented by first loading the sperm sorting devices with grafting solution to remove any air inside the device and then gently placing them into the reactor. In addition, it was thought that the thermal bonding step accelerated the hydrophobic recovery of the activated PDMS, which, in turn, would reduce the available radicals necessary for the surface-induced graft-*co*-polymerization of PEG-MA to the PDMS surface.

Table 1 Contact angle measurements as determined by the sessile drop method

Sample	PDMS reference*	Grafted PDMS after 28 days	Grafted PDMS after 42 days	Grafted PDMS after 56 days
Average	111°	60°	60°	59°

*PDMS was treated in the same way as all the other samples, but without previous UV/ozone activation.

In a series of bonding experiments, we found that the thermal bonding step was not necessary to achieve good sealing and could be eliminated. After eliminating the thermal bonding step, the sperm sorters still showed bonding comparable to devices bonded with thermal post-treatment and fluid flow through all devices appeared to be more consistent. Due to the design of the device, portions of the sperm sorter contained only a small amount of PDMS available for bonding. Initially, the seal in those areas were prone to leaking. This problem was resolved by reducing the UV/ozone treatment time to 15 minutes, which minimized leaking without compromising the sealing of the device or fluid flow through the device. Finally, the polymerization rate of the PEG-MA in the solution was difficult to assess. Typically, the PEG-MA solution could be reused for 3 to 6 reactions. These differences may be due to the presence of oxygen or impurities and the grafting solution should be inspected prior to each run. In some cases, polymerization of the PEG-MA within the microfluidic channel obstructed fluid movement. These obstacles were easily removed by sonicating the device followed by blowing argon gas through the channel. In summary, the above-mentioned optimization steps resulted in a reliable process for surface modification and sealing of PDMS-based microfluidic devices.

Evaluation of UV/ozone-initiated graft-*co*-polymerization process

After the sperm sorting devices were modified via surface-initiated graft-co-polymerization, an evaluation of the fluid handling performance was carried out twofold. The goal of these tests was to demonstrate that this process could generate a stable hydrophilic environment within the PDMS microfluidic channel. The first study involved determining whether or not the operating conditions were sufficient to graft PEG-MA onto PDMS. The methods used to characterize the grafted surface were contact angle measurement, ATR-IR, and a protein adsorption test. The second set of experiments was designed to test the microfluidic devices under fluid flow conditions. Initially, fluid was passed through the device to show that the microfluidic channel was hydrophilic enough for this purpose. Then, semen containing live sperm was introduced into the device to prove that the grafting did not adversely affect the performance of the sperm sorter.

Physico-chemical characterization of the surface-modified PDMS

During each reaction step, pieces of PDMS were activated and grafted along with the devices. We measured the contact angle to determine the hydrophilic nature of a surface. For this analysis, two pieces of grafted PDMS were used. One piece of PDMS was grafted, but was not exposed to UV/ozone. The other piece of PDMS was activated before grafting and consequently contained initiator groups for graft-co-polymerization. As shown in Table 1, the difference in contact angle measurements of about 40° clearly shows that the grafted surfaces that were treated with UV/ozone were more hydrophilic than the piece without the treatment. The measurement for the grafted PDMS without UV/ozone treatment is also consistent with contact angle measurements of PDMS reported at 109° (Hu et al., 2002). Furthermore, these tests were conducted at time points of 28, 42, and 56 days to show that the PEG-MA grafted surface was stable over extended time periods.

The contact angle measurements were complemented by ATR-IR spectroscopy. The FTIR spectra shown in Fig. 2 revealed the presence of the PEG-MA on the surface of PDMS and support the results obtained from the contact angle study. Routinely, spectra for three different PDMS samples were taken. The first sample was a piece of unmodified PDMS used as reference. The second sample was a piece of PDMS that was treated in the same way as the other grafted samples, but without UV/ozone treatment. The third sample was a piece of PDMS that was grafted following UV/ozone activation. Only for the grafted sample that was previously exposed to UV/ozone, does the IR spectra (Fig. 3) indicate a carbonyl band at 1728 cm^{-1}. This peak confirms that grafting was successful because it indicates the presence of the carbonyl functional group, which is found on PEG-MA and not on PDMS. A second characteristic signal is found in the 3300–3500 cm^{-1} range, which is due to either the formation of Si-OH caused by UV/ozone and/or the presence of water (Graubner et al., 2004).

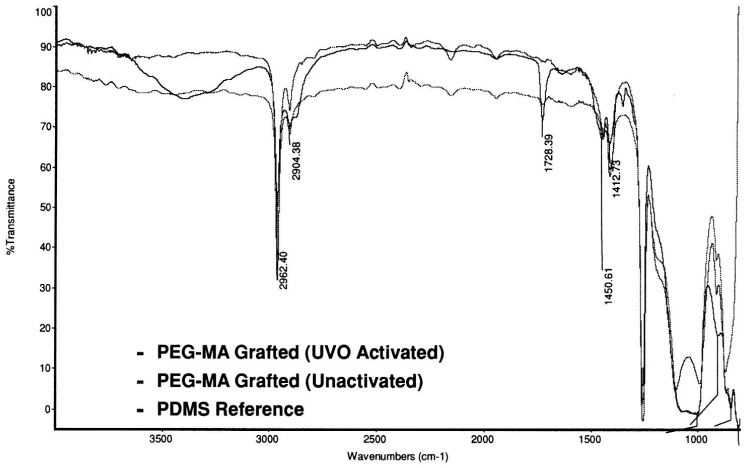

Fig. 2 ATR-FTIR spectra of PEG-MA-grafted PDMS surfaces compared to virgin PDMS and PDMS that was treated analogue to the grafted samples, but without UV/ozone activation

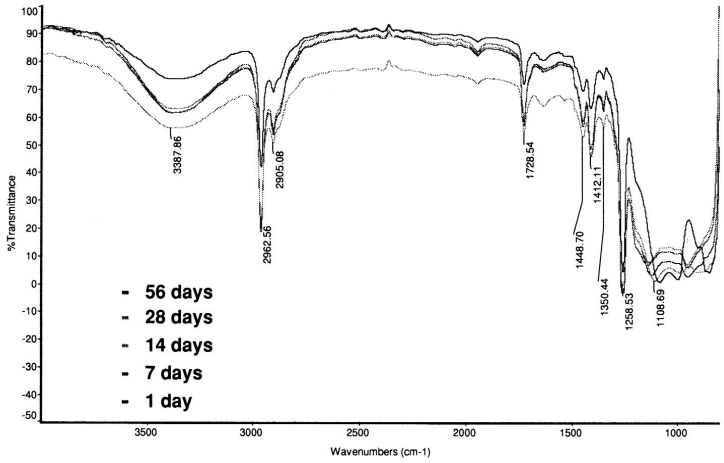

Fig. 3 ATR-FTIR spectra of PEG-MA-Grafted PDMS recorded over a period of 56 days. Samples were stored in air at room temperature

The grafted sample was also monitored by ATR-IR-stored in air over the course of 56 days—to determine the stability of the surface modification. As shown in Fig. 3, the spectra for the sample taken at time points over a period of 1, 7, 14, 28, and 56 days are similar, because they all display the key peak of a carbonyl group stemming from the PEG-MA group. This further proves the stability of the PEG-MA coating. Furthermore, a fluorescence-based protein adsorption test was conducted to demonstrate that this process allows for the creation of a non-fouling surface. Fibrinogen was incubated in circular wells placed on the surface of a piece of PDMS and a piece of PEG-MA grafted PDMS. After washing, the samples were examined with a fluorescence microscope to detect circular patterns indicative of adsorbed protein. In Fig. 4, the fluorescence signal is evidence of the presence of adsorbed fibrinogen at the surface and follows the expected result that PDMS allows adhesion of biological matter, such as proteins. The absence of the white circle illustrates PEG-MA's anti-fouling capabilities. In addition, these images were examined to measure the intensity of the fluorescence to evaluate the protein repelling capability of the PEG-MA modification. Figure 4 shows that the intensity of the fluorescence stemming from adsorbed fibrinogen is significantly higher for unmodified PDMS than for the PEG-MA-grafted PDMS. From these data, we concluded that PEG-MA grafting reduces fibrinogen adsorption and imparts non-fouling

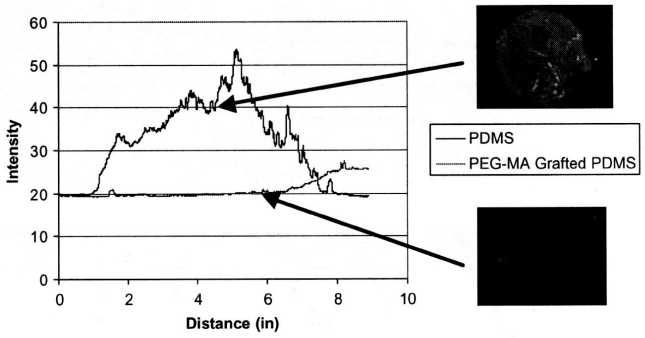

Fig. 4 Fluorescence measurements of virgin PDMS and surface-modified PDMS. The assay is based on the detection of fluorescence-labeled fibrinogen. The two inlets show the actual fluorescence micrographs, from which the data on the left were extracted

properties to PDMS. Taken together, the contact angle measurements, FTIR spectra, and protein assays confirm that the PEG-MA has successfully grafted to the surface of PDMS and exhibit long-term stability of the surface hydrophilicity.

Microfluidic sperm sorting experiments

Before testing the devices with live sperm, the grafted sperm sorters were examined to ensure that fluid flow occurred as designed. An important design criterion that needs to be fulfilled by this grafting process is that the channels be hydrophilic enough to enable ready introduction of the sorting samples and fluids, that the channels be resistant to clogging by unwanted adsorption of proteins and cellular debris, and that the contact angles at all the reservoirs be similar to balance the capillary forces generated at the various reservoirs. In addition, the sperm sorter is designed so that the flow within the microfluidic channel is laminar. The fluid flowing through the semen inlet and the fluid flowing through from the medium inlet should move parallel to each other and then exit through their respective outlets. The sorting is done based on the ability of motile sperm to swim across the streamline into the medium stream and be recovered. Our fluid test is designed to show that even after grafting, the device still functions as designed. When colored DI water was loaded into the sperm sorters and steady laminar flows were observed. The two streams move through the channel system and then exiting through their respective outlets [Fig. 5(a)]. The fluid flow test was carried out using the same time points used for the FTIR study; namely 1 day, 7 days, 14 days, 28 days and 56 days after grafting and subsequent storage in an air environment. In contrast, a sperm sorter that is bonded together by UV/ozone, but does not undergo grafting, has poor fluid handling and does not have flows through the channels as shown in [Fig. 5(b)].

After the stability of the PEG-MA grafted sperm sorters with laminar flow conditions was established, it was essential to test the device with human semen samples containing live sperm. Figure 6 shows how the sorting of motile sperm occurs. A simplified scheme visualizes the underlying concept. The picture on the left illustrates that initially there are two separate streams. One containing semen and the other containing medium. In the middle picture, it can be seen that

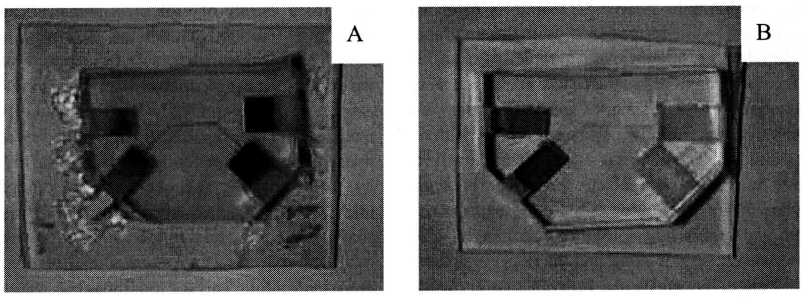

Fig. 5 Fluid flow evaluation of surface-modified PDMS-based sperm sorting devices. The dimensions of the microfluidic channel system are as follow: sperm inlet and outlet channels were 120 μm wide, 5000 μm long, and 150 μm deep, media inlet and outlet channels were 360 μm wide, 5000 μm long, and 150 μm deep, and the main channel was 500 μm wide, 5000 μm long, and 150 μm deep. (A) PEG-MA Grafted PDMS device and (B) and unmodified PDMS device

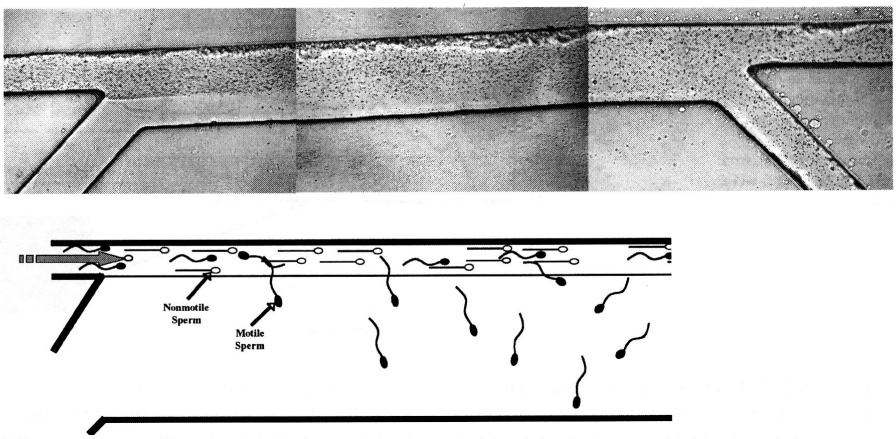

Fig. 6 Human semen sample consisting of a mixture of motile and immotile sperm enters the device from the top right. A laminar flow of medium is introduced from the bottom right. Motile sperm migrate towards the medium and are harvested on the outlet at the bottom left. Immotile sperm and round cells are collected in the reservoir at the top left

motile sperm are beginning to swim out of the semen and into the medium stream. Finally, the picture on the right displays the separation that occurs as motile sperm are recovered in one outlet while the remnants of the semen sample are collected in another outlet. Preliminary sperm sorting data involving semen samples containing 50% motile sperm are promising. The sperm sorting experiments were done directly without any additional channels treatments using a device that was grafted 14 d prior to its use. Compared to conventional PDMS devices that would require plasma treatment to make the surface hydrophilic and coating by albumin or other proteins to make the channels resistant to adhesion of biological matter, this greatly reduces the time from having device in hand to performing sorting experiments. Eliminating the plasma treatment and protein coating steps greatly simplifies the translation into clinical practice, because the devices now have the potential to be pretreated, stored for extended periods, and used immediately as needed. With these surface-modified PDMS devices, human sperm samples were sorted and 74% of the sperm captured in the motile sperm recovery outlet found to be motile. The samples were straightforward to load and experiments could be performed rapidly with no channel pretreatments. The device did suffer from flow fluctuations caused by changes in meniscus shape at the inlet and outlet reservoirs during the course of a sorting experiment. When smooth and highly hydrophilic (contact angle < 20 degrees) materials are used to construct the reservoirs, there is little contact angle hysteresis and little change in meniscus shape during the course of a sperm sorting experiment as the fluid volumes in the reservoirs change (Cho et al., 2003). The relatively high contact angle hysteresis of the current PEG-MA grafted devices, however, made it difficult to maintain optimal flow conditions for extended sorting periods and led to a lower selectivity in motile sperm over the course of an experiment. Thus, the PEG-MA surfaces are excellent for allowing easy introduction of aqueous solutions into the microfluidic channels and in reducing unwanted cell and debris buildup within the channels, but further optimization of the yield and selectivity of recovered motile sperm will require more hydrophilic surface modifications especially at the reservoirs to match closer the extremely hydrophilic surfaces of devices used immediately after plasma oxidation.

Conclusion

PDMS based microfluidic devices have been increasingly used for a variety of biological and medical applications, including reproductive medicine. However, further progress would benefit from surface modification protocols. Herein, we established a protocol based on UV/ozone-initiated graft-*co*-polymerization of poly(ethylene glycol) methyl ether methacrylate to equip PDMS microfluidic systems with more hydrophilic and non-fouling surfaces for long-term stability. This capability will become more crucial as microfluidic devices, such as the sperm sorting devices used in this study, gain commercial relevance. Future work with surface-modified sperm sorting devices will revolve around even more hydrophilic surface modifications with extended shelf lives to further improve reliability and selectivity of the device. The proposed technology may extend the applicability of microfluidic devices by offering a workable solution to

clinical settings, where small amounts of sperm need to be sorted. It also may open an avenue towards convenient bioassays to assess sperm motility, such as at-home motile sperm tests.

Acknowledgments JL gratefully acknowledges support from the NSF in form of a CAREER grant (DMR-0449462), while ST thanks the Whitaker Foundation (TF-04-0032) and the University of Michigan Engineering Technology Development Fund for partial support of this study. We thank Damon Davis and Lourdes Cabrera for sperm samples collecting, media preparation, and sperm motility measurement.

References

D. Belder and M. Ludwig, Electrophoresis **24**, 3595 (2003).
Y. Berdichevsky, J. Khandurina, A. Guttman, and Y.-H Lo, Sensors and Actuators **97**, 402 (2004).
B.S. Cho, T.G. Schuster, X. Zhu, D. Chang, G.D. Smith, and S. Takayma, Anal Chem **75**, 1671 (2003).
K. Efimenko, W.E. Wallace, J. Genzer, J. Colloid Interface Sci **254**, 306 (2002).
V.-M Graubner, R. Jordan, O. Nuyken, B. Schnyder, T. Lippert, R. Kotz, and A. Wokaun, Macromolecules **37**, 5936 (2004).
S. Hu, X. Ren, M. Bachman, C.E. Sims, G. P. Li, and N.L. Allbritton, Langmuir **20**, 5569 (2004).
S. Hu, X. Ren, M. Bachman, C.E.Sims, G.P. Li, and N.L. Allbritton, Anal Chem **74**, 4117 (2002).
B.J. Jeong, J.H. Lee, and H.B. Lee, J. Colloid Inerface Sci **178**, 757 (1996).
J. Lahann, M. Balcells, H. Lu, T. Rodon, K.F. Jensen, and R. Langer, Analytical Chemistry **75**, 2117 (2003).
J.M.K. Ng, I. Gitlin, A.D. Stroock, and G.M. Whitesides, Electrophoresis **23**, 3461 (2002).
A. Olah, H. Hillborg, and G.J. Vancso, Applied Surface Science **239**, 410 (2005).
S.K. Sia and G.M. Whitesides, Electrophoresis **24**, 3563 (2003).
R.S. Suh, N. Phadke, D.A. Ohl, S. Takayma, and G.D. Smith, Human Reprod. Update **9**, 451 (2003).
F. Zhang, E.T. Kang, K.G. Neoh, P. Wang, and K.L. Tan, Biomaterials **22**, 1541 (2001).
X.P. Zou, E.T. Kang, and K.G. Neoh, Plasmas and Polymers **7**, 151 (2002).
X.P. Zou, E.T. Kang, and K.G. Neoh, Surface and Coatings Technology **149**, 119 (2002). http://www.jelight.com/uvo-ozone-cleaning.php http://rsb.info.nih.gov/ij/download.html

Reference

1. Burger, J.A. and T.J. Kipps, *CXCR4: a key receptor in the crosstalk between tumor cells and their microenvironment.* Blood, 2006. **107**(5): p. 1761-7.
2. Cooper, C.R., et al., *Stromal factors involved in prostate carcinoma metastasis to bone.* Cancer, 2003. **97**(3 Suppl): p. 739-47.
3. Kang, H., et al., *Stromal cell derived factor-1: its influence on invasiveness and migration of breast cancer cells in vitro, and its association with prognosis and survival in human breast cancer.* Breast Cancer Res, 2005. **7**(4): p. R402-10.
4. Mosadegh, B., et al., *Epidermal growth factor promotes breast cancer cell chemotaxis in CXCL12 gradients.* Biotechnol Bioeng, 2008. **100**(6): p. 1205-13.
5. Porcile, C., et al., *CXCR4 activation induces epidermal growth factor receptor transactivation in an ovarian cancer cell line.* Ann N Y Acad Sci, 2004. **1030**: p. 162-9.
6. Porcile, C., et al., *Stromal cell-derived factor-1alpha (SDF-1alpha/CXCL12) stimulates ovarian cancer cell growth through the EGF receptor transactivation.* Exp Cell Res, 2005. **308**(2): p. 241-53.
7. Vaday, G.G., et al., *CXCR4 and CXCL12 (SDF-1) in prostate cancer: inhibitory effects of human single chain Fv antibodies.* Clin Cancer Res, 2004. **10**(16): p. 5630-9.
8. Sun, Y.X., et al., *Skeletal localization and neutralization of the SDF-1(CXCL12)/CXCR4 axis blocks prostate cancer metastasis and growth in osseous sites in vivo.* J Bone Miner Res, 2005. **20**(2): p. 318-29.
9. Taichman, R.S., et al., *Use of the stromal cell-derived factor-1/CXCR4 pathway in prostate cancer metastasis to bone.* Cancer Res, 2002. **62**(6): p. 1832-7.
10. Boldajipour, B., et al., *Control of chemokine-guided cell migration by ligand sequestration.* Cell, 2008. **132**(3): p. 463-73.
11. Ferguson, S.S., *Evolving concepts in G protein-coupled receptor endocytosis: the role in receptor desensitization and signaling.* Pharmacol Rev, 2001. **53**(1): p. 1-24.
12. Boyden, S., *The chemotactic effect of mixtures of antibody and antigen on polymorphonuclear leucocytes.* J Exp Med, 1962. **115**: p. 453-66.
13. Kamholz, A.E., et al., *Quantitative analysis of molecular interaction in a microfluidic channel: the T-sensor.* Anal Chem, 1999. **71**(23): p. 5340-7.
14. Li Jeon, N., et al., *Neutrophil chemotaxis in linear and complex gradients of interleukin-8 formed in a microfabricated device.* Nat Biotechnol, 2002. **20**(8): p. 826-30.
15. Burger, J.A. and T.J. Kipps, *CXCR4: a key receptor in the crosstalk between tumor cells and their microenvironment.* Blood, 2006. **107**(5): p. 1761-7.
16. Cooper, C.R., et al., *Stromal factors involved in prostate carcinoma metastasis to bone.* Cancer, 2003. **97**(3 Suppl): p. 739-47.
17. Kang, H., et al., *Stromal cell derived factor-1: its influence on invasiveness and migration of breast cancer cells in vitro, and its association with prognosis and survival in human breast cancer.* Breast Cancer Res, 2005. **7**(4): p. R402-10.
18. Mosadegh, B., et al., *Epidermal growth factor promotes breast cancer cell chemotaxis in CXCL12 gradients.* Biotechnol Bioeng, 2008. **100**(6): p. 1205-13.

19. Porcile, C., et al., *CXCR4 activation induces epidermal growth factor receptor transactivation in an ovarian cancer cell line.* Ann N Y Acad Sci, 2004. **1030**: p. 162-9.
20. Porcile, C., et al., *Stromal cell-derived factor-1alpha (SDF-1alpha/CXCL12) stimulates ovarian cancer cell growth through the EGF receptor transactivation.* Exp Cell Res, 2005. **308**(2): p. 241-53.
21. Vaday, G.G., et al., *CXCR4 and CXCL12 (SDF-1) in prostate cancer: inhibitory effects of human single chain Fv antibodies.* Clin Cancer Res, 2004. **10**(16): p. 5630-9.
22. Sun, Y.X., et al., *Skeletal localization and neutralization of the SDF-1(CXCL12)/CXCR4 axis blocks prostate cancer metastasis and growth in osseous sites in vivo.* J Bone Miner Res, 2005. **20**(2): p. 318-29.
23. Taichman, R.S., et al., *Use of the stromal cell-derived factor-1/CXCR4 pathway in prostate cancer metastasis to bone.* Cancer Res, 2002. **62**(6): p. 1832-7.
24. Boldajipour, B., et al., *Control of chemokine-guided cell migration by ligand sequestration.* Cell, 2008. **132**(3): p. 463-73.
25. Ferguson, S.S., *Evolving concepts in G protein-coupled receptor endocytosis: the role in receptor desensitization and signaling.* Pharmacol Rev, 2001. **53**(1): p. 1-24.
26. Boyden, S., *The chemotactic effect of mixtures of antibody and antigen on polymorphonuclear leucocytes.* J Exp Med, 1962. **115**: p. 453-66.
27. Kamholz, A.E., et al., *Quantitative analysis of molecular interaction in a microfluidic channel: the T-sensor.* Anal Chem, 1999. **71**(23): p. 5340-7.
28. Li Jeon, N., et al., *Neutrophil chemotaxis in linear and complex gradients of interleukin-8 formed in a microfabricated device.* Nat Biotechnol, 2002. **20**(8): p. 826-30.
29. Postlethwaite, A.E. and A.H. Kang, *Collagen-and collagen peptide-induced chemotaxis of human blood monocytes.* J Exp Med, 1976. **143**(6): p. 1299-307.
30. Albini, A., et al., *A rapid in vitro assay for quantitating the invasive potential of tumor cells.* Cancer Res, 1987. **47**(12): p. 3239-45.
31. Fong, C.J., et al., *Utilization of the Boyden chamber to further characterize in vitro migration and invasion of benign and malignant human prostatic epithelial cells.* Invasion Metastasis, 1992. **12**(5-6): p. 264-74.
32. Li, Y.H., et al., *Prognostic significance of elevated hemostatic markers in patients with acute myocardial infarction.* J Am Coll Cardiol, 1999. **33**(6): p. 1543-8.
33. Zigmond, S.H., *Orientation chamber in chemotaxis.* Methods Enzymol, 1988. **162**: p. 65-72.
34. Zigmond, S.H. and J.G. Hirsch, *Leukocyte locomotion and chemotaxis. New methods for evaluation, and demonstration of a cell-derived chemotactic factor.* J Exp Med, 1973. **137**(2): p. 387-410.
35. Zicha, D., G.A. Dunn, and A.F. Brown, *A new direct-viewing chemotaxis chamber.* J Cell Sci, 1991. **99 (Pt 4)**: p. 769-75.
36. Gundersen, R.W. and J.N. Barrett, *Neuronal Chemotaxis - Chick Dorsal-Root Axons Turn toward High-Concentrations of Nerve Growth-Factor.* Science, 1979. **206**(4422): p. 1079-1080.

37. Gundersen, R.W. and J.N. Barrett, *Characterization of the Turning Response of Dorsal Root Neurites toward Nerve Growth-Factor.* Journal of Cell Biology, 1980. **87**(3): p. 546-554.
38. Lohof, A.M., et al., *Asymmetric modulation of cytosolic cAMP activity induces growth cone turning.* J Neurosci, 1992. **12**(4): p. 1253-61.
39. Bradke, F. and C.G. Dotti, *The role of local actin instability in axon formation.* Science, 1999. **283**(5409): p. 1931-4.
40. Ming, G.L., et al., *cAMP-dependent growth cone guidance by netrin-1.* Neuron, 1997. **19**(6): p. 1225-35.
41. Ming, G.L., et al., *Adaptation in the chemotactic guidance of nerve growth cones.* Nature, 2002. **417**(6887): p. 411-8.
42. Wang, S.J., et al., *Differential effects of EGF gradient profiles on MDA-MB-231 breast cancer cell chemotaxis.* Exp Cell Res, 2004. **300**(1): p. 180-9.
43. Abhyankar, V.V., et al., *Characterization of a membrane-based gradient generator for use in cell-signaling studies.* Lab Chip, 2006. **6**(3): p. 389-93.
44. Frevert, C.W., et al., *Measurement of cell migration in response to an evolving radial chemokine gradient triggered by a microvalve.* Lab Chip, 2006. **6**(7): p. 849-56.
45. Futai, N., et al., *Handheld recirculation system and customized media for microfluidic cell culture.* Lab Chip, 2006. **6**(1): p. 149-54.
46. Abdelgawad, M., et al., *Soft lithography: masters on demand.* Lab Chip, 2008. **8**(8): p. 1379-85.
47. Gu, W., et al., *Computerized microfluidic cell culture using elastomeric channels and Braille displays.* Proc Natl Acad Sci U S A, 2004. **101**(45): p. 15861-6.
48. Heo, Y.S., et al., *Characterization and resolution of evaporation-mediated osmolality shifts that constrain microfluidic cell culture in poly(dimethylsiloxane) devices.* Anal Chem, 2007. **79**(3): p. 1126-34.
49. Gundelfinger, E.D., M.M. Kessels, and B. Qualmann, *Temporal and spatial coordination of exocytosis and endocytosis.* Nat Rev Mol Cell Biol, 2003. **4**(2): p. 127-39.
50. Lambeir, A.M., et al., *Kinetic investigation of chemokine truncation by CD26/dipeptidyl peptidase IV reveals a striking selectivity within the chemokine family.* J Biol Chem, 2001. **276**(32): p. 29839-45.
51. Chary, S.R. and R.K. Jain, *Direct measurement of interstitial convection and diffusion of albumin in normal and neoplastic tissues by fluorescence photobleaching.* Proc Natl Acad Sci U S A, 1989. **86**(14): p. 5385-9.
52. Dafni, H., et al., *Overexpression of vascular endothelial growth factor 165 drives peritumor interstitial convection and induces lymphatic drain: magnetic resonance imaging, confocal microscopy, and histological tracking of triple-labeled albumin.* Cancer Res, 2002. **62**(22): p. 6731-9.
53. Jain, R.K., R.T. Tong, and L.L. Munn, *Effect of vascular normalization by antiangiogenic therapy on interstitial hypertension, peritumor edema, and lymphatic metastasis: insights from a mathematical model.* Cancer Res, 2007. **67**(6): p. 2729-35.

54. Weinbaum, S., S.C. Cowin, and Y. Zeng, *A model for the excitation of osteocytes by mechanical loading-induced bone fluid shear stresses.* J Biomech, 1994. **27**(3): p. 339-60.
55. Ng, C.P. and M.A. Swartz, *Fibroblast alignment under interstitial fluid flow using a novel 3-D tissue culture model.* Am J Physiol Heart Circ Physiol, 2003. **284**(5): p. H1771-7.
56. Fleury, M.E., K.C. Boardman, and M.A. Swartz, *Autologous morphogen gradients by subtle interstitial flow and matrix interactions.* Biophys J, 2006. **91**(1): p. 113-21.
57. Hsu, P.P., et al., *Effects of flow patterns on endothelial cell migration into a zone of mechanical denudation.* Biochem Biophys Res Commun, 2001. **285**(3): p. 751-9.
58. Li, S., et al., *The role of the dynamics of focal adhesion kinase in the mechanotaxis of endothelial cells.* Proc Natl Acad Sci U S A, 2002. **99**(6): p. 3546-51.
59. Li, S., N.F. Huang, and S. Hsu, *Mechanotransduction in endothelial cell migration.* J Cell Biochem, 2005. **96**(6): p. 1110-26.
60. Lin, X. and B.P. Helmke, *Micropatterned structural control suppresses mechanotaxis of endothelial cells.* Biophys J, 2008. **95**(6): p. 3066-78.
61. Noria, S., et al., *Transient and steady-state effects of shear stress on endothelial cell adherens junctions.* Circ Res, 1999. **85**(6): p. 504-14.
62. Tardy, Y., et al., *Shear stress gradients remodel endothelial monolayers in vitro via a cell proliferation-migration-loss cycle.* Arterioscler Thromb Vasc Biol, 1997. **17**(11): p. 3102-6.
63. Urbich, C., et al., *Shear stress-induced endothelial cell migration involves integrin signaling via the fibronectin receptor subunits alpha(5) and beta(1).* Arterioscler Thromb Vasc Biol, 2002. **22**(1): p. 69-75.
64. Walker, G.M., et al., *Effects of flow and diffusion on chemotaxis studies in a microfabricated gradient generator.* Lab Chip, 2005. **5**(6): p. 611-8.
65. Song, J.W., et al., *Computer-controlled microcirculatory support system for endothelial cell culture and shearing.* Anal Chem, 2005. **77**(13): p. 3993-9.
66. Poznansky, M.C., et al., *Active movement of T cells away from a chemokine.* Nat Med, 2000. **6**(5): p. 543-8.
67. Yu, X., et al., *Stromal cell-derived factor-1 (SDF-1) recruits osteoclast precursors by inducing chemotaxis, matrix metalloproteinase-9 (MMP-9) activity, and collagen transmigration.* J Bone Miner Res, 2003. **18**(8): p. 1404-18.
68. Brummelkamp, T.R., R. Bernards, and R. Agami, *A system for stable expression of short interfering RNAs in mammalian cells.* Science, 2002. **296**(5567): p. 550-3.
69. Wang, J., et al., *Diverse signaling pathways through the SDF-1/CXCR4 chemokine axis in prostate cancer cell lines leads to altered patterns of cytokine secretion and angiogenesis.* Cell Signal, 2005. **17**(12): p. 1578-92.
70. Rutkowski, J.M. and M.A. Swartz, *A driving force for change: interstitial flow as a morphoregulator.* Trends Cell Biol, 2007. **17**(1): p. 44-50.
71. Moissoglu, K. and M.A. Schwartz, *Integrin signalling in directed cell migration.* Biol Cell, 2006. **98**(9): p. 547-55.

72. Hoogewerf, A.J., et al., *Glycosaminoglycans mediate cell surface oligomerization of chemokines.* Biochemistry, 1997. **36**(44): p. 13570-8.
73. Dinauer, M.C., T.L. Steck, and P.N. Devreotes, *Cyclic 3',5'-AMP relay in Dictyostelium discoideum IV. Recovery of the cAMP signaling response after adaptation to cAMP.* J Cell Biol, 1980. **86**(2): p. 545-53.
74. Paliwal, S., et al., *MAPK-mediated bimodal gene expression and adaptive gradient sensing in yeast.* Nature, 2007. **446**(7131): p. 46-51.
75. Isbister, C.M., et al., *Gradient steepness influences the pathfinding decisions of neuronal growth cones in vivo.* J Neurosci, 2003. **23**(1): p. 193-202.
76. Janetopoulos, C., et al., *Chemoattractant-induced phosphatidylinositol 3,4,5-trisphosphate accumulation is spatially amplified and adapts, independent of the actin cytoskeleton.* Proc Natl Acad Sci U S A, 2004. **101**(24): p. 8951-6.
77. Harmatz, M.G., et al., *Seasonal variation of depression and other moods: a longitudinal approach.* J Biol Rhythms, 2000. **15**(4): p. 344-50.
78. Hachet-Haas, M., et al., *Small neutralizing molecules to inhibit actions of the chemokine CXCL12.* J Biol Chem, 2008. **283**(34): p. 23189-99.
79. Herzmark, P., et al., *Bound attractant at the leading vs. the trailing edge determines chemotactic prowess.* Proc Natl Acad Sci U S A, 2007. **104**(33): p. 13349-54.
80. Loberg, R.D., et al., *CCL2 is a potent regulator of prostate cancer cell migration and proliferation.* Neoplasia, 2006. **8**(7): p. 578-86.
81. Loberg, R.D., et al., *Inhibition of decay-accelerating factor (CD55) attenuates prostate cancer growth and survival in vivo.* Neoplasia, 2006. **8**(1): p. 69-78.
82. Goldbeter, A., *Oscillations and waves of cyclic AMP in Dictyostelium: a prototype for spatio-temporal organization and pulsatile intercellular communication.* Bull Math Biol, 2006. **68**(5): p. 1095-109.
83. Ashall, L., et al., *Pulsatile stimulation determines timing and specificity of NF-kappaB-dependent transcription.* Science, 2009. **324**(5924): p. 242-6.
84. Wells, A., *Tumor invasion: role of growth factor-induced cell motility.* Adv Cancer Res, 2000. **78**: p. 31-101.
85. Rosenberg, M. and S. Ravid, *Protein kinase Cgamma regulates myosin IIB phosphorylation, cellular localization, and filament assembly.* Mol Biol Cell, 2006. **17**(3): p. 1364-74.
86. Ben-Ya'acov, A. and S. Ravid, *Epidermal growth factor-mediated transient phosphorylation and membrane localization of myosin II-B are required for efficient chemotaxis.* J Biol Chem, 2003. **278**(41): p. 40032-40.
87. Phillips, R.J., et al., *Epidermal growth factor and hypoxia-induced expression of CXC chemokine receptor 4 on non-small cell lung cancer cells is regulated by the phosphatidylinositol 3-kinase/PTEN/AKT/mammalian target of rapamycin signaling pathway and activation of hypoxia inducible factor-1alpha.* J Biol Chem, 2005. **280**(23): p. 22473-81.
88. Cullen, J.P., et al., *Pulsatile flow-induced angiogenesis: role of G(i) subunits.* Arterioscler Thromb Vasc Biol, 2002. **22**(10): p. 1610-6.
89. Voermans, C., et al., *SDF-1-induced actin polymerization and migration in human hematopoietic progenitor cells.* Exp Hematol, 2001. **29**(12): p. 1456-64.

90. Voermans, C., P.B. van Hennik, and C.E. van der Schoot, *Homing of human hematopoietic stem and progenitor cells: new insights, new challenges?* J Hematother Stem Cell Res, 2001. **10**(6): p. 725-38.